International Telecommunication Union

ITU-R
Radiocommunication Sector of ITU

Report ITU-R M.2376-0
(07/2015)

Technical feasibility of IMT in bands above 6 GHz

M Series

Mobile, radiodetermination, amateur
and related satellite services

Foreword

The role of the Radiocommunication Sector is to ensure the rational, equitable, efficient and economical use of the radio-frequency spectrum by all radiocommunication services, including satellite services, and carry out studies without limit of frequency range on the basis of which Recommendations are adopted.

The regulatory and policy functions of the Radiocommunication Sector are performed by World and Regional Radiocommunication Conferences and Radiocommunication Assemblies supported by Study Groups.

Policy on Intellectual Property Right (IPR)

ITU-R policy on IPR is described in the Common Patent Policy for ITU-T/ITU-R/ISO/IEC referenced in Annex 1 of Resolution ITU-R 1. Forms to be used for the submission of patent statements and licensing declarations by patent holders are available from http://www.itu.int/ITU-R/go/patents/en where the Guidelines for Implementation of the Common Patent Policy for ITU-T/ITU-R/ISO/IEC and the ITU-R patent information database can also be found.

Series of ITU-R Reports

(Also available online at http://www.itu.int/publ/R-REP/en)

Series	Title
BO	Satellite delivery
BR	Recording for production, archival and play-out; film for television
BS	Broadcasting service (sound)
BT	Broadcasting service (television)
F	Fixed service
M	**Mobile, radiodetermination, amateur and related satellite services**
P	Radiowave propagation
RA	Radio astronomy
RS	Remote sensing systems
S	Fixed-satellite service
SA	Space applications and meteorology
SF	Frequency sharing and coordination between fixed-satellite and fixed service systems
SM	Spectrum management

Note: This ITU-R Report was approved in English by the Study Group under the procedure detailed in Resolution ITU-R 1.

Electronic Publication
Geneva, 2015

© ITU 2015

REPORT ITU-R M.2376-0

Technical feasibility of IMT in bands above 6 GHz

(2015)

TABLE OF CONTENTS

1 Introduction

The experiences of current mobile and wireless communications networks have shown that data traffic is growing more than anticipated (see Report ITU-R M.2243). This development is providing a significant challenge to the development of future mobile and wireless communication networks. It is envisioned that future IMT systems, in addition to other features, will need to support very high throughput data links to cope with the growth of the data traffic. There has been academic and industry research and development ongoing related to suitability of mobile broadband systems in frequency bands above 6 GHz.

In ITU-R, studies are underway on further developments of IMT and its future needs. Recommendation ITU-R M.2083 – Framework and overall objectives of the future development of IMT for 2020 and beyond; describes "*the framework of the future development of IMT for 2020 and beyond, including a broad variety of capabilities associated with envisaged usage scenarios.*" For some of these new usage scenarios "*contiguous and broader channel bandwidths than available to current IMT systems would be desirable to support continued growth.*" Report ITU-R M.2320 – Future technology trends of terrestrial IMT systems; highlights the development of technologies such as small cells, 3D beamforming and massive MIMO techniques that "*may realize their full potential when applied to smaller wavelengths, which are characteristic of higher frequency bands*".

Recently, considerable research has been carried out by various organizations on a global scale on feasibility of IMT in spectrum above 6 GHz. The corresponding results have been presented at various workshops and conferences. In particular, several presentations were made during the 'workshop on research views of IMT beyond 2020'[1] hosted by the ITU in February 2014. During this workshop, most research organizations expressed their interest in utilizing higher frequencies for IMT and mobile broadband usage. It is expected that usage of higher frequencies will be one of the key enabling components of future IMT.

2 Scope

The scope of this Report is to study and provide information on the technical feasibility of IMT in the bands between 6 GHz and 100 GHz. Technical feasibility includes information on how current IMT systems, their evolution, and/or potentially new IMT radio interface technologies and system approaches could be appropriate for operation in the bands between 6 GHz and 100 GHz, taking into account the impact of the propagation characteristics related to the possible future operation of IMT in those bands. Technology enablers such as developments in active and passive components, antenna techniques, deployment architectures, and the results of simulations and performance tests are considered.

3 Related documents

Report ITU-R M.2320

Recommendation ITU-R M.2083

Recommendation ITU-R P.676

Recommendation ITU-R P.833

Recommendation ITU-R P.837

Recommendation ITU-R P.838

---

[1] http://www.itu.int/dms_pub/itu-r/oth/0a/06/R0A060000630001MSWE.docx

Recommendation ITU-R P.525

ITU-R Handbook on Radiometeorology

4 Radiowave propagation in bands above 6 GHz

This section contains material which is the combination of existing ITU-R Recommendations and Reports as well as new preliminary material contributed through research work done outside ITU-R to address certain new use cases and applications. Further investigations are ongoing and applicable ITU-R Recommendations are being developed.

4.1 Propagation losses

4.1.1 Path loss

One of the challenges of mobile communications in the higher bands for outdoor access will be to overcome the expected difficulties in propagation conditions. Understanding the propagation conditions will be critical to designing an appropriate air interface and determining the type of hardware (particularly the array size) needed for reliable communications. The most obvious obstacle will be the higher pathloss of the bands above 6 GHz relative to traditional cellular bands. Just looking at free-space pathloss, the expected loss (dB) will be

$$L_p = 92.4 + 20 \log f + 20 \log d \tag{1}$$

where f is the frequency (GHz) and d is the distance (km) between transmitter and receiver (Recommendation ITU-R P.525). For example, an additional 22.9 dB and 30.9 dB of losses are expected to result in the ranges from 2 GHz to 28 GHz and 70 GHz respectively which will need to be compensated by some means, for example, larger antenna array sizes with higher antenna gains and MIMO technologies.

Due to variation of propagation characteristics in bands above 6 GHz, it is appropriate to investigate the propagation characteristics of these frequency bands independently. Some preliminary investigations were conducted by both industry and academy The combined effects of all contributors to propagation loss can be expressed via the path loss exponent.

Some preliminary experiments in urban micro cell outdoor-to-outdoor and indoor scenarios, with transmitter and receiver antenna heights below rooftop, measured path loss exponents for 10 GHz, 18 GHz, 28GHz, 38 GHz, 60 GHz and 72 GHz in both line-of-sight (LoS) and non-line-of-sight (NLoS) environments which are summarized below. Please note that every experiment at each frequency could have different measurement setup.

Despite these losses, higher frequencies nevertheless could be applicable for IMT use. In fact, frequencies above 6 GHz can actually provide large chunks of spectrum with sufficiently low atmospheric attenuation in the case of small cells.

Figure 1 (Fig. 6.1 of the ITU-R Handbook on Radiometeorology) shows the specific gas, rain and fog attenuation (dB/km) as a function of frequency. As seen in Fig. 1, these effects exhibit a high degree of frequency dependent variation. Rain loss can be more significant compared to other atmospheric losses, except near the peaks in gaseous attenuation, but is relatively infrequent.

Atmospheric gas loss is approximately 0.10 dB/km and 0.15 dB/km at 28 GHz and 38 GHz, respectively, and about 0.40 dB/km at frequencies between 70 and 90 GHz. Since urban microcells will be designed for inter-site distances within 200 m (both for backhaul and cellular), the gas attenuation could be of little concern. Thus, frequencies above 6 GHz can provide access to spectrum with sufficiently low atmospheric attenuation in the case of small cells.

Generally, rain effects are analysed in terms of system outages which are typically required to be on the order of 0.01% or even 0.001% (i.e. 99.999% system availability) against expected mm/hr rainfall in a geographical region (Recommendation ITU-R P.837). For small cell radii below 200 m, the effects do not seem to be insurmountable. A 30 GHz carrier will see less than 1 dB loss over 200 m in a "heavy rain" (25 mm/h), while a 60 GHz carrier would see less than 2 dB. However, tropical downpours, hurricanes, and the like where reliable mobile communications links are vital, must be taken into consideration [26].

Even those frequencies represented by the peaks in Fig. 1 that are more susceptible to molecular oxygen and water vapour losses than other bands could still be used for small cell applications where the atmospheric attenuation is not a limitation. In these frequency ranges, the inherent atmospheric loss also limits reach of interfering signals, allowing tighter reuse of carrier frequencies.

FIGURE 1

Atmospheric attenuation vs. frequency

Since the size of raindrops is similar to the wavelength around the millimetric wave frequency bands, it causes the scattering effect of the signal propagation.

Detailed information on oxygen and water vapour loss can be found in Recommendation ITU-R P.676. Information on rain loss can be obtained from Recommendation ITU-R P.838. Also, the ITU-R Handbook on Radiometeorology will provide good supporting material.

The total specific attenuation (dB/km) caused by atmospheric gasses and rain is:

$$\gamma = \gamma_G + \gamma_R = \gamma_0 + \gamma_w + k \cdot R^a \tag{2}$$

where

γ_G: sum of the specific attenuations (dB/km) of oxygen and water vapour, respectively:

$$\gamma_G = \gamma_0 + \gamma_w$$

and

γ_R: specific attenuations (dB/km) due to the rainfall:

$$\gamma_R = k \cdot R^a$$

R is the rain rate (mm/h); values for the coefficients k and a are determined as functions of frequency, f (GHz) and the polarization type (Recommendation ITU-R P.838).

For outdoor usage, there are other signal impairments that must be considered. Local environmental factors such as trees and shrubs cause additional attenuation of the millimetric signal. The associated loss is caused by a combination of diffraction, ground reflection and through-vegetation scattering. Recommendation ITU-R P.833 includes information for calculation of foliage loss for up to 60 GHz for terrestrial and slant paths. For terrestrial links, the loss is expressed in the form of:

$$L_{total} = -10 \log_{10}\left\{10^{\left(\frac{-L_{sidea}}{10}\right)} + 10^{\left(\frac{-L_{sideb}}{10}\right)} + 10^{\left(\frac{-L_{top}}{10}\right)} + 10^{\left(\frac{-L_{ground}}{10}\right)} + 10^{\left(\frac{-L_{scat}}{10}\right)}\right\}$$

In which L_{sidea} and L_{sideb} represent loss due to diffraction from either side of the vegetation, L_{top} represents the diffraction loss above the vegetation, L_{ground} is the loss due to ground reflection, and L_{scat} is the loss due to scattering through the vegetation. Formulas for calculating the above losses, which depend on frequency, depth of the vegetation, and type of the vegetation, are included in Recommendation ITU-R P.833. The figure below depicts attenuation due to vegetation for 0.5 m^2 and 2 m^2 illumination area, for in leaf and out of leaf situations.

FIGURE 2

Attenuation for 0.5m² and 3m² illumination area, a) in leaf, b) out of leaf

a)

b)

- - - - - - - -   5 GHz, 0.5 m²   — — — 10 GHz, 2 m²

——————   5 GHz, 2 m²   —— – · 40 GHz, 0.5 m²

———— · —— 10 GHz, 0.5 m²   ———— — 40 GHz, 2 m²

* The curves show the excess loss due to the presence of a volume of foliage
which will be experienced by the signal passing through it. In practical
situations the signal beyond such a volume will receive contributions due
to propagation both through the vegetation and diffracting around it. The
dominant propagation mechanism will then limit the total vegetation loss.

P.0833-07

4.2 Recent activities on radiocommunication channel characteristics and modelling

4.2.1 General

In general, an appropriate channel model for higher bands including millimetric bands should fulfil a set of requirements including those listed below:

– provide accurate space-time characteristics of the propagation channels in three-dimensional (3D) space for LoS and NLoS conditions;

– support beamforming with steerable directional antennas on both transmitter and receiver sides with no limitation on the antenna type and technology;

– account for polarization characteristics of antennas and signals;

– support non-stationary characteristics of the propagation channel arising from UE motion and non-stationary environment (e.g. moving people causing communication link attenuation or full blockage).

The channel models can be divided in two categories, geometry based stochastic approach, and deterministic/quasi-deterministic, depending on the approach taken. The geometry based stochastic approach characterizes the channel as a number of probabilistic rays with different delay and angular spread representative of a particular multi-path propagation environment. The spatial and temporal statistics are collected in a measurement campaign for a given frequency in an environment typical to the desired deployment. The purely deterministic model would use electromagnetic equations and the model of the scatterer environment to predict the channel between the transmitted and the receiver, whereas the quasi-deterministic approach is based on the representation of the channel impulse response as superposition of a few quasi-deterministic strong rays and a number of relatively weak random rays, and the parameters for a given frequency in a particular environment are based on a measurement campaign. A large body of work by industry and academia has already gone into channel measurements and modelling, due to the multitude of different propagation environments and the large frequency range. This will continue, and a set of channel models will be developed for the IMT propagation environments for bands above 6 GHz, which will be described in ITU-R Recommendations..

One advantage of millimetric wave systems is in the inherently small antennas required, which can be arranged in relatively small-footprint phased-arrays for high directivity and beamsteering.

Generally, RMS delay spread is increased for lower gain antennas which employ wider beams, as the wider profile collects signals from more directions with similar or equal gain to the boresight angle. This particularly applies to UE equipment whose size and power requirements do not support large arrays and have a more omni-directional pattern.

Conversely, RMS delay spread is decreased for higher gain antennas and the associated narrower beamwidth. The transmit beamwidth from the base station limits the direction of the generated energy and thus the opportunities to scatter. Likewise, in spite of the higher gain, scattered energy of the multipath link may not be picked up by the spatial range of the receive antenna boresight.

As an example, assuming a transmitter beamwidth of 5 degrees and the transmitter distance of 100 m, the UE receiver will be illuminated by the primary transmitter energy and its reflections over an arc length of about 9 m.

The reflections will thus be primarily bounded by delays around 30 ns. This model is theoretical, of course, and does not account for sidelobe energy or reflections behind the UE.

Meanwhile, as outlined through an outdoor ray-tracing analysis of [32], higher-order rays (i.e. rays with more reflections) have larger angles of incidence and are, therefore, more likely to fall outside of the receiver antenna beamwidth. Theoretically, for a typical geometry of lampposts several meters

above the ground and several hundred metres separate, second order systems are often deemed sufficient approximations. A model for this system is outlined later in this section.

Thus, for a given environment and use cases with different transmitter and receiver antenna radiation patterns, one may observe different scattering effects as illustrated, in a rather ideal sense for ease of conceptualization, in Fig. 3. The primary point is that delay spread is mitigated by the beamforming paradigm. This is a key area of exploration, simulation and prototyping.

FIGURE 3

Scattering effects

As stated, recently there have been experiments conducted at millimetric wave frequencies in outdoor environments. These experiments involved both LoS and NLoS scenarios over a variety of distances, antenna gains and beamwidth for several frequencies. Following subsections provide detailed information. The findings are summarized in Table 3.

TABLE 3

Summary of channel rms delay spread for NLoS experiments in different environments

	28 GHz	38 GHz	60 GHz	73 GHz
Mean RMS delay spread		23.6 ns	7.4 ns	
Max RMS delay spread	454.6 ns	185 ns	36.6 ns	248.8 ns

4.2.2 Frequency range 6-30 GHz

Delay spread in ~30 GHz

From measurements made at 28 GHz in New York, the urban-micro type environment at 28 GHz can be characterized as follows [41] [42].

• From the NYU WIRELESS 28 GHz outdoor Manhattan database using a 5 dB detectable multipath component threshold, the maximum RMS delay spread values in LoS and NLoS locations are 309.6 ns and 454.6 ns, respectively and the max 20 dB down maximum excess delay (MED) in LoS and NLoS locations are 1291.4 ns and 1387.4 ns respectively.

• Azimuth angle of arrival spreads of 15.5 degrees for NLoS.

• Azimuth angle of departure spreads of 10.2 degrees for NLoS.

• Elevation angle of arrival spreads of 6.0 degrees.

Measurements of building entry losses at 28 GHz

Experiments [62] have shown that the attenuation/excess loss limits the coverage rather than multipath interference. In the scenario studied, coverage was obtained at all measured locations with a loss between 3 and 60 dB above the reference level at 70 m LoS distance. If all windows in the office had been of the coated glass kind, then at least 20 dB higher excess loss would be expected and the coverage would be significantly more limited. Thus, the deployment opportunities strongly depend on the specific location and the kind of windows that are present.

4.2.3 Frequency range 30-70 GHz

Channel model in ~60 GHz

During the IEEE Std 802.11ad^{TM} standardization process for frequencies around 60 GHz, a large body of work on systematization and unification of the channel model was performed [33] [34] [35] [36]. This resulted in a unified, 3-dimensional (3D), statistical channel model for different indoor scenarios [37] used for development of the IEEE Std 802.11ad standard.

Millimetric wave outdoor channels have been experimentally investigated in a number of papers and reports, for various deployments at the 60 GHz band [38] [39] [40]. However, there is still on-going work on 3D models for typical outdoor environments.

Following the same methodology used for indoor environments, a set of statistical channel models for outdoor scenarios could be developed. As a starting point, one can assume the channel model developed in [43]. When considering an LoS path plus both first-order and second-order reflected paths, the (m, n)-th element of the channel matrix **H** can be modelled for a second-order channel as:

$$h_{m,n} = h_{LOS}(m,n) + \sum_{i=1}^{K_1} h_{1,i}(m,n) + \sum_{k=1}^{K_2} h_{2,k}(m,n)$$

where K_1 and K_2 are the numbers of first-order and second-order reflected paths respectively. The additive terms are defined as:

$$h_{LOS}(m,n) = \frac{\lambda}{4\pi p_{LOS}(m,n)} \exp\left(-j\frac{2\pi}{\lambda} p_{LOS}(m,n)\right)$$

$$h_{1,j}(m,n) = \Gamma(\theta_{1,j}) \frac{\lambda}{4\pi p_{1,i}(m,n)} \exp\left(-j\frac{2\pi}{\lambda} p_{1,i}(m,n)\right)$$

$$h_{2,k}(m,n) = \Gamma_1(\theta_{2,k})\Gamma_2(\phi_{2,k}) \frac{\lambda}{4\pi p_{2,k}(m,n)} \exp\left(-j\frac{2\pi}{\lambda} p_{2,k}(m,n)\right)$$

where $\Gamma(q)$ is the perpendicular Fresnel reflection coefficient and λ is the wavelength. This channel model is quite well formulated and tractable and captures the key features of the millimetric wave channel. As a starting point, this simple channel model can be considered for design and analysis until other more accurate millimetric wave channel models are available.

A quasi-deterministic (Q-D) approach for modelling outdoor and indoor millimetric wave channels is presented here. From measurements made at 60 GHz [63] with three kinds of scenarios, i.e. (i) *mobile access scenarios* including open area (university campus), street canyon, hotel lobby, (ii) *backhaul/front haul scenarios* including above roof top (ART), street canyon, and (iii) *device-to-device (D2D) scenarios* including open area D2D, street canyon D2D, hotel lobby D2D, the measurement in 60 GHz can be characterized as follows (detailed in § A4.2):

1)   Link budget drawn from the measurements indicate the necessity of directional transmission. Interference will therefore be a much less limiting factor than at legacy frequencies. Transmit power limitation on the other hand and the achievable gain of adaptive or multiple antennas will limit the achievable range, especially in NLoS cases.

2)   There are significant propagation paths besides the LoS path with considerable power. Their number is limited and strongly depends on the propagation environment. The reflection from the ground plays an important role.

3)   Blockage of particular propagation paths by persons and other objects (e.g. street furniture or vehicles), especially of the direct path has severe effects on the overall channel. This applies to indoor as well as to outdoor environments. However, a communication system can make use of propagation paths that are not blocked.

4)   For a mobile RX (or TX) and dynamic propagation environments, the propagation channel is highly time-variant. The time variance is caused by temporary blockage of particular paths as well as by additionally appearing paths related to moving reflectors. Passing vehicles can result in strong temporary reflected paths.

5)   The cross-polarization ratio (XPR) is relatively small, especially for outdoor scenarios with a limited number of paths. The measured XPR for the ground-reflected ray was less than −25 dB.

6)   The time delay difference of paths can become very small, especially for outdoor scenarios and increasing distance between TX and RX.

7)   A millimetric wave channel model for link and system-level simulations must support (must be combinable with) arbitrary antenna patterns, multi-antenna configurations (beamforming and MIMO), time-variant effects (including Doppler and blockage effects) related to mobile RX, TX and dynamic outdoor environments.

8)   A quasi-deterministic (Q-D) channel modelling methodology is well-suited to describe the channel on a scenario-specific basis. A corresponding approach is presented in the annex. The Q-D approach is based on the representation of the channel impulse response as superposition of a few quasi-deterministic strong rays (D-rays) and a number of relatively weak random rays (R-rays). The model has already been verified and parameterized for several of the above-mentioned scenarios by two independent 60 GHz channel measurement campaigns.

Delay spread in ~40 GHz

From measurements made at 38 GHz [7a], the urban-micro type environment in Austin at 38 GHz can be characterized as follows:

•   From the NYU WIRELESS 38 GHz measurement results which were performed at the University of Texas at Austin campus, most LoS measurements had very minimal RMS delay spread, on the order of 1 ns, due solely to the transmitted pulse shape with one partially obstructed LOS link resulting in a maximum of 15.5 ns. The NLoS measurements exhibited higher and more varied RMS delay spreads, with a mean of 14.8 ns for the 25-dBi receiver antenna and 13.7 ns for the 13.3-dBi receiver antenna. The maximum NLoS RMS delay spreads were 185 and 166 ns for the 25- and 13.3-dBi receiver antennas, respectively.

        Nonetheless, more than 80% of the NLoS links had RMS delay spreads under 20 ns and 90% of the NLoS links had RMS delay spreads under 40 ns.

•   In both LoS and NLoS, 25 dBi narrow beam with the beamwidth of 7.8 degree horn antennas at the transmitter (TX) and receiver (RX) were systematically and iteratively steered in the azimuth and elevation directions, emulating a beam-steering antenna-array architecture. For LoS, the transmitter and receiver were pointed directly at each other in both azimuth and

elevation directions, corresponding to zero degree azimuth scanning angles for the transmitter and receiver.

- It is possible to receive many NLoS links for different transmitter/receiver pointing angle combinations, with multipath signals often 10-20 dB weaker from the strongest received signal.

Delay spread in ~60 GHz

From measurements made at 60 GHz [6a] with three kinds of scenarios, i.e. (i) *mobile access scenarios* including open area (university campus), street canyon, hotel lobby; (ii) *backhaul/front haul scenarios* including above roof top (ART)and street canyon; and (iii) *device-to-device (D2D) scenarios* including open area D2D, street canyon D2D, hotel lobby D2D, and the measurement in 60 GHz can be characterized as follows (detailed in Annex 2):

- The use of directional antennas at both TX and RX led to the discovery that the considered experimental scenario was adequately characterized by only two strongest propagation paths (or rays). The first path corresponded to the LoS component and the second path corresponded to the reflection from the ground (asphalt) surface. All other propagation paths caused by reflections from surrounding objects were more than 15-20 dB lower than these two strongest components.

- The peaks corresponding to the LoS and ground-reflected components are found 2.5 ns apart from each other. The power difference between those two peaks is approximately equal to the ground reflection coefficient (–6 dB) in line with the given scenario geometry where the horizontal distance between the transmitter and receiver is 30.6 m. Initially, the dependency of the channel transfer function (CTF) on the RX vertical motion was investigated for a distance $L_0 = 30.6$ m. According to the measurement results, the millimeter-wave channel has highly frequency selective in an 800 MHz bandwidth. In addition, millimeter-wave channel has very fast variations when the RX height is changing.

- The cross-polarization ratio (XPR) was also measured and the value of XPR was less than −25 dB for the ground-reflected ray in the considered experimental scenario. For that purpose, orthogonal antenna polarization configurations were used at the TX and RX.

- It was identified that typical (not very highly-directional) mobile user antenna will receive two rays (the direct LoS ray and the ground-reflected ray) with rather small time delay (2.5 ns for 30 m). It should be noted, that as the distance between the TX and RX sites increases, the difference between the time delays and angles of arrival between these rays decreases.

4.2.4 Frequency range 70-100 GHz

Delay spread in ~70 GHz

Using the measurements at 73 GHz from [64] as well as ray tracing, an initial channel model was developed [65]. It was found that in urban-micro type environments in New York the 73 GHz channel has the following characteristics:

1. From the NYU WIRELESS 73 GHz outdoor Manhattan database using a 5 dB detectable multipath component threshold, the maximum RMS delay spread values in LoS and NLoS locations are 219.2 ns and 248.8 ns, respectively and the max 20 dB down maximum excess delay (MED) in LoS and NLoS locations are 762.3 ns and 1 053 ns respectively.

2. Azimuth angle of arrival spreads of 3.0 degrees for LoS and 20 degrees for NLoS.

3. Azimuth angle of departure spreads of 3.5 degrees for LoS and 12 degrees for NLoS.

4. Elevation angle of arrival and departure spreads and biases (deviation from the LoS elevation angle) were distant-dependent.

5. A Ricean factor of 12 dB for the LoS channels.

6.   A cross-polarization discrimination factor for the NLoS path of 15 dB, based on the limited set of measurements available.

In addition to considerable studies to date, further measurements and analyses are underway to accurately develop channel models including but not limited to characterization of the angular domain of the channel, consideration of accurate space-time characteristics, polarization characteristics, scattering, etc.

Millimetric wave angular spread

For millimetric wave bands, the spatial propagation characteristics, especially angular domain characteristics can have influence on beamforming key technologies design. The results in [61] showed that the directional dispersion of 72 GHz indoor channels is sparser than those obtained in lower frequencies. The observation of angular spreads implies that spatial beamforming techniques are preferable in both backhaul transmission and radio access.

4.3   Summary of the results of the studies

In order to evaluate the feasibility of IMT in spectrum above 6 GHz, it is essential to understand how the radio signal will propagate in typical hotspot scenarios for IMT deployment. Both academia and industry have studied propagation characteristics of IMT deployment scenarios above 6 GHz, which are different from deployment scenarios for other services. Measurement campaigns that have been conducted cover frequency ranges from 10 GHz to 73 GHz. Both LoS and NLoS for indoor and outdoor, as well as outdoor-to-indoor measurement cases have been studied. Propagation pathloss has been investigated in order to estimate the coverage and link budget of the radio system. Other channel modelling and measurement activities have studied propagation phenomena, such as delay spread caused by multi-path propagation of radio signals, which can be helpful for system design. The results described in this Section support the feasibility of IMT in spectrum above 6GHz, and studies are continuing.

5   Characteristics of IMT in the bands above 6 GHz

The use of bands above 6 GHz for small cells is expected to provide the scalability, capacity and density required for a seamless integration of these cells into the cellular network infrastructure [26] [27]. These higher bands contain large frequency ranges with existing primary allocations to the mobile service, and offer the potential for increased network capacity as well as network densification. All of these benefits, on the other hand, come at the expense of added system complexity particularly in terms of radio frequency (RF) front end, complex antenna design, and the need to combat higher atmospheric losses. However, recent advancements in technologies developed for spectrum around 60 GHz (see § 6) have produced cost effective solutions that can be leveraged to overcome many of these challenges. The following sections discuss some of these challenges while § 6 describes technologies that could provide potential solutions associated with these problems.

5.1   Outdoor-to-outdoor coverage and link budget

The first consideration for link budget analysis is the signal power attenuation due to propagation loss over the air. The inverse Friis equation for isotropic radiators relates the free space path loss (FSPL) of an RF carrier as proportional to the square of its frequency. FSPL also increases in proportion to the square of the distance between the transmitter and receiver (Recommendation ITU-R P.525). As such, a 30 GHz signal transmitted over a distance of 20 m loses 88 dB of power just covering this relatively short distance between transmitter and receiver. At 100 m, the loss is increased to 102 dB.

Coverage can be analysed from the link budget perspective. Since the typical outdoor urban environments will include NLoS paths, the analysis should include the NLoS cases. For the given

system parameters of Table 4, the maximum distances that can support 1 Gbit/s data rate in various environments can be found in this section.

In the analysis presented in Table 5, the 28 GHz frequency band is considered for the centre frequency of systems with 1 GHz bandwidth. Tx e.i.r.p. and Rx antenna gain are assumed to be 65 dBm, which can be realized by low-power base stations. For example, 30 dBm Tx power with 25 dBi Tx antenna gain and 10 dBi Rx antenna gain can be used for the systems.

TABLE 4

System parameters for link budget analysis

Carrier Frequency (GHz)	28	
Tx e.i.r.p.+ Rx antenna Gain (dBm)	65	
Bandwidth (GHz)	1	
Rx noise figure (dB)	7	
Other losses (dB)	10	
Target data rate (Gbit/s)	1	0.1
Target SNR (dB)	0	−11.4

TABLE 5

Example link budget analysis for various environments at 28 GHz

Environments	Open Space	Campus	Dense Urban	Dense Urban
LoS / NLoS	LoS	NLoS	NLoS	NLoS
Reference	Friis Equation	[R5]	[R6]	[R7]
Path loss model	$PL(d) = 61.4 + 20*\log10(d)$	$PL(d) = 47.2 + 29.8*\log10(d)$	$PL(d) = 96.9 + 15.1*\log10(d)$ (for $d<100$) $PL(d) = 127.0 + 87.0*\log10(d/100)$ (for $d>100$)	$PL(d) = 61.4 + 34.1*\log10(d)$
Max. distance for 1 Gbit/s	978 m	304 m	40 m	57 m
Max. distance for 100 Mbit/s	3,634 m	734 m	116 m	122 m

As shown in the Table 5, the low-power base station can provide 1 Gbit/s using 1 GHz bandwidth for the outdoor coverage with from tens to hundreds meter cell radius depending on cell environments. For example, the campus in [17] which is similar to sub-urban environments could serve a 300 m distance at 1 Gbit/s data rate while the dense urban environments like New York City [19] could provide 1 Gbit/s data rate for the distance of up to around 50 m even if the channel link is blocked by buildings. If the channel link is clearly secured without any obstacles between the transmitter and the receiver, the distance would be increased similar to the case of free space.

As indicated in Table 6, a small cell situation at 39 GHz and 60 GHz is assumed wherein the base station is presumed to transmit at the maximum transmit power of 19 dBm and has a transmit antenna gain of 24 dBi due to the directivity provided by a beam steerable patch array antenna. On the user

equipment (UE) side, the constraint is to a maximum transmitter power of 10 dBm and only 15 dBi of antenna gain, e.g. using a small-size patch antenna, due to form factor limitations.

The results are summarized in Table 6. It should be noted that baseband techniques such as coding gain and shadowing effects on the channel model are not considered. Nevertheless, the results in Table 6 give a good indication of the challenges presented by the link budget.

TABLE 6

Example DL LoS link budgets for 60 GHz and 39 GHz

		60 GHz		39 GHz	
Tx power	dBm	19		19	
Tx ant gain	dB	24		24	
e.i.r.p.	dBm	43		43	
Path loss	dB	LoS: $PL(d) = 92.44 + 20\log10(60) + 20\log10(d/1000)$ (source: Recommendation ITU-R P.2001)	Street Canyon: $PL(d) = 82.02 + 23.6*\log10(d/5)$ (source: Reference [37] in § A4.3)	LoS: $PL(d) = 92.44 + 20\log10(39) + 20\log10(d/1000)$ (source: Recommendation ITU-R P.2001)	Street Canyon: $PL(d) = 78.28 + 23.6*\log10(d/5)$ (Source: Reference [37] in § A4.3)
Rx ant gain	dB	15		15	
Signal BW	GHz	2		0.5	
Input noise power	dBm	−80.9			
Radio NF	dBm	10			
Implement. loss	dB	10			
Capacity (achievable rates)	Gbit/s	LoS: 16.54 Gbit/s in 20 m 7.47 Gbit/s in 100 m 4.05 Gbit/s in 200 m	NLoS: 15.08 Gbit/s in 20 m 4.73 Gbit/s in 100 m 1.71 Gbit/s in 200 m	LoS: 4.75 Gbit/s in 20 m 2.64 Gbit/s in 100 m 1.52 Gbit/s in 200 m	NLoS: 4.39 Gbit/s in 20 m 1.72 Gbit/s in 100 m 0.77 Gbit/s in 200 m

The salient point of this analysis is the high degree of antenna gain required for any appreciable small cell radii. Much higher gain is needed to achieve high data rates. Indeed, large 60 GHz patch antennas on the market today are advertising gain of 29 dBi. However, they are designed to support highly directive point-to-point installations. This issue is addressed further in § 6.1, where an alternative approach is presented.

Example link budgets for 72 GHz are summarized in Table 7. Since the antenna array can be much denser and compact, high antenna gain of 34 dBi can be achieved in the 72 GHz band. The link budgets show that the coverage at 1 Gbit/s can be about 120 m under NLoS propagation conditions. For LoS conditions, the coverage at 1 Gpbs can be enlarged to more than 470 m. 72 GHz band can meet the requirements of most of the use cases introduced in § 7.1.

TABLE 7

Example DL outdoor link budget for 72 GHz

Parameters	72 GHz	
	NLoS	LoS
Transmitter power (dBm)	26.00	
Path loss (dB)	PL(d)= 69.59 + 36.7·log(d)	PL(d)= 69.59 + 28.6·log(d)
Transmitter antenna gain (dBi)	34.00	
Transmitter e.i.r.p. (dBm)	60.00	
Receiver antenna gain (dBi)	21.00	
Bandwidth (GHz)	2.00	
Receiver noise figure (dB)	7.00	
Receiver noise power (dBm)	–73.99	
Implementation loss (dB)	10.00	
Capacity and coverage	1 Gbit/s: 122.92 m 10 Gbit/s: 37.98 m	1 Gbit/s: 477.18 m 10 Gbit/s: 105.86 m

5.2 Outdoor-to-indoor coverage

For cost reasons it would be desirable to provide indoor coverage using base stations located outdoors. A discussion of building penetration losses for these scenarios along with illustrations of simulated indoor-to-outdoor path gain maps for different building types at frequencies above 6 GHz can be found in § A3.1 in Annex 3. Section A3.1 in Annex 3 also contains simulated user throughput performance for these scenarios, for a range of frequencies up to 60 GHz. The results of the simulations conducted are shown in the table below for two types of building (A and B), and, for each building, two types of indoor propagation models; further, for each model, three different frequencies):

	Building A (old building construction)		Building B (new building construction, with infrared reflective glass)	
	Indoor Model 1	Indoor Model 2	Indoor Model 1	Indoor Model 2
10 GHz	1 BS >100 Mbit/s	1 BS >100 Mbit/s	>1 BS >10 Mbit/s	>2 BSs >10 Mbit/s
30 GHz	>1 BS >10 Mbit/s	>2 BSs >10 Mbit/s	>6 BSs >10 Mbit/s	>6 BSs >10 Mbit/s
60 GHz	>6 BSs >10 Mbit/s	>6 BSs >10 Mbit/s	>10 Mbit/s: Not achievable even with narrow beam entering through the window as the IRR glass loss is comparable to that of the concrete wall (~40 dB)	>10 Mbit/s: Not achievable even with narrow beam entering through the window as the IRR glass loss is comparable to that of the concrete wall (~40 dB)

5.3   Mobility

Since the Doppler shift is a linear function of the velocity and the operating frequency, frequency bands above 6 GHz will experience higher Doppler shift than do current cellular frequency bands under 6 GHz. For example, if the velocity of the mobile station is 120 km/h, the maximum Doppler shift at 30 GHz is 3.33 kHz, which is 10 times greater than at 3 GHz if other conditions are kept the same.

The channel link between the base station and the mobile station usually includes multi-path components which have different routes with different time delays, angles of departure and angles of arrival. From the perspective of the receiver, every path with a different route may result in a different Doppler shift because of potentially different angles of departure/arrival, relative to the direction of travel of the mobile station. Therefore, multipath environments introduce a spread of Doppler shifts at the mobile station; the magnitude of Doppler shift is proportional to frequency and will therefore be larger above 6 GHz, while the minimum Doppler shift remains as zero. Consequently, the enlarged Doppler spread in frequency bands above 6 GHz results in faster channel fluctuations in the time domain than that in current cellular frequency bands.

In mobile communication systems, channel fluctuations in the time domain necessitate a feedback mechanism for various information including channel quality to properly adapt system operation to the channel fluctuations so that system performance can be maximized. Since the latency of the feedback mechanism is a decisive factor to deal with the channel variation from mobility, it is important to minimize the latency. One limiting factor for the feedback latency is the symbol duration, which is directly determined by the bandwidth size. In frequency bands above 6 GHz, the available bandwidth could be much larger and the symbol duration could be shortened, making it possible to reduce the feedback loop latency.
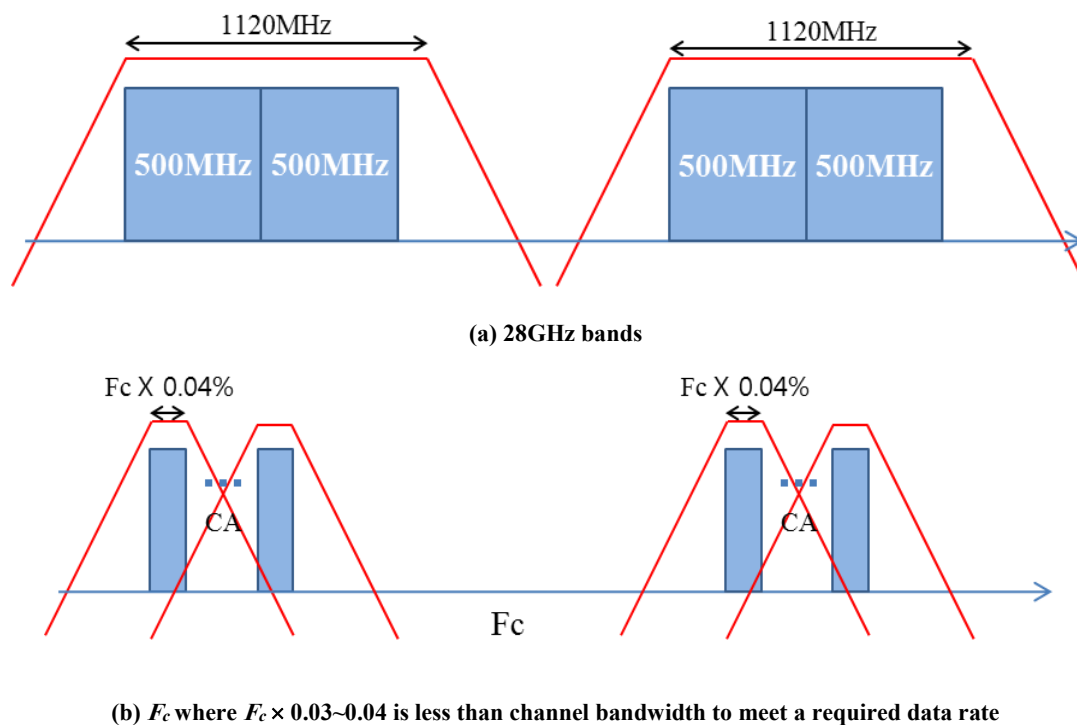
Another factor determining the amount of channel fluctuation is the number of multi-paths. If the number of multi-path components is reduced, then the channel fluctuation becomes smoother in the time domain. Therefore if the multi-path components impinging on the receiver are reduced by using narrow beamforming, channel fluctuation will be less than in the case of wide beamforming.

5.4   Impact of bandwidth

One benefit of adopting higher frequency for mobile communication is a capability to implement wide channel bandwidths with a bandpass filter. For FDD implementation, a duplex filter is needed. Tuneable and reconfigurable radio frequency (RF)/microwave duplex filters are important building blocks in modern wireless systems used for channel selection and noise reduction and they can represent a major bottleneck in performance. With the ever-increasing demand for use of spectrum above 6 GHz for mobile services, there is an urgent need for hardware that is tuneable and reconfigurable, so it can be used for multiple applications while facilitating efficient utilization of the available spectrum. This includes a large variety of novel planar/hybrid tuneable circuit realizations for spectrum management and dynamic broad-band filtering, as well as new low-loss micro-electromechanical systems (MEMS)-based reconfigurable duplex filters for wide tuning ranges and their realization through cutting-edge technologies. The current state-of-the-art allows for a maximum duplex filter size of around 3-4% of the centre frequency of the band [20] which means that it is very difficult to implement a wider channel bandwidth. For example, at a 12.5 GHz centre frequency, it is feasible to implement a duplex filter for a 500 MHz channel bandwidth. A duplex filter at 28 GHz can cover a 1 120 MHz channel bandwidth or two 500 MHz channels. If centre frequency (Fc) × 0.03~0.04 is less than the channel bandwidth necessary to meet a specific data rate, carrier aggregation is required to achieve that data rate as shown as Fig. 5.

FIGURE 5

The number of duplex filter to cover BW to meet required data rate

(a) 28GHz bands

(b) F_c where $F_c \times 0.03{\sim}0.04$ is less than channel bandwidth to meet a required data rate

6 Enabling technologies toward IMT in bands above 6 GHz

6.1 Antenna technology

Antennas naturally scale well with frequency and hence user devices and wireless access points can certainly exploit the smaller required footprint by implementing additional elements. If one were to consider a typical handset size of 120 mm × 60 mm, it would be feasible to fit upwards of 24 antenna elements across the shortest edge (60 mm) operating at 60 GHz. An 8 × 8 array would occupy a footprint of 20 mm × 20 mm.

The integration of higher bands with lower bands (such as 700 MHz, 1.9 GHz, 2.6 GHz) requires a much larger footprint. It is difficult to design antennas that can operate well at both 700 MHz and 60 GHz and as such, it is possible that the two bands would require separate antennas.

The shorter wavelengths of above 6 GHz frequency bands make it possible to put more antenna elements in the limited size of the form factor. The antenna technology with the enlarged number of antenna elements can be used to provide high beamforming gain so that the increased path loss of above 6 GHz frequency bands can be mitigated by beamforming techniques with correctly pointing direction.

Considering the enlarged number of antennas with wider bandwidth, however, having ADC/DAC per antenna element might be challenging because of the overall cost and power consumption. For the reason, communication systems in above 6 GHz frequency bands have utilized the phased array architecture in radio frequency or inter frequency instead of base band, which can reduce the number of ADC/DAC while keeping the high beamforming gain. ADC is a bottleneck for multi gigabit communication. The high signal bandwidth requires very fast A/D and D/A-converters. Recently the hybrid beamforming structure has been suggested which combines phased array beamforming with the digital precoder [21, 22].
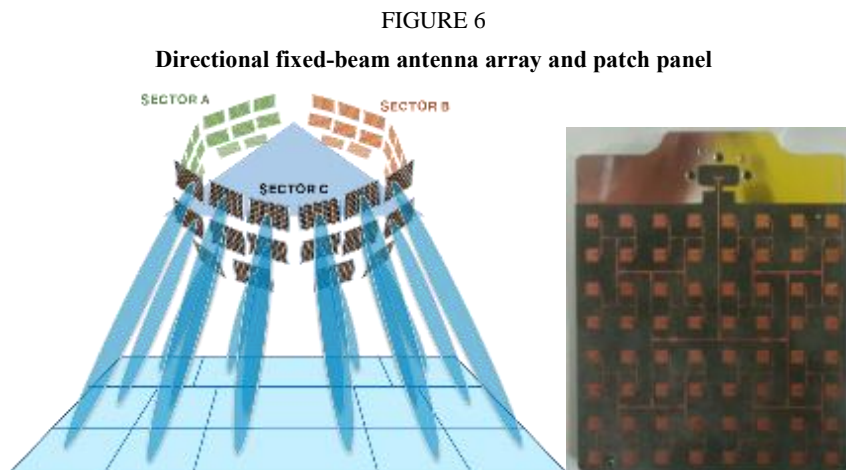
The phased array beamforming is used to enhance the received signal power by using beamforming gain, and the base band signal processing at the digital precoder is used to manage multiple streams for the further improvement.

Though greater antenna gains may be achieved with narrower beams, this may be of detriment to MIMO communications as some scattering environments call for broader beam antennas to maximize channel capacity, i.e. narrow beams are not always ideal. If the beams are too narrow, then beamforming may not be able to properly synthesize a broad, omni-like aggregate pattern.

6.1.1   Directional fixed-beam antenna array

Fixed-beam antenna array is a beamforming technology that the direction of multiple beams are pre-adjusted and fixed in order to provide overall good service coverage in whole cellular area. The fixed beamforming has advantage of simplicity because it doesn't require phase shifters. Phase shifter usually requires complex calibration process that precise adjustment often needs skilled experience.

Figure 6 below shows a schematic view of fixed beam antennas. In this configuration of antennas, an area of cell (or sectors) is covered by multiple fixed beams of which the exact number of beams and beam-width can be varied according to deployment plan. The figure shows an example of cell area covered by 48 fixed beams, in other words, 48 patch antenna panels. Each panel of patch antenna array consists of 8×8 or 8×12 patches of simple mmWAVE components. Note that using 28 GHz carrier frequency band, the size of one antenna patch becomes so tiny that the size of one panel can be made smaller than typical smart phone.

FIGURE 6

Directional fixed-beam antenna array and patch panel

6.1.2   Full adaptive antenna array

From the antenna perspective, traditional copper-based printed designs remain viable at 60 GHz. The issues at 60 GHz are mainly the complexity and performance of the Tx/Rx modules. Thus, a fully adaptive antenna array is feasible strictly from the antenna element design perspective both in cost and performance. Some alternatives such as reflect array and transmit array antennas and parasitic array antennas can be used to enhance the size and gain without additional transmission line loss.

An example of capacity improvement using full adaptive antenna array is presented below. The path loss is compensated through a combination of multiple elementary antenna components, allowing ranges in the order of several hundred meters in LoS conditions, resulting from coherent combining of signals transmitted and/or received on multiple elementary antennas.

It should be noted that the use of such large scale antenna systems (LSAS) for massive MIMO is studied for TDD operation.

Each elementary antenna can have only a modest gain, here assumed as 8 dBi, (though lower radiation efficiencies at higher frequencies may drop this gain by 1-2 dB in practice), due to the need to receive from a wide range of possible directions. This is also consistent with typical patch antennas used in current small cells. The rest of the gain has to be achieved through adaptive beamforming to accommodate random mobile locations and angular spread.

FIGURE 7

Data rate vs system bandwidth under outdoor LoS conditions

The above results are produced assuming a transmitter power of 1W, and a noise figure of 10 dB, at 60 GHz frequency in LoS conditions.

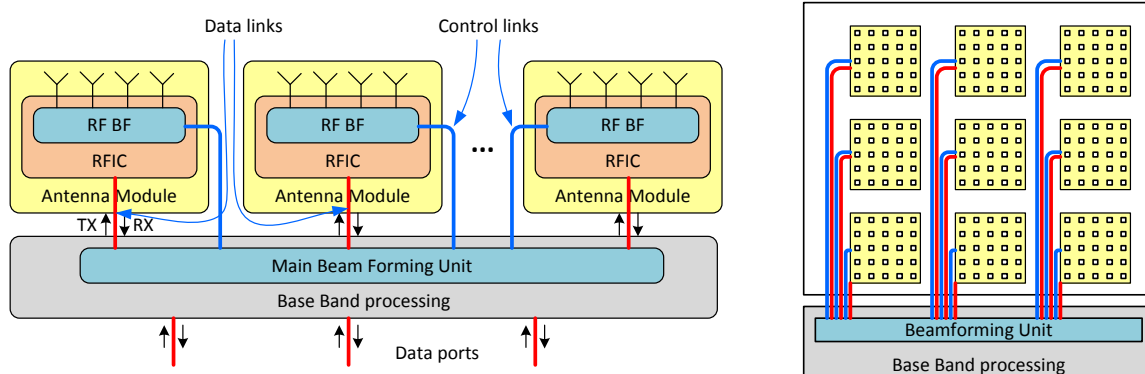### 6.1.3 Modular antenna array overview

There are many sources of propagation loss, as discussed earlier in section 4.1, at frequencies above 6 GHz for which antennas with high directivity may be used to compensate for such losses. Meanwhile, modern communication systems often require a station to be capable of covering relatively wide sector around it to communicate with other stations regardless of their locations. Traditional antenna architectures are generally not capable of combining wide angle coverage with high directivity. Reflective, parabolic dishes and lenses can create narrow beam thus delivering the needed 30-40 dB antenna gain, but they lack the flexibility to cover wide angle and are relatively bulky. Phased patch antenna arrays allow steering the beam to a desired direction. However, to achieve the necessary directivity, the array must consist of a large number of elements (several hundred to thousands).

Antenna array architectures currently used for mass production and intended for personal devices, comprise a single module containing an RFIC chip that includes controlled analogue phase shifters capable of providing several discrete phase shifting levels. The antenna elements are connected to the RFIC chip via feeding lines. Due to the loss on the feeding lines, this approach allows implementing antenna arrays with relative small dimensions of up to 8×8 thus achieving gains of about 15-20 dB.

One novel antenna array architecture for the millimetric wave band that provides simultaneous flexibility in form factor choice, beam steering, and high array gain in a conceivably more cost-efficient manner is to construct modular, composite antenna arrays. Each module is implemented

in a traditional way with dedicated RFIC chip serving several antenna elements and an RF beamforming unit. The architecture is shown in Fig. 8.

FIGURE 8

**High level block diagram of the proposed large antenna array and example of layout
for the case of planar sub-array modules**

The aperture of the modular antenna array and total transmitted power may exceed that of an individual sub-array module proportionally to the number of the sub-array modules used (e.g. ten times or more). Therefore, much narrower beams may be created and, therefore, much greater antenna gains may be achieved with the modular array as opposed to individual sub-arrays.

It is also possible that sectors of different sub-arrays may be configured in such a way as to vary the coverage angle of the composite array, thereby creating several coverage angles (e.g. to communicate with several peer stations simultaneously).

6.1.4 Multi-antenna transmission using modular phased antenna structures

The propagation properties of the frequencies above 6 GHz channel also contribute to creating several beams by greatly attenuating multi-path components of the signals, thus allowing the advantage of directed transmissions over line-of-sight ray or over the best reflected ray. However, there are several technical challenges that affect applicability of traditional multi-antenna transmission techniques in the frequencies above 6 GHz.

Traditional multi-antenna transmission implementations assume each antenna can make use of an independently coded spatial stream with its own transceiver chain. In practice, this may be too challenging for systems in frequencies above 6 GHz owing to the sheer number of elements involved for any degree of antenna gain.
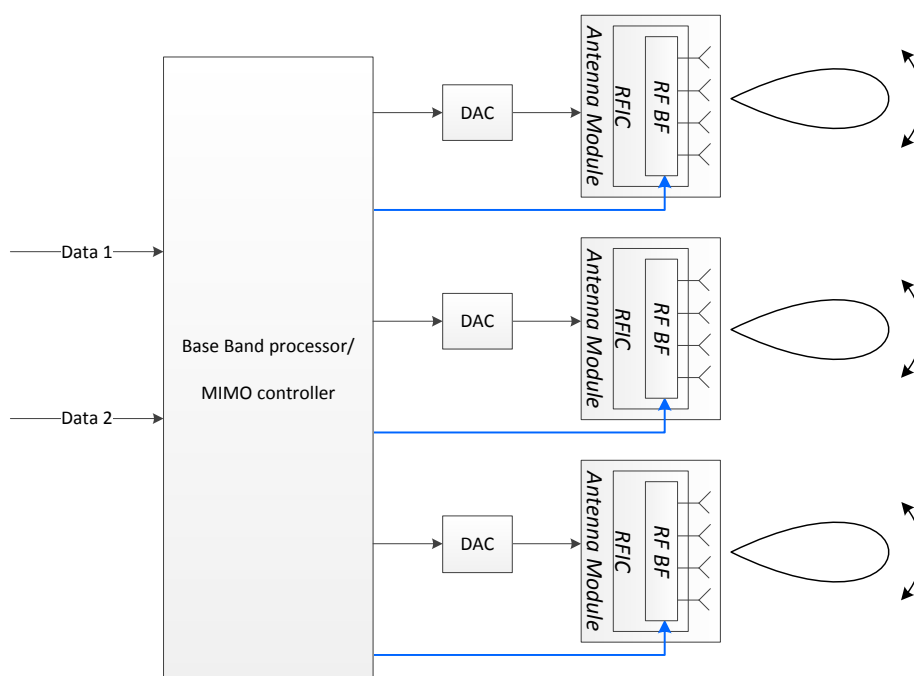
Even though it is true that coupling between antenna elements may become an issue at higher frequencies e.g. 60 GHz, it is easier to mitigate such effects at higher frequencies. Reducing spatial correlation between antenna elements will become easier as frequencies increase. Increasing element separation by 10% of a wavelength (to reduce coupling, for example) requires a small change of 0.5 mm at 60 GHz. The same requirement at 700 MHz would require more than 40 mm of additional separation, which is difficult on many mobile devices. As a result, antenna designers generally can obtain superior MIMO performance at higher frequencies than lower frequencies (e.g. 700 MHz, 2.6 GHz) because of the reduced space constraints on antenna footprint.

In the modular phased array architecture (see § 6.1.2), however, each phased array module has a dedicated transceiver with an RF beamforming unit and, therefore, may create a dedicated RF beam as shown in Fig. 9. The beamforming network (BFN) is implemented at the RF or at the baseband of the transceiver unit. Different architectures exist to implement the shaped beam array such as Analog Beamforming and digital beamforming.

Beams of individual sub-arrays may be steered in various directions to achieve a number of goals. For example, one may want to steer all sub-array beams in different directions and configure each one to communicate with a different user. This may create the equivalent of an omnidirectional antenna pattern which may be useful to train antenna system of a peer station. Alternatively, when steered to different directions, each sub-array may communicate with its own user, simultaneously with other sub-arrays which are also serving other users. This may substantially increase the throughput delivered to users by the small cell. In addition, the idea of adaptive sub-array can also improve the *C*/*I* beside its gain advantage and increasing coverage.

FIGURE 9

Multi-antenna transmission using modular phased arrays

Each antenna sub-array module may be also seen as a single antenna port in the context of a MIMO system. The beamforming gain is provided by the proper array phasing of each element within a module and each module within the entire antenna system. Sub-arraying could lead to grating lobes, which can impact performance when attempting to perform direction finding and/or perform null-steering.

Instead of throughput, one may want to combine the beams for extended distance. The appropriate phasing of sub-arrays with respect to each other may result in a very narrow beam to communicate over extended distances (e.g. to cover very remote users) and to reduce the interference in the entire deployment.

More compelling is the challenge of combining all of the above scenarios and to do so adaptively in a mobile environment. This would involve the real-time combining and recombining of modules and user groupings dependent on channel conditions, user data rate requirements, and dynamic locations. The understanding of the trade-offs and complexities of the algorithms involved is quite important.

Table 8 illustrates the theoretical downlink throughput performance for a single-user over several different distances. The results are calculated for the 60 GHz band. It is assumed that each module has 16 elements and that the user terminal has a quasi-omni (5 dBi) antenna gain. Both Single Carrier (SC) and OFDM modulations are considered.

TABLE 8

Theoretical downlink performance in a single-user case

Modular antenna array				Range for 385 Mbit/s (SC, π/2-BPSK, 1/4) (m)	Range for 3.465 Gbit/s (OFDM, π/2-16-QAM, 5/8) (m)	Range for 6.756 Gbit/s (OFDM, π/2-64QAM, 13/16) (m)
# of modules	TX power (dBm)	Tx array antenna (dBi)	e.i.r.p. (dBm)			
1	10	15	25	31 m	8 m	3 m
4	16	21	37	105 m	31 m	12 m
8	19	24	43	184 m	58 m	22 m
16	22	27	49	299 m	105 m	42 m

NOTE – In Table 8: SC: single carrier, OFDM: Orthogonal Frequency Division Multiplexing, π/2-BPSK and π/2-64-QAM are modulation schemes and ¼, ½, and 13/16 are code rates.

6.2 Semiconductor technology

Although most of current cellular frequency bands fall into the spectrum from 300 MHz to 3 GHz, there are commercial systems in frequencies above 6 GHz for a variety of systems like satellite systems, fixed wireless systems, radars etc. However, the semiconductor technology of above 6 GHz frequency bands for terrestrial mobile applications has mainly been developed toward academic or non-commercial purpose.

Recently, technologies above 6 GHz frequency bands have been developed in areas including circuits, antennas and communication protocols, in order to exploit the large chunks of bandwidths in those frequency bands as the 60 GHz MGWS (multi gigabit wireless systems) products are developed for the commercial market.

For example, the silicon-based CMOS (complementary metal oxide semiconductor) technologies are implementing integration system-in-package including mixers, LNAs, PAs, and IF amplifiers in above 6 GHz frequency bands. Cost effective implementations of CMOS nano-process under 100 nm have facilitated the utilization of 60 GHz spectrum bands.

Also GaAs MMIC technologies are mature enough to have a dominant presence for power amplifiers (PAs), low noise amplifiers (LNAs), switches for digital attenuators and phase shifters, voltage controlled oscillators (VCOs) and passive components from a few GHz to 100 GHz already.

GaN MMIC's will challenge GaAs technology mostly in high-bandwidth, highpower applications, because, due to the smaller required device periphery for a given specified output power, good impedance matching can be achieved for GaN FET's over a broader frequency range than for GaAs pHEMT's. Besides being used for high power RF applications, GaN HFET technology also has strong potential for implementation in a harsh environment. Also, GaN HFET devices are well suited to receiver applications, due to the robust nature and good low noise performance of these devices. Noise Figures (NF) of less than 0.7 dB at a frequency of 10 GHz have been reported for GaN HFETs.

One of key elements for the communication systems of above 6 GHz frequency bands is the use of RFIC because using RFIC provides highly integrated solutions with benefits of the reduction in size, power consumption and cost perspectives. Therefore the RFIC semiconductor process needs to provide sufficient fidelity as discussed in [23-25].

Semiconductor manufacturers have successfully shrunk the gate length of transistors into deep submicrometer levels below 50 nm, allowing transit frequencies of CMOS transistors to reach hundreds of gigahertz, much higher than the 60 GHz carrier frequency thereby allowing analogue microwave circuitry to be fabricated on the same circuit die and in the same semiconductor process as digital circuitry. Remarkably, today's ability to integrate millimetric wave analogue circuits in the
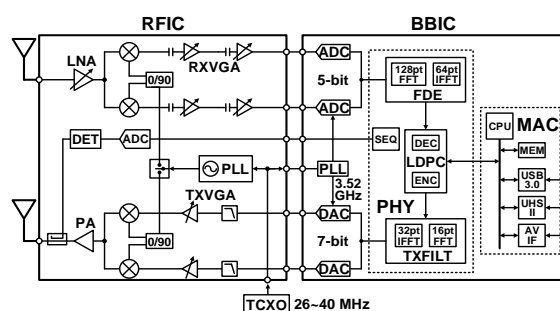
same process and die as high-speed digital circuitry is a by-product of Moore's Law, which has been predicting greater integration densities and computations per unit energy for digital circuitry rather than for analogue. Still, there remain challenges to using CMOS for millimetric wave analogue components, including increasingly lossy substrates with each new process generation due to higher substrate doping concentrations.

6.2.1 Device for low power consumption

Below, an example of a state-of-the-art low power millimetric wave CMOS transceiver based on WiGig specifications is discussed. Even though recent works have realized 60 GHz transceivers in a cost-effective CMOS process [44] [45] [46], achieving low power consumption as well as small form factor remains a difficult challenge. By employing sophisticated built-in self-calibrations, the developed chipset achieves MAC throughput of 1.8 Gbit/s while dissipating less than 1 W total power. Figure 10 shows the block diagram of the transceiver [47].

FIGURE 10

Block diagram of RFIC

The RFIC employs direct conversion architecture, supporting all four channels allocated at 60 GHz. Direct conversion is uniquely well-suited to monolithic integration due to the lack of image filtering, and its intrinsically simple architecture. However, the direct conversion receiver has not gained widespread acceptance in mobile Base Station transceivers to date, due to its intrinsic sensitivity to DC offset problems, even harmonics of the input signal and local oscillator leakage problems back to the antenna (which may be the most serious).

Offset arises from a) transistor mismatch in signal path b) LO signal leaking to the antenna c) near-channel interferer leaking into the LO part of the mixer, then self-down-converting to DC. The BBIC includes PHY and MAC layers as well as high speed interfaces. The chipset is developed for single-carrier (SC) modulation, which is suitable for reduced power consumption as compared to OFDM modulation. To overcome performance degradations due to in-band amplitude variations, which are primarily a result of gain variations of analogue circuits and multipath delay spread, the chipset employs built-in transmitter in-band calibration and a receiver Frequency Domain Equalizer (FDE) [47]. These techniques relax the requirement of the gain flatness and process variations for high speed analogue circuits, leading to less power consumption with minimum hardware overhead.

FIGURE 11

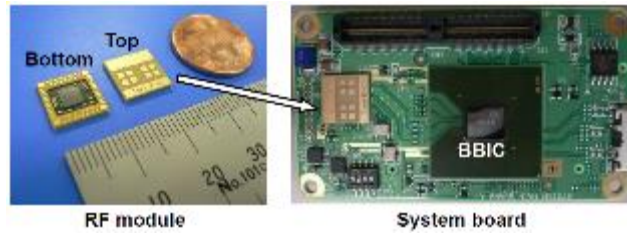**RF antenna module and system board**

Figure 11 shows the photograph of an RF module and a system board. The RF module employs a cavity structure with the RFIC mounted by flip chip technology. Each Tx/Rx antenna consists of four patch elements, providing 6.5 dBi gain with 50 degree beamwidth. The RFIC and the BBIC are fabricated in 90 nm CMOS and 40 nm CMOS respectively. In the transmit mode, the chipset consumes 347 mW in the RFIC and 441 mW in the BBIC with the output power of +8.5 dBm e.i.r.p.. In the receive mode, it consumes 274 mW in the RFIC and 710 mW in the BBIC with 7.1 dB noise figure.

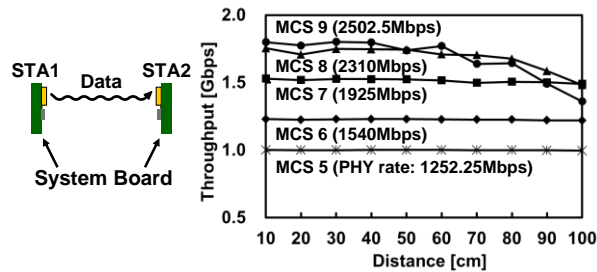FIGURE 12

Measured MAC throughput over the air

Figure 12 shows the measured MAC throughput from one station to the other using different modulation and coding schemes (MCS). The chipset achieves 1.8 Gbit/s up to 40 cm and 1.5 Gbit/s up to 1 m. For small cell access or backhaul/fronthaul usage, however, longer communication distance will be required. This is achieved by either increasing the output power or antenna gain. For instance, link margin can be increased by using N_{Tx} or N_{Rx} elements in a phased-array configuration, which can be installed in base stations where size and power constraints are less critical. Ignoring second order effects such as feeding loss from the RFIC to antenna elements, the link margin is increased by a factor of $10\log10\left(N_{Tx}^2 \cdot N_{Rx}\right)$ due to the phased-array gain and the transmitted power increase. As a numerical example, $N_{Tx} = 32$ and $N_{Rx} = 4$ gives 36.1 dB, which translate to 65 times improvement in the communication distance.

6.2.2 Device for high gain beamforming

Latest advances in the millimetric wave antenna and packaging technology [48] allow the creation of phased antenna arrays but with a limited number of elements, due to large losses in the feeding lines. Next evolution in millimetric wave technology is modular antenna arrays (MAA) [49] [50], comprised of large number of sub-array modules. Clearly, the traditional discrete front-end technology cannot be used for millimetric wave purposes because of weight, volume and cost. The only viable alternative is the use of microwave monolitically integrated circuits (MMICs). From simplicity point of view it is essential that the number of components on the PCB board is kept to a minimum as losses in RF chip intercomnection can easily become significant at higher frequencies. So, the level of integration should be as high as possible.

In the MAA, each module has built-in sub-array phase control and coarse beam steering capability. MAA's flexible and scalable architecture accomplishes a wide range of antenna gain and apertures challenging today's regulatory e.i.r.p. limits. For example, Fig. 13 left shows one module which may be used for constructing the MAA by any configuration or, as a single phased antenna array, for a UE.
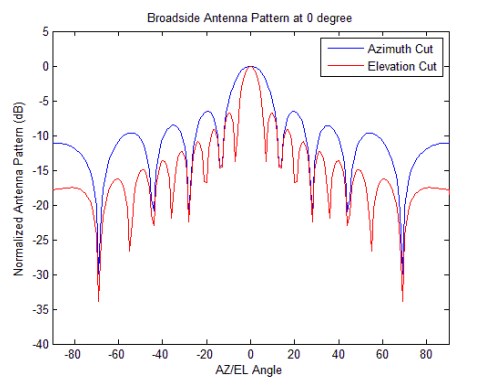
FIGURE 13

Single MAA element (left) and schematics of an 8-module MAA architecture

The 8-module MAA architecture (each sub-array module is an $8 \times 2 = 16$ elements, vertical $\times$ horizontal) and its 2D antenna pattern are shown in Fig. 13 right and Fig. 14, respectively.

FIGURE 14

2D antenna patterns for 8-module MAA

Capable of realizing massive MIMO in baseband with independently phase-controlled antenna elements (totally $8 \times 32 = 128$), such MAA can increase range up to 400 m for LoS backhaul/fronthaul, and up to 100 m for millimetric wave capable small cell access range.

First downlink access link budget (BS 8-module MAA with 19 dBm Tx power, 24 dBi antenna gain, single carrier, $\pi/2$-16 QAM modulation, ½ coding rate, and UE with Rx quasi-omni antenna with 5 dBi gain) estimates show a small cell edge throughput of about 3 Gbit/s for ISD (inter-site distance) of 100 m. First uplink access link budget (BS 32-module MAA with 30 dBi antenna gain and UE with 10 dBm Tx power, quasi-omni antenna with 5 dBi gain, single carrier, $\pi/2$-64 QAM modulation, ½ coding rate) estimates show a small cell edge throughput of about 3 Gbit/s for ISD of 100 m. First backhaul/fronthaul link budget (BS 8-module MAA with 19 dBm Tx power, 24 dBi antenna gain, single carrier, $\pi/2$-64 QAM modulation, ½ coding rate at both sides) estimates show a highest data rate of 6.5 Gbit/s at 150 m range.

7 Deployment scenarios and architectures

7.1 Use cases for IMT in bands above 6 GHz

IMT technologies adopted for bands above 6 GHz will be mainly used in dense urban environments to provide high data rate services. However, such transmissions can also provide wide area coverage

to mobile users by exploiting tracking capabilities and adaptive beamforming. Following use cases have been identified.

Dense hotspot in an indoor shopping mall

Deployment of small cells is an efficient solution to cope with the ever-increasing demand of high data rate applications. Environments such as shopping malls may be located outside the city centre i.e. in rural and suburban areas where the capacity of the macro cell based network might not be sufficient. Also, bringing optical fibre in these locations may be unaffordable and wireless backhaul/fronthaul solutions may be preferred to efficiently enable high data rate services in the mall.

Inside such buildings, small cell deployment avoids outdoor to indoor propagation losses and benefits of the favourable radio environment characteristics to offer an enhanced wireless service. Technologies based on bands above 6 GHz allow larger bandwidth at the cost of an increased number of cells.

Dense hotspot in an indoor enterprise environment

Proving ubiquitous coverage and high capacity in enterprise space is a big challenge for mobile service providers. Since enterprises buildings are characterized by different characteristics in terms of location, age, size, shape, number of rooms, etc. finding a unique solution to offer high data rate mobile services could be difficult for cost and scalability reasons. Technologies above 6 GHz can provide high data rate to users in their offices while other systems such as macro cell network using IMT in bands below 6 GHz may provide ubiquitous connectivity.

Dense hotspot in home and indoor environments

RLANs are a common way to access wireless applications/services at home. However, RLAN performance can suffer from interference. Moreover, current solutions do not provide seamless handover between cellular networks and RLANs. With use of indoor small cells in bands above 6 GHz inside each apartment small cells will benefit from the favourable radio environment characteristics that avoid interference between neighbouring apartments to offer an enhanced wireless service. Therefore, in locations where dense deployment of small cells in existing IMT bands is not a viable solution due to the insufficient capacity and/or strong inter-cell interference, small cells in bands above 6 GHz can be used as an alternative to provide high quality of experience in indoor environment.

Dense urban hotspot in a square/street

This use case focuses on a square or street located in the city centre where thousands of people may spend part of their daily life. The area is characterized by several possible indoor and outdoor hotspots like bus stops, restaurants, enterprises, and recreation parks. Due to the variety of uses in this environment and the high data rate requirements for multimedia broadband services, conventional solutions may not be sufficient.

For this dense area, the mobile operators may greatly benefit from upgrading their network through deployment of small cells in bands above 6 GHz, which will enhance the quality of experience of nearby users while providing sufficient capacity. Examples include cases such as users sitting in a cafe or waiting for their bus may launch real time video streaming applications, gaming, video calls, etc.

In big cities with tall sky-scrapers, networks and street canyons are truly 3-dimensional. There may be need for small cells to provide services at different altitudes.

Mobility in the city

A challenge for mobile operators is to provide high capacity inside public transportation. In this use case, a high number of users may require access to high data rate services in a relatively small indoor

location that is characterized by high mobility (around 50 km/h or more). For example, people using trams to move from home to work/the city centre may access internet to read emails, update the software of their devices, download movies and files, or play videogames.

IMT in bands above 6 GHz could be used to provide access and backhaul/fronthaul dedicated to public transportation capable of providing ubiquitous high data rates to users as they enter and leave public transportation. Backhaul/fronthaul nodes distributed on the railways or on street level can use IMT in bands above 6 GHz to transport data towards the trams and other public transportation along their routes. Devices installed on public transportation would provide connectivity to street level small cells infrastructure.

Deployment of access nodes in main streets is another possible usage to provide access to fast mobile users in cars and public transportations even if these vehicles are not equipped with small cells.
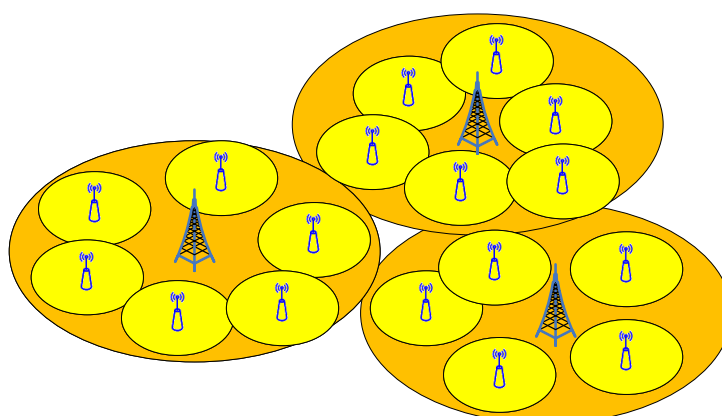
7.2 Deployment architecture

The deployment architecture are in general classified into standalone and overlay architectures, where the standalone architecture refers to the network deployment consisting of mere millimetric wave small cells and the overlay architecture refers to the network deployment of millimetric wave small cells rolled out on top of the existing macro networks.

By leveraging the existing macro cell deployment, millimetric wave small cells are rolled out on top of the existing network to form the overlay network architecture, as shown in Fig. 15. In this case, the existing macro-cell layer serves mainly for coverage purpose, whereas the millimetric wave small-cell layer serves for capacity boost. Thanks to the wide bandwidth and beam-forming capability as well as reduced access-link distances, the overlaid millimetric wave small cells are capable of bringing substantial system capacity boost. An essential merit of such overlay network architecture is facilitating separation of control signalling and data transmission, where all control signalling is transmitted by existing macro cells and millimetric wave small cells intend to provide high-rate data transmission only.

In addition, communication links that require critical reliability can also be established to macro cells. Overlay network architecture overcomes the mobility and signalling issues of the standalone architecture.

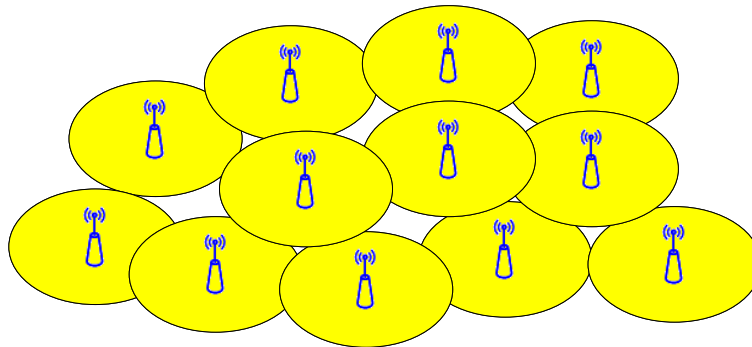The overlay architecture provides an example of how bands below and above 6 GHz could be coordinated on a complementary manner for the development of the future IMT for 2020 and beyond, with baseline coverage ensured by frequency bands utilized for macrocell operation, and additional elements to be developed at higher frequencies for improved capacity, where and when necessary.

FIGURE 15

Overlay network architecture

In the standalone architecture, as shown in Fig. 16, millimetric wave small cells are deployed seamlessly over the designated area for provisioning of full mobile services. By virtue of advanced antenna technology, compact antenna arrays with massive antenna elements provide high beam-forming gains, which is a key for overcoming excessively high path loss at millimetric wave frequencies, as well as reducing interference between users through narrow beam communications. Together with much wider bandwidth available, millimetric wave small cell deployment can provide area throughput on magnitude orders higher than the existing macro cell networks. However, due to much shorter inter-site distance between small-cells, mobility management and excessive signalling exchange become critical issues for mobile users.
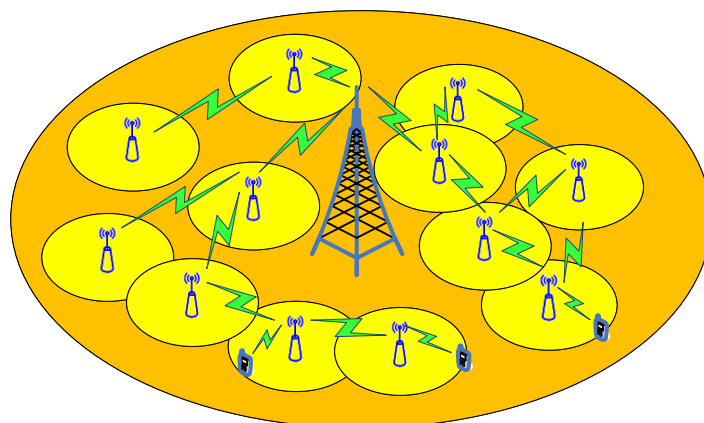
FIGURE 16

Standalone network architecture

Besides the access network architecture, backhauling is another critical challenge to fulfil the demands of future mobile traffic. In the context of dense deployment of millimetric wave small cells, average cell throughput on the magnitude of multi- Gbit/s and as small service area as tens of meters, conventional wired backhauling is not feasible in many cases due to excessive deployment costs for large number of small cells, or physically unavailability for wired-line deployment, and wireless backhauling deems to be the only alternative.

In terms of backhaul operational frequency, both in-band and out-band backhauling are optional, where backhaul links operate in the same spectrum as access links for the in-band backhauling and operate in a separate spectrum for the out-band backhauling. In-band backhauling for millimetric wave small cells facilitates single antenna usage for both access and backhauling purpose, with concerns over mutual interference and capacity trade-offs between access and backhaul links. Millimetric wave spectrum is in nature applicable for backhauling due to its directive propagation characteristics. Out-band backhauling, on the other hand, requires additional spectrum resources. Dense small-cell deployment also requires flexible and robust one- or multi-hop backhauling. For this purpose, mesh-alike backhaul networking, as shown in Fig. 17, is preferred to provide balanced backhaul links over multiple routes and robustness over single-point failure.
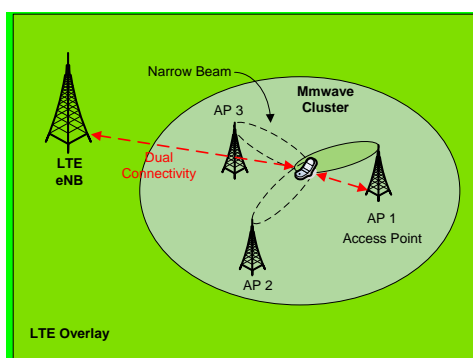
FIGURE 17

Wireless backhauling

Different combinations of the above networks can be implemented. A combined network of wireless backhauling and overlay network is a promising network which could well reduce network deployment while meeting a smooth evolution of current cellular network and future high frequency network. Another way is to combine standalone high frequency network and wireless backhauling.

7.3 Deployment scenarios

Various deployment scenarios are envisaged for IMT in bands above 6 GHz. For instance, cooperating radio nodes in bands above 6 GHz, denoted as a cluster, can be deployed to cope with propagation characteristics in bands above 6 GHz. Figure 18 shows an example of a cluster which is deployed with IMT systems in existing bands in overlay architecture. In this case, a user can be covered by multiple radio nodes within the cluster and also covered by IMT systems in existing bands.

FIGURE 18

An example of a cluster in IMT systems above 6 GHz

Recent field measurement campaigns with base stations clusters have been conducted in dense urban environment aiming to create statistical spatial channel modelling for future cellular networks operating at millimetric or sub-millimetric frequency ranges [66].

The studies described in this reference suggest that, even under NLoS conditions, statistical spatial channel models could be used to derive beam steering algorithms to optimize the angle of departure and angle of arrival of the link between the base station and the terminal. In addition the deployment of several base stations in a cluster results in terminals being connected to more than one base station. These studies show that, in some dense areas in New York City this type of deployment scenario provides on average 2.5 usable links per terminal, each of these links being optimized by beam steering algorithm.

One approach to increase capacity of existing networks is to combine different networks in different bands, as well to extend indoor systems to outdoor hot spot extensions utilizing bands above 6 GHz. See an example in Fig. 19 below.

FIGURE 19

An example of a combination of different networks

The main distinctive characteristic of a small cell is its range. For small cells developed using cellular technologies, the range is expected to be typically around 10 to 200 m under NLoS conditions, which is much shorter than the range of a cellular macrocell which might be several kilometres [51].

Small cells can be deployed indoor (e.g. femto cells) or outdoor. When deployed outdoor, small cells are typically deployed at a lower height than a macro cell (e.g. on street lamp posts) and with lower transmit power to serve a targeted area. Therefore, a number of small cells are needed especially in the dense urban area where more obstacles of signal propagation exist and where the mobile traffic keeps increasing.
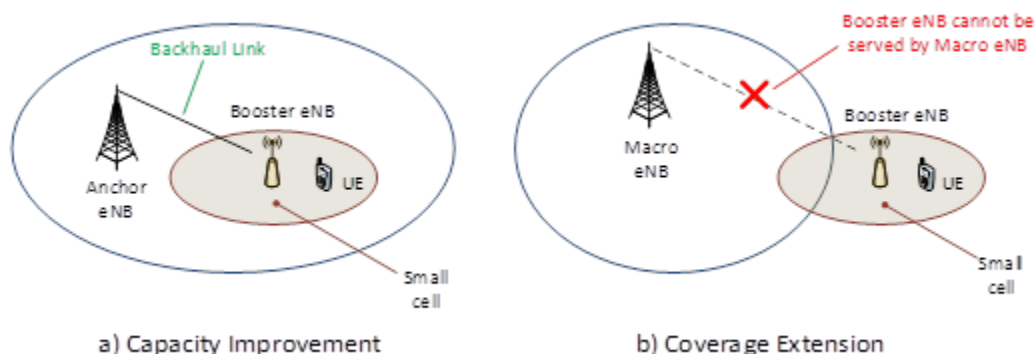
Small cells can be managed or unmanaged. Managed small cells are those that are deployed under the control of the cellular operator. Unmanaged small cells are those deployed by end users, such as Home base stations. Considering vast deployment of small cells with the low operating expenditure (OPEX) and low cost per bit, it is helpful to have the feature of self-organizing network (SON) capability.

Small cells are deployed with one of two primary targets (Fig. 20):

– Coverage extension/enhancement: by deployment of small cells at the edge of a macro cell to extend the coverage of the cellular communication system. Coverage of the small cell and coverage of the macro cell may partially overlap. This type of small cell is engineered to enhance user perceived experience with respect to service availability, and not primarily designed for targeted capacity. This type of small cell can be deployed both indoor and outdoor, and can be thought of as a range extension for macro cells where peripheral coverage areas at cell edge requires quality of service (QoS) and enhanced data throughput.

– Capacity improvement: by deployment of small cells within the coverage of a macro cell to improve data throughput of the cellular communication system. Usually, the coverage of the small cell and the coverage of the macro cell overlap to a large extent.

FIGURE 20

Capacity improvement (left) and coverage extension (right)

a) Capacity Improvement   b) Coverage Extension

An increase in cell density for the given area usually leads to an increase in inter-cell interference and difficulty of managing more frequent handover request. For these reasons, it is desirable to consider interference management techniques and also enhanced mobility management schemes to relieve the degradation of mobility performance.

For example, the dual connectivity allows a UE to connect to a macro cell and a small cell simultaneously so that the small cell is used for data transmission while the connection management is taken care of by the macro cell.

On the basis of types of deployments, three categories of small cells deployment scenarios can be identified [51]:

7.3.1 Hotspot

Hotspot is a type of small cell deployed to ease congestion from the macro cell, within the macro cell coverage. Therefore, this type of small cell provides targeted capacity in areas with high traffic density.

7.3.2 Indoor

Indoor small cells are often deployed to improve indoor public spaces with steady daily nomadic (non-mobile) traffic and occasional peaks within the enclosed structures such as hotels and office spaces, often isolated from the macro cell outdoor coverage. As such, indoor small cells provide coverage enhancement. Indoor scenarios could be further divided into a) large indoor area such as shopping malls, airports, stadiums, etc. and b) multi-room scenario such office buildings.

One typical deployment scenario is an airport terminal lounge, in which small cell base stations operating at high carrier frequency are installed on the wall or ceiling, or collocate with the air conditioner. Most of the links of indoor scenario are LoS channel, but some can be NLoS channel because of obstacles created by human body or furniture, such as, table, chair, cabinet, etc.

FIGURE 21

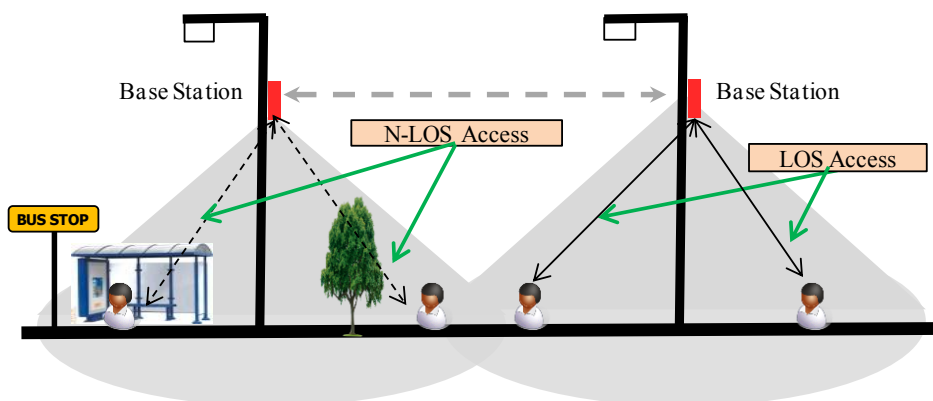**Example of Indoor small cell deployment**

7.3.3   Outdoor

Outdoor small cells are deployed to provide coverage and/or capacity in concert with macro cells coverage or in isolation of the macro cells such as in disaster recovery support and in rural areas. Although small cells are typically mounted on street facilities (i.e. deployed at a lower height than a macro cell), it is noteworthy that in some scenarios the beams of outdoor small cells may be directed at higher locations, such as window panes (e.g. in order to cater for indoor coverage with or without additionally deployed repeaters), or elevated train tracks, and like.

The typical outdoor deployment scenario is to collocate high frequency small cell base stations with the public facilities, such as, light poles along the street, bus stop, etc. Figure 22 shows an example of outdoor small cell deployment in an urban street.

FIGURE 22

Example of outdoor small cell deployment

Some cells can form a cluster to provide users with contiguous accesses of high throughput. E.g. tourist can share the interesting places with their friends by video phone calling as walking in a tour street. The high frequency point-to-point link between cells can be also exploited to improve throughput by taking advantage of cooperation between nodes. The users' access links can be LoS channels, or NLoS channels caused by foliage, cars, pedestrians, etc., while the links between base stations are usually LoS since the height of light pole is more than that of most obstacles.

Outdoor scenarios could be further divided into a) contiguous coverage, b) non-contiguous coverage, and c) backhaul and fronthaul.

In a distributed base station architecture, the base band unit (BBU) is physically separate from the radio remote unit (RRU). Multiple RRUs typically share one BBU to improve the processing efficiency of baseband data. Fronthaul refers to the link between BBU and RRU. The fronthaul may also include the link between RRHs in some deployment cases. In the existing network deployments the fronthaul is typically connected with a fibre optic cable introducing deployment complexity and decreasing the data transmission efficiency. Therefore, in the considered deployment scenarios, it is beneficial to connect the fronthaul link wirelessly using frequency bands above 6 GHz. Backhaul refers to two links, 1) the link between Macro/Pico BS and Core Network, 2) the link between Macro/Pico BSs. An overview of the overall network architecture is shown in Fig. 23. All the backhaul, fronthaul and access link can operate on bands above 6 GHz.

FIGURE 23

Description of distributed base station deployment

7.4   Flexible deployment of access and backhaul

The previous sub sections presented scenarios of how IMT systems in bands above 6 GHz could be used for the interface between the base station and the mobile users (the access) to enhance data services, being either for capacity in dense urban environment or for wide area coverage. However, another perspective is worth considering due to the uniqueness of the spectrum bands above 6 GHz. This is the flexible spectrum use, which could be defined as the flexibility of using the spectrum for either mobile applications or fixed applications. This has already been alluded to in § 7.3.3, where bands above 6 GHz can be used for fronthaul point-to-point links , as well as in § 7.1 on use cases, where use of wireless backhaul/fronthaul may be more cost effective than optical fiber to enable high data rate services in some locations (e.g. in a shopping mall). Having the possibility to use the same spectrum above 6 GHz for both access and fronthaul/backhaul links would be advantageous. An operator could manage the use of the spectrum based on the service and deployment needs, allowing for more rapid and cost-effective system deployment by using the same spectrum for both access and front/backhaul link, when technically feasible, rather than requiring two different frequency bands or a cable connection. As an example, enabling the bands currently used for fixed applications[6] to be also used for mobile would be advantageous.
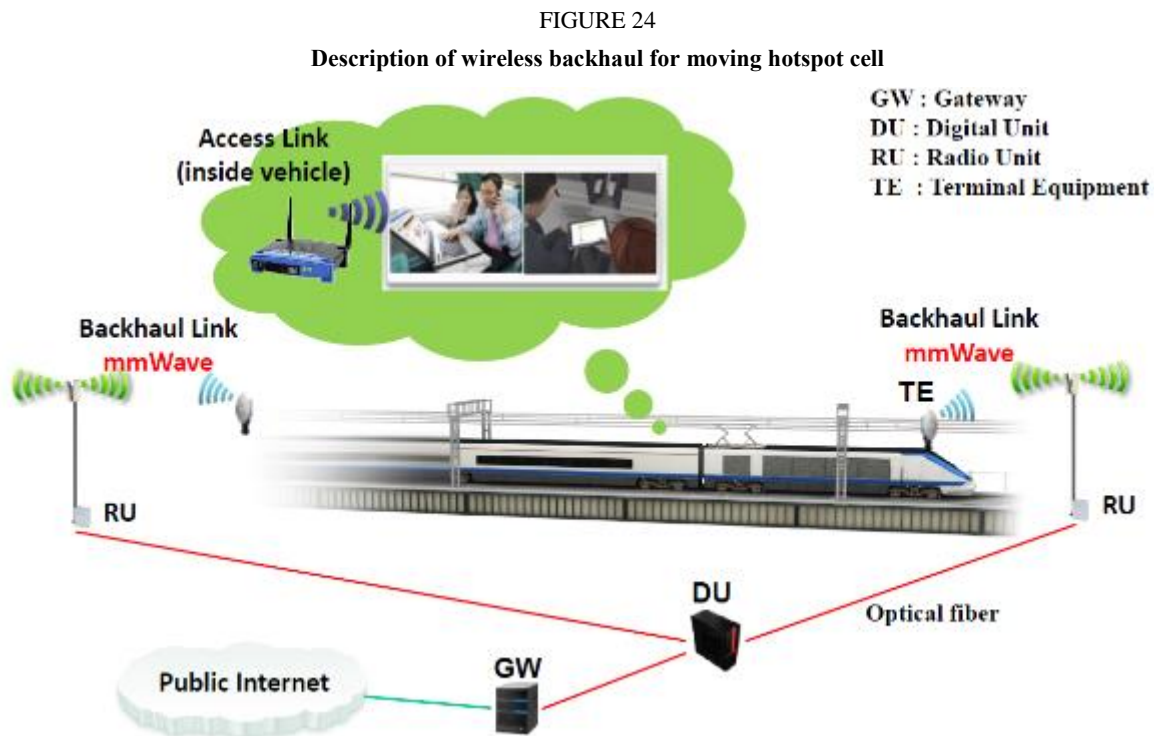
---

6   Recommendation ITU-R F.746.

7.4.1   Wireless backhaul for moving hotspot

One promising area that will be benefitted by high data-rate service using millimetric technology is public transportation, such as subway, bus or high speed train. Growing number of users uses mobile internet in public transportation every day. During rush-hour, thousands of passengers are carried in one subway train and each cabin becomes dense hotspot area. Cellular service (LTE/WCDMA) or Wi-Fi is typical means to access mobile internet inside the cabin, however the overall throughput is limited by capacity of external link per vehicle. Current feasible technology to provide wireless backhaul for moving vehicle is using IMT-200/IMT-Advanced access.

In whatever means, the capacity is far insufficient than user expectation. In future IMT, there will be solutions for delivering broadband access to passengers using millimetric technology. One feasible option is deploying one or several relay node(s) mounted on the vehicles.

The wide spectrum in above 6 GHz can be used for supporting moving hotspot cell users such as high speed train moving 500 km/hr. The access link inside the vehicle can use both existing sub 6 GHz radio transmission technologies (such as, Wi-Fi, LTE-A Femto) and above 6 GHz technologies (WiGig).

When the access link and backhaul link use above 6 GHz spectrum, they can employ in-band or out-of-band relaying. Figure 24 shows an example of wireless backhaul system for moving hotspot cell (train environment).

FIGURE 24

Description of wireless backhaul for moving hotspot cell

8   Conclusions

This Report investigates the technical feasibility of IMT in the frequencies between 6 and 100 GHz based on recently conducted and still ongoing studies carried out by a large number of sector members in different organizations globally. The Report also describes a number of channel measurement campaigns carried out by the industry and academia aiming at investigating the propagation channel characteristics in these bands under different propagation condition, e.g. LoS and NLoS. This work is needed to develop a representative set of channel models for different portions of the frequency ranges and for different propagation environments. Large-scale path loss models are useful in

estimating the coverage and link budget of the radio system, and other modelling is used when investigating phenomena like outdoor-to-indoor coverage, mobility and performance of different deployment scenarios utilizing a given bandwidth and the frequencies between 6 and 100 GHz.

This Report collects measurement data on some examples and reference points in ranges from 10 GHz to higher than 70 GHz in several different environments and refers to a number of other publications on the matter. Both LoS and NLoS as well as outdoor-to-indoor measurement cases have been studied in this Report. Further, several different deployment scenarios for systems operating in the frequencies between 6 and 100 GHz have been envisioned and some of these simulated for performance. Generally the results are as expected; the lower bands have better propagation characteristics for coverage and indoor penetration, whereas the higher bands are more suitable for outdoor hot-spot and indoor deployments with relatively poor outdoor-to-indoor coverage capabilities.. At the same time it has been noted that solutions based on MIMO and beamforming with large number of antennas compensating for the propagation loss are becoming increasingly feasible with higher frequencies due to the smaller antenna sizes and the ability to exploit chip-scale antenna solutions. Bands below and above 6 GHz could be used in a complementary manner for future IMT for the year 2020 and beyond.

The practical feasibility of building commercial transmitters and receivers for the frequencies between 6 and 100 GHz was also investigated as evidenced by availability of commercial 60 GHz multi-gigabit wireless systems (MGWS) products and prototyping activities that are already underway in other frequencies, such as 11, 15, 28, 44, 70 and 80 GHz. It is first noted that there are already products available for a large variety of bands between 6 GHz and 100 GHz, showing that there is nothing in these bands that inherently prevents their commercial mobile usage. The Report takes a more detailed look at state-of-the art solutions for building a cost and energy efficient large-scale adaptive antenna arrays not requiring ADC/DAC per antenna element and notes that modular phased antenna arrays are a promising technology enabling this. Recent advancements in semiconductor technology processes in manufacturing RFICs for the frequencies between 6 and 100 GHz allow for using several different processes such as CMOS and GaAS MMIC to be used to manufacture integrated and cost effective system-in-package modules consisting of mixers, LNAs, PAs and IF amplifiers. Further references to the work in this area have been covered as well.

Finally the Report notes that the allowing for flexible usage of the frequencies between 6 and 100 GHz in IMT systems could be beneficial to facilitate rapid roll out of high-capacity networks. There could be advantages to use the same spectrum for both access and fronthaul/backhaul as compared with using two different frequencies for access and fronthaul/backhaul, or fibre access.

During the development of this Report, ITU-R has been in contact with external organizations and research projects, such as METIS, MiWaveS and MiWEBA, researching and developing practical aspects, solutions and deployment considerations for the frequencies between 6 and 100 GHz .

The theoretical assessment, simulations, measurements, technology development and prototyping described in this Report indicate that utilizing the bands between 6 and 100 GHz is feasible for studied IMT deployment scenarios, and could be considered for the development of IMT for 2020 and beyond.

List of References

[1]   E. Ben-Dor, et. al., "Millimeter-wave 60 GHz Outdoor and Vehicle AOA Propagation Measurements using a Broadband Channel Sounder," *in Proc. Globecomm 2011*, December 2011.

[2]   R. Daniels and R. Heath, Jr., "60 GHz Wireless Communications: Emerging Requirements and Design Recommendations," *IEEE Vehicular Technology Magazine*, Vol. 2., Issue 3, 2007.

[3]   T. S. Rappaport, J. N. Murdock, and F. Gutierrez, "State of the Art in 60-GHz Integrated Circuits and Systems for Wireless Communications," *Proceedings of the IEEE*, vol. 99, no. 8, pp. 1390−1436, August 2011.

[4]   Rappaport, T.S., Sun, S., Mayzus, R., Zhao, H., Azar, Y., Wang, K., Wong, G.N., Schulz, J.K., Samimi, M., and Gutierrez, F., "Millimeter Wave Mobile Communications for 5G Cellular: It Will Work!" *IEEE Access Journal*, Vol 1, No. 1, May 2013.

[5]   Y. Azar, G.N. Wong, K. Wang, R. Mayzus, J.K. Schulz, H. Zhao, F. Gutierrez, D. Hwang, and T. S. Rappaport, "28 GHz Propagation Measurements for Outdoor Cellular Communications Using Steerable Beam Antennas in New York City," *2013 IEEE International Conference on Communications (2013 ICC)*, June 9–13 2013.

[6]   P. Mogensen et al., "*Beyond 4G local area: high level requirements and system design,*" in the Proc. Globecom 2012, International workshop on emerging techniques for LTE-Advanced and Beyond 4G.

[7]   H. Holma and A. Toskala, "LTE for UMTS: OFDMA and SC-FDMA Based Radio Access". Wiley, 2009.

[8]   G. W. O. Da Costa, "Dynamic Spectrum Sharing among Femtocells: Coping with Spectrum hScarcity in 4G and Beyond", PhD dissertation, Aalborg University, 2012.

[9]   G. Berardinelli, F. M. L. Tavares, N. H. Mahmood, O. Tonelli, A.F. Cattoni, T.B. Sørensen and P. Mogensen, "*Distributed Synchronization for Beyond 4G Indoor Femtocells*", Proceedings of 20th International Conference on Telecommunications, May 2013.

[10]   F. M. L. Tavares, G. Berardinelli, N. H. Mahmood, T. B. Sørensen and P. Mogensen, "*On the potential of Interference Rejection Combining in Beyond 4G networks*", in Proc. IEEE VTC2013-Fall, September 2013.

[11]   F. M. L. Tavares, G. Berardinelli, N. H. Mahmood, T. B. Sørensen, and P. Mogensen, "*On the impact of receiver imperfections on the MMSE-IRC receiver performance in 5G networks*", accepted in IEEE VTC2014-Spring, May 2014.

[12]   M. Cudak, A. Ghosh, T. Kovarik, R. Ratasuk, T. Thomas, F. Vook and P. Moorut, "Moving Towards mmWave-Based Beyond-4G (B-4G) Technology," in *Proc. IEEE VTC-Spring 2013*, June 2-5, 2013.

[13]   H. Bruce Wallace, "Millimetre-wave propagation through snow," Proc. SPIE 0414, Optical Engineering for Cold Environments, Sep. 1983.

[14]   F. Nadeem, E. Leitgeb, M.S. Awan and G. Kandus "Comparing the snow effects on hybrid network using optical Wireless and GHz links," IEEE IWSSC (Satellite and Space Communications), Sept. 2009.

[15]   "Attenuation due to clouds and fog," Recommendation ITU-R P.840-5, Feb. 2012.

[16]   "Atmospheric Effects on Terrestrial Millimeter-Wave Communications," A Report prepared for DARPA, Mar. 1974.

[17]   S. Hur, et al., "Millimeter-wave Channel Modeling based on Measurements in In-building and Campus Environments at 28 GHz", will be presented on COST IC1004 10th Meeting, May 2014.

[18]   Y. Chang, et al., "A Novel Two-Slope mmWave Channel Model Using 3D Ray-Tracing Technique in Urban Environments", submitted to IEEE PIMRC 2014.

[19]   M. K. Samimi, et al., "Ultra-Wideband Statistical Channel Model for Non Line of Sight Millimeter-Wave Urban Channels," submitted to IEEE Globecom 2014.

[20]   APT Report 24, "Implementation issues associated with use of the band 698-806 MHz by mobile services", Sep. 2011.

[21]   T. Kim, et al., "Tens of Gbps Support with mmWave Beamforming Systems for Next Generation Communications," IEEE Globecom, 2013.

[22]   O. E. Ayach, et al., "Spatially Sparse Precoding in Millimeter Wave MIMO Systems," IEEE Trans. on Wireless Communications, Vol. 13, No. 3, March 2014.

[23]   A. Valdes-Garcia, et al., "A SiGe BiCMOS 16-Element Phased-Array Transmitter for 60 GHz Communications", 2010 IEEE International Solid-State Circuits Conference, Feb. 2010.

[24]   S. Emami, et al., "A 60GHz CMOS Phased-Array Transceiver Pair for Multi-Gb/s Wireless Communications", 2011 IEEE International Solid-State Circuits Conference, Feb. 2011.

[25]   S. Alexandre, et al., "A 65nm CMOS Fully Integrated Transceiver Module for 60 GHz Wireless HD Applications", 2011 IEEE International Solid-State Circuits Conference, Feb. 2011.

[26]   Z. Pi and F. Khan, "An introduction to mm-wave mobile broadband systems," IEEE Communications magazine, June, 2011.

[27]   T. S. Rappaport, "The massively broadband future," Spectrum 20/20 conference, June 2012 (http://www.spectrum2020.ca/presentations/Rappaport.pdf).

[28]   Naval Air Systems Command, Avionics Department AIR-4.5, Electronic Warfare and Radar Systems Engineering Handbook, Apr 1999.

[29]   Theodore S. Rappaport, Eshar Ben-Dor, James N. Murdock and Yijun Qiao, "38 GHz and 60 GHz Angle-dependent Propagation for Cellular & Peer-to-Peer Wireless Communications," IEEE International Conference on Communications, Ottawa, Canada, June 2012.

[30]   LightPointe White Paper Series, Millimeter-Wave Radio Transmission: Atmospheric Propagation, Link Budget and System Availability, 2010.

[31]   Michael Marcus and Bruno Pattan, "Propagation: Spectrum Management Implications," IEEE Microwave Magazine, June 2005.

[32]   Hong Zhang, Sriram Venkateswaran, Upamanyu Madhow, "Channel Modeling and MIMO Capacity for Outdoor Millimeter Wave Links," IEEE WCNC, 2010.

[33]   A. Matlsev et. al., "Impact of polarization characteristics on 60 GHz indoor radio communication systems," IEEE Antennas and Wireless Propagation Letters, vol. 9, pp 413 – 416, 2010.

[34]   A. Maltsev, R. Maslenninkov, A. Khoryaev and A. Lomayev, "Experimental investigations of 60 GHz wireless systems in office environment," IEEE Journal on Selected Areas in Communications, vol 9, no. 8, pp 1488-1499, 2009.

[35]   A. Maltsev et al., "Experimental investigation of polarization impact on 60 GHz WLAN systems," IEEE doc. 802.11-09/0552r0, 2009.

[36]   A. Maltsev, R. Maslennikov, A. Lomayev, A. Sevastyanov and A. Khoryaev, "Statistical Channel Model for 60 GHz WLAN Systems in Conference Room Environment," Radioengineering, vol. 20, no. 2, pp 409-422, June 2011.

[37]   A. Maltsev et. al., "Channel Models for 60 GHz WLAN Systems," IEEE doc. 09/0334r8, 2010.

[38]   A.M. Hammoudeh, M.G. Sanchez and E. Grindrod, "Experimental Analysis of Propagation at 62 GHz in Suburban Mobile Radio Microcells," 1999.

[39]   M. Rasekhi, F. Farzaneh and A. Shishegar, "A street canyon approximation model for the 60 GHz propagation channel in an urban environment with rough surfaces," 2010.

[40]   B. Langen, G. Lober and W. Herzig, "Reflection and transmission behavior of building materials at 60 GHz," in PIMRC, 1994.

[41]   C. Briso-Rodriguez, M. Vazquez-Castro and J. Alonso-Montes, "28 GHz LMDS channel measurements and modeling for parameterized urban environments," 2001.

[42]   S. Seidel and H. Arnold, "Propagation measurements at 28 GHz to investigate the performance of local multipoint distribution service (LMDS)," 1995.

[43]   E. Torkildson, U. Madhow and M. Rodwell, "Indoor millimeter wave MIMO: Feasibility and Performance," IEEE Trans. Wireless Communications, vol. 10, no. 12, pp. 4150-4160, Dec. 2011.

[44]   S. Emami, R. F. Wiser, E. Ali, M. G. Forbes, M. Q. Gordon, X. Guan, S. Lo, P. T. McElwee, J. Parker, J. R. Tani, J. M. Gilbert and C. H. Doan, "A 60 GHz CMOS phased-array transceiver pair for multi-Gb/s wireless communications," IEEE ISSCC Dig. Tech. Papers, Feb. 2011.

[45]   A. Siligaris, O. Richard, B. Martineau, C. Mounet, F. Chaix, R. Ferragut, C. Dehos, J. Lanteri, L. Dussopt, S. D. Yamamoto, R. Pilard, P. Busson, A. Cathelin, D. Belot and P. Vincent, "A 65 nm CMOS fully integrated transceiver module for 60 GHz wireless HD applications," IEEE ISSCC Dig. Tech. Papers, Feb. 2011.

[46]   K. Okada, K. Kondou, M. Miyahara, M. Shinagawa, H. Asada, R. Minami, T. Yamaguchi, A. Musa, Y. Tsukui, Y. Asakura, S. Tamonoki, H. Yamagishi, Y. Hino, T. Sato, H. Sakaguchi, N. Shimasaki, T. Ito, Y. Takeuchi, N. Li, Q. Bu, R. Murakami, K. Bunsen, K. Matsushita, M. Noda and A. Matsuzawa, "A full 4-channel 6.3 Gb/s 60 GHz direct-conversion transceiver with low power analog and digital baseband circuitry," IEEE ISSCC Dig. Tech. Papers, Feb. 2012.

[47]   T. Tsukizawa, N. Shirakata, T. Morita, K. Tanaka, J. Sato, Y. Morishita, M. Kanemaru, R. Kitamura, T. Shima, T. Nakatani, K. Miyanaga, T. Urushihara, H. Yoshikawa, T. Sakamoto, H. Motozuka, Y. Shiraka, N. Yosoku, A. Yamamoto, R. Shiozaki and N. Saito, "A fully integrated 60 GHz CMOS transceiver chipset based on WiGig/IEEE802.11ad with built-in self calibration for mobile applications," IEEE ISSCC Dig. Tech. Papers, Feb. 2013.

[48]   Advanced Millimeter-wave Technologies: Antennas, Packaging and Circuits, Wiley, 2009.

[49]   A. Sadri, "Evolution of mmWave Technology from WiGig to Cellular and Backhaul Systems," IEEE The Brooklyn 5G Summit, Apr. 2014.

[50]   A. Maltsev, A. Sadri, A. Pudeyev, R. Nicholls, R. Arefi, A. Davydov, I. Bolotin, G. Morozov, K. Sakaguchi and T. Haustein, "MmWave Smallcells is a Key Technology for Future 5G Wireless Communication Systems," European Conference on Networks and Communications (EuCNC'2014), Bologna, Italy, Jun. 2014

[51]   "Backhaul Technologies for Small Cells Use cases, requirements and recommendations," Small cell forum, draft white paper, Oct. 2012.

[52]   Report ITU-R M.2135-1 (12/2009): Guidelines for evaluation of radio interface technologies for IMT-Advanced.

[53]   3GPP TR 36.814 v9.0.0 (2010-03): E volved Universal Terrestrial Radio Access (E-UTRA); Further advancements for E-UTRA physical layer aspects (Release 9).

[54]   Mathew Samini, Kevin Wang, Yaniv Azar, George N. Wong, Rimma Mayzus, Hang Zhao, Jocelyn K. Schulz, Shu Sun, Felix Guttierez, Jr., and Theodore S. Rappaport, "28 GHz Angle of Arrival and Angle of Departure Analysis for Outdoor Cellular Communications using Steerable Beam Antennas in New York City", IEEE Vehicular Technology Conference (VTC), June 2-5, 2013.

[55]   T. S. Rappaport, et al., "Millimeter wave mobile communications for 5G cellular: It will work!," *IEEE Access*, vol. 1, pp. 335-349, 2013.

[56]   W. Roh, et al., "Millimeter-wave beamforming as an enabling technology for 5G cellular communications: Theoretical Feasibility and Prototype Results," *IEEE Communications Magazine*, pp. 106-113, February 2014.

[57]   M. R. Akdeniz, et al., "Millimeter Wave Channel Modeling and Cellular Capacity Evaluation," *IEEE Journal on Selected Areas in Communications*, Special Issue on 5G, July, 2014.

[58]   T. A. Thomas, et al., "3D mmWave Channel Model Proposal," *in Proc. IEEE VTC-Fall/2014*, Vancouver, Canada, September 14-17, 2014.

[59]   A. Maltsev, et al., "WP5: Propagation, Antennas and Multi-Antenna Techniques," MiWEBA EU Contract No. FP7-ICT-608637, 2014.

[60]   T.S. Rappaport, F. Gutierrez Jr., E. Ben-Dor, J.N. Murdock, Y. Qiao, and J.I. Tamir, "Broadband Millimeter-Wave Propagation Measurements and Models using Adaptive-Beam Antennas for Outdoor Urban Cellular Communications," *IEEE Transactions on Antennas and Propagation*, vol. 61, no. 4, pp. 1850 - 1859, April 2013.

[61]   N. Zhang, et al, "Measurement-based Angular Characterization for 72 GHz Propagation Channels in Indoor Environments". Accepted by Globecom 2014, WS MCHFB, Dec. 2014.

[62]   Larsson, C., Harrysson, F., Olsson, B.-E., and Berg, J.-E., "An Outdoor-to-Indoor Propagation Scenario at 28 GHz". The 8th European Conference on Antennas and Propagation (EuCAP 2014), pp. 3301-3304, April 2014

[63]   A. Maltsev, et al., "WP5: Propagation, Antennas and Multi-Antenna Techniques," MiWEBA EU Contract No. FP7-ICT-608637, 2014.

[64]   [Reference 1] A. Ghosh, et al., "Millimeter wave enhanced local area systems: A high data rate approach for future wireless networks," IEEE Journal on Selected Areas in Communications, vol. 32, no. 6, pp. 1152-1163, June, 2014.

[65]   T. A. Thomas, et al., "3D mmWave Channel Model Proposal," in Proc. IEEE VTC-Fall/2014, Vancouver, Canada, September 14-17, 2014.

[66]   28 GHz Angle of Arrival and Angle of Departure Analysis for Outdoor Cellular Communications using Steerable Beam Antennas in New York City, by Mathew Samini, Kevin Wang, Yaniv Azar, George N. Wong, Rimma Mayzus, Hang Zhao, Jocelyn K. Schulz, Shu Sun, Felix Guttierez, Jr., and Theodore S. Rappaport, 2013 IEEE Vehicular Technology.

Acronyms and Abbreviations

3GPP	Third Generation Partnership Project
ADC/DAC	Analogue-to-digital converter/digital-to-analogue converter
AMC	Adaptive modulation/coding
AP	Access point
AOA	Angle of arrival
AOD	Angle of departure
ART	Above roof top
BBIC	Base band integrated circuit
BBU	Base band unit
BF	Beam-forming
BLER	Block error rate
BS	Base station
CEPD	Canal enregistré de propagation
CIR	Channel impulse response
CMOS	Complementary metal oxide semiconductor
CTF	Channel transfer function
D-rays	Quasi-deterministic rays
D2D	Device to device
DL	Downlink
e.i.r.p.	Effective isotropic radiated power
F-ray	Flashing rays
FDD	Frequency division duplex
FPGA	Field-programmable gate array
FSPL	Free space path loss
GaAs MMIC	Gallium arsenide monolithic microwave integrated circuit
H-H	Horizontal-to-horizontal
HARQ	Hybrid automatic repeat request
HetNet	Heterogeneous network
IF	Inter-frequency
IMT	International mobile telecommunications
IRR	Infrared reflective glass
ISD	Inter-site distance
LDPC	Low density parity check
LMDS	Local multipoint distribution system
LNA	Low noise amplifier

LOS	Line-of-sight
LSAS	Large scale antenna systems
LTE	Long term evolution
MAA	Modular antenna array
MAC	Medium access control
MCS	Modulation and coding scheme
MED	Maximum excess delay
METIS	Mobile and wireless communications enablers for twenty-twenty (2020) information society
MGWS	Multi-gigabit wireless systems
MIMO	Multiple input multiple output
MiWEBA	Millimetre-wave evolution for backhaul and access
MMW	Millimetric wave (30-300 GHz)
MS	Mobile station
NLoS	Non-line-of-sight
OFDM	Orthogonal frequency division multiplexing
PA	Power amplifier
PAPR	Peak-to-average power ratio
PDP	Power delay profile
PLE	Path loss exponent
Q-D	Quasi-deterministic
QAM	Quadrature amplitude modulation
QPSK	Quaternary phase shift keying
PHY	Physical layer
R-rays	Random rays
RF	Radio frequency
RLAN	Radio local area network
RMS	Root mean squared
RFIC	Radio frequency integrated circuit
RRU	Remote radio unit
RSRP	Reference signal received power
RX	Receive or receiver
SC	Single carrier
SCM	Spatial channel model
SINR	Signal-to-interference-plus-noise ratio
SNR	Signal-to-noise ratio

TDD	Time division duplex
TX	Transmit or transmitter
UE	User equipment
VCO	Voltage controlled oscillator
VOIP	Voice over internet protocol
WiGig	Wireless gigabit alliance
XPR	Cross-polarization ratio

Annex 1

Semiconductor technology status

A1.1   Introduction

Driven by unprecedented growth in the demand for mobile data, and with no signs of a slowdown, industry and academia alike are looking for solutions that go beyond what can be offered by finding spectrum fragments of 10 MHz here and there. In particular, there is interest in finding large contiguous chunks of spectrum providing wide bandwidths that can be used for addressing the traffic explosion problem in a more fundamental way.

This in turn has spurred interest in investigating the suitability of utilizing a very wide continuous bandwidth in millimetric wave bands for mobile broadband access [1-4].

Advances in semiconductor technology have made millimetric wavewireless systems feasible [5-9].Commercial products in millimetric wave bands are now readily available. Notable examples are products in the 60 GHz Band (for personal area networks (PAN) are available soon under the labels of WiGig [10][11]), products in the 28 and 38 GHz bands (for wireless backhaul) as well as products in the 71-76 and 81-86 GHz bands.

This annex provides semiconductor technology status for millimetric wavebands with an aim to show the feasibility of using the lower millimetric wave bands for IMT system.

A1.2   Semiconductor technology

Millimetric wave technologies have been developed in all areas including circuits, antennas and communication protocols, in order to exploit the large chunks of bandwidths in millimetric wave bands.
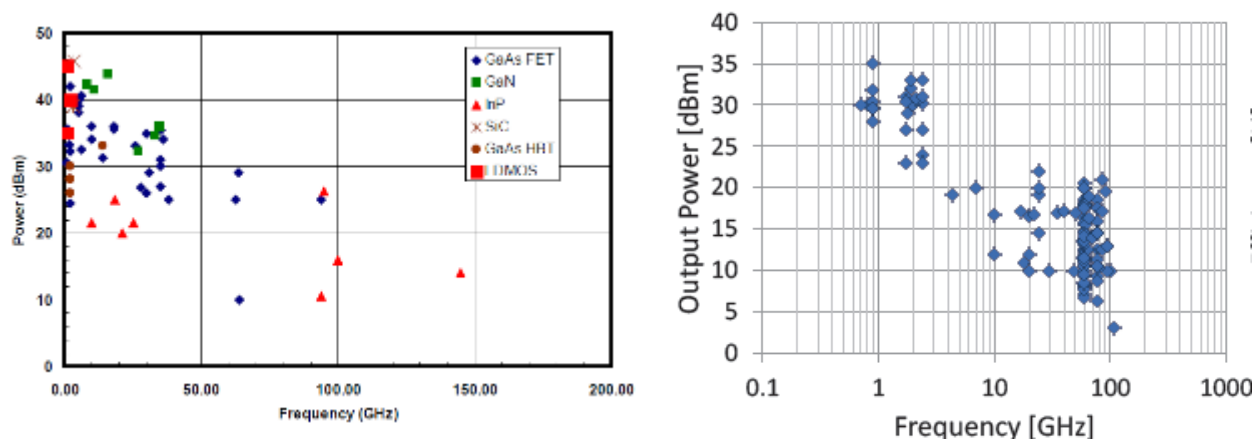
Gallium Arsenide (GaAs)Monolithic Microwave Integrated Circuit(MMIC) technologies are mature enough to have a dominant presence for power amplifiers (PAs), low noise amplifiers (LNAs), switches for digital attenuators and phase shifters, voltage controlled oscillators(VCOs) and passive components from a few GHz to 100 GHz already.

At the same time, recent technologies of Silicon-based CMOS (Complementary Metal Oxide Semiconductor) processes are capable of implementing integration systems-in-package including mixers, LNAs, PAs, and inter-frequency (IF) amplifiers in millimetric wave bands, especially for 60 GHz commercialized products (with the label of WiGig). Cost effective implementations of CMOS nano-process under 100 nm have facilitated the utilization of 60 GHz spectrum bands.

Figure A1.2-1 shows the survey of output power for both MMIC-based PA and Silicon-based PA. PA output power level for the frequency range of 10 GHz to 100 GHz is relatively small compared to those for up to 10 GHz. However, e.i.r.p. can be boosted up with a beamforming technique that provides a high antenna gain by utilizing a large number of antenna elements.

FIGURE A1.2-1

Left: Power MMIC Survey [9], Right: Silicon Power Amplifier Survey

A key element of the future system solution relies upon the use of RFIC for bands above 6 GHz providing the core radio technology for the system. RFICs provide highly integrated solutions with benefits of reduced size, power consumption and cost. The RFIC semiconductor process needs to provide sufficient fidelity when operating in 60 GHz spectrum bands as discussed in [11], [12], [13].

The size of the array has a significant impact on the transmitter e.i.r.p. as well as receiver sensitivity and thus directly impacts the system link budget. Likewise, the size of the array, particularly the transmitter array, has a significant impact on the RFIC power consumption as well as cost. Device side applications will often be constrained for minimum power consumption, size and cost and will need small sized arrays while base station applications will need to utilize larger sized arrays to establish sufficient link gain. Scalable and adaptable solutions are likely to be needed, particularly during the early stages of this future system deployment.

References

[1]   Assessment of the global mobile broadband deployments and forecasts for International Mobile Telecommunications. Report ITU-R M.2243.

[2]   Pi Z; Khan, F., "An Introduction to Millimeter-wave Mobile Broadband Systems," Communications Magazine, IEEE.2011, Jun.

[3]   Amitabha Ghosh, et al, "Towards Millimeter Wave Beyond-4G Technology," IWPC, 2012 Dec.

[4]   Suyama, S., Fukuda, H., Suzuki, H., Fukawa, K., "11 GHz Band 4x4 MIMO-OFDM Broadband Experimental System for 5 Gbps Super High Bit-Rate Mobile Communications," IEEE 75th VTC Spring, 2012.

[5]   P. VanDerVoorn et al, "A 32nm low power RF CMOS SOC technology featuring high-k/metal gate," VLSI Tech. Symp. 2010.

[6]   T.S. Rappaport, J.N. Murdock, and F. Gutierrez, "State of the Art in 60-GHz Integrated Circuits and Systems for Wireless Communications,"Proceedings of the IEEE, vol. 99, no. 8, pp. 1390-1436, Aug. 2011.

[7]   A. Shamim, L. Roy, N. Fong, and N. G. Tarr.,"24 GHz On-chip Antennas and Balun on Bulk Si for Air Transmission," IEEE Trans. Antennas Propag. 2008, Feb.

[8]   Ali M. Niknejad, "0-60 GHz in Four Years: 60 GHz RF in Digital CMOS,"IEEE SSCS NEWS. 5. Research highlights. Spring 2007.

[9]   Amin K. Ezzeddine, "Advances in Microwave & Millimeter-wave Integrated Circuits,"http://amcomusa.com/downloads/publications/June2007a.pdf.

[10]   http://www.engadget.com/2011/06/01/qualcomm-unleashes-tri-band-wifi-and-new-mobile-wireless-chipset/.

[11]   A. Valdes-Garcia, S. Nicholson, J. Lai, A. Natarajan, P. Chen, S. Reynolds, J. Zhan, B. Floyd, "A SiGe BiCMOS 16-Element Phased-Array Transmitter for 60 GHz Communications", 2010 IEEE International Solid-State Circuits Conference, Feb 2010, pp. 218-220.

[12]   S. Emami, R. Wiser, E. Ali, M. Forbes, M. Gordon, X. Guan, S. Lo, P. McElwee, J. Parker, J. Tani, J. Gilbert, C. Doan, "A 60GHz CMOS Phased-Array Transceiver Pair for Multi-Gb/s Wireless Communications", 2011 IEEE International Solid-State Circuits Conference, Feb 2011.

[13]   S. Alexandre, O. Richard, B. Martineau, C. Mounet, F. Chaix, R. Ferragut, C. Dehos, J. Lanteri, L. Dussopt, S. Yamamoto, R. Pilard, P. Busson, A. Cathelin, D. Belot, P. Vincent "A 65 nm CMOS Fully Integrated Transceiver Module for 60 GHz Wireless HD Applications", 2011 IEEE International Solid-State Circuits Conference, Feb 2011.

Annex 2

Measurement results in bands above 6 GHz

There are prototyping activities ongoing in various spectrum bands including 11, 15, 28, 44, 70 and 80 GHz.[7]

A2.1 Test results of prototype mobile system

This section introduces a prototype of millimetric wave mobile communication system and provides various test results in three categories:

the transmission range tests include LoS environments,

transmissions are made to a moving receiver with speed of 8 km/h in NLoS environments,

two case studies for outdoor-to-indoor building penetration.

Overview of a millimetric wave prototype mobile system

The millimetric wave prototype mobile system was developed for mobile communications by using FPGA and analog RF components to transmit and receive signals and to perform real time processing.

The system operates at the frequency of 27.925 GHz with a bandwidth of 500 MHz, and a pencil beamforming technique is applied to both the base station (BS) and mobile station (MS) transceivers. Figure A2.1-1 shows the overall system configuration, which is composed of BS, MS, and DM (diagnostic monitor). The DM provides the status of RX signal processing, and selected beams at BS and MS are visualized in real time.

---

[7] https://www.nttdocomo.co.jp/english/info/media_center/pr/2014/0508_00.html

https://www.nttdocomo.co.jp/english/info/media_center/pr/2013/0227_00.html

http://pr.huawei.com/en/news/hw-328622-ictmwc.htm#.VXiBiFJr_Gc

http://www.ericsson.com/news/1810070

http://www.ericsson.com/news/1897060

http://company.nokia.com/fi/news/press-releases/2015/03/02/ntt-docomo-nokia-networks-showcase-high-speed-data-transmission-in-5g

http://www.mitsubishielectric.com/news/2015/0302-b.html

FIGURE A2.1-1

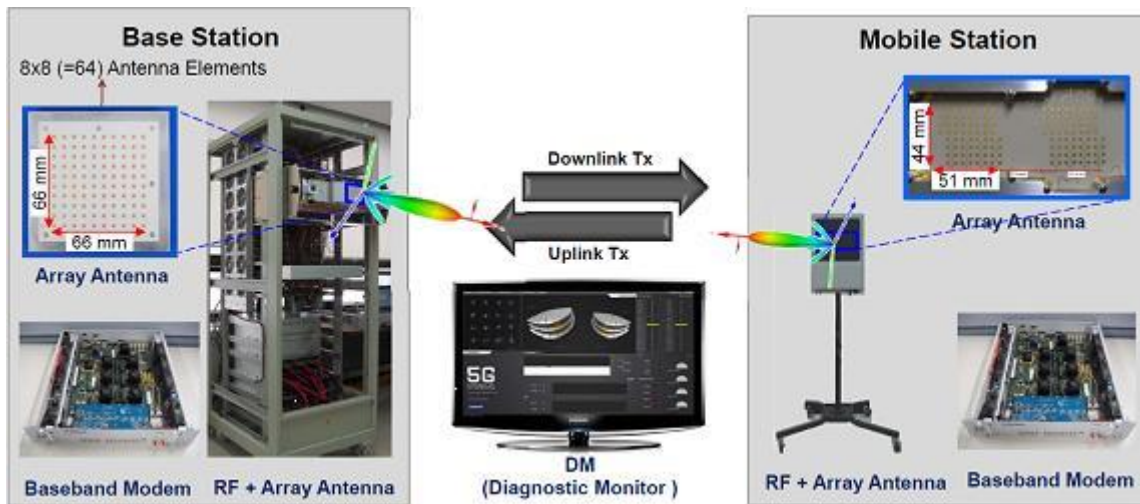**Overview of the prototype mobile system at 28 GHz band**

Figure A2.1-2 shows the key system parameters. Half power beam-width (HPBW) is 10 degrees, and either 64 or 32 antenna elements are used to generate a beam. As for TX output power, 36 dBm is the maximum power after considering PAPR backoff, but some power margin was available for all test cases. OFDM using QPSK or 16-QAM modulation with LDPC channel coding was used. For system operation, fundamental functions like synchronization, beam searching, and channel estimation were implemented, and data transmission is performed using the remaining resources.

FIGURE A2.1-2

Key system parameters and values

PARAMETER	VALUE
Carrier Frequency	27.925 GHz
Bandwidth	500 MHz
Duplexing	TDD
Array Antenna Size	8x8 (64 elements) 8x4 (32 elements)
Beam-width (Half Power)	10º
Channel Coding	LDPC
Modulation	QPSK / 16QAM

LoS range test results

The first question regarding millimetric wave signal transmission in outdoor environments would be "How far can the signal be transmitted in millimetric wave bands?" In order to investigate this question, a range test has been performed in Samsung Campus in Suwon, Korea. The LoS environments which can be found in the Campus provide a maximum distance of 1.7 km. Figures A2.1-3 and A2.1-4 show the scene of LoS environments in Suwon Campus from the satellite view and ground view.

Please note that the BS is located on the rooftop of a4-story building and the mobile station (MS) is located on the road.

FIGURE A2.1-3

Ground view of LoS range test in Suwon Campus

For the given 1.7 km distance, a communication link between the BS and MS was verified with more than 10 dB TX power margin. The data rate of 264 Mbit/s using QPSK shows no block error rate and a data rate of 528 Mbit/s using 16-QAM shows 10^{-6} block error rate. The target error rate of the system link is usually 10% thanks to the HARQ operation. Taking account of these results and conditions, we expect the maximum range to be more than 2 km in LoS environments for the given system configurations.

FIGURE A2.1-4

Satellite view of LoS range test in Suwon Campus

NLoS mobility test results

Secondly, NLoS transmission has been investigated, combined with mobility tests. The BS is located on the 4-th floor rooftop of the building R2, and the MS is located on the road where there is no LoS between BS and MS. The BS transmits a signal toward the building R3, and this signal may reflect from the building and then arrive at the receiver. The distance in total from BS to MS is approximately 160 m. At the receiver side, the MS is not nomadic but moving with the speed of approximately 8~10 km/h.

In the conditions mentioned above, a data rate 528 Mbit/s (16-QAM) was verified with block error rate of no more than 0.5%. The data rate of 256 Mbit/s (QPSK) did not show any block errors. The best TX beam and RX beams have been tracked continuously during movement, and the necessary information was fed back to the BS.

This TX-RX beam tracking made it possible for the MS to move without disconnect of transmission as long as the MS dwells in the BS service coverage. The mobility speed that is allowed in beamforming systems is tightly related to beamforming configurations and beam-tracking period. For example, if the beamwidth is getting narrower, the allowable speed to be supported would be getting slower if the beam-tracking period is retained. On the contrary, for the given beamwidth, making the beam tracking period shorter would support a higher speed of mobility.
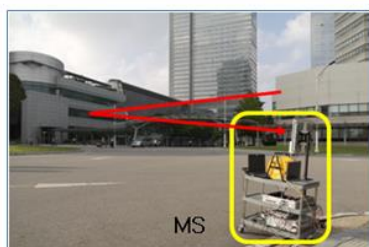
FIGURE A2.1-5

View of NLoS environments for mobility test in Suwon Campus

During the experiments, the best TX beam of BS is continuously searched by the MS and fed back to BS so that the BS can apply the TX beam for transmission.

Outdoor-to-indoor penetration test results

The final test was to investigate the system performance in outdoor-to-indoor penetration environments. Two case tests were conducted and the environments for the tests are shown in Figs A2.1-6 and A2.1-7, respectively.

In the first case, the BS is located at the rooftop of the 2nd floor of the building R1, and the MS is located at the 7th floor office inside the building R2. The distance between BS and MS is approximately 65 m. For the data rate of 256 Mbit/s (QPSK), a block error rate up to 0.6 % was obtained.

In the second case, the BS is located at the rooftop of the 4th floor of the building R2, and the MS is located at the 1st floor lobby inside the building R4. The distance between BS and MS is approximately 150 m. For the data rate of 256 Mbit/s (QPSK), a block error rate up to 0.3 % was obtained.

The BS had more than 10 dB TX power margin for both cases and the MS was located inside the building up to 15 m away from the window; the environments inside the building were not necessarily LoS.

FIGURE A2.1-6

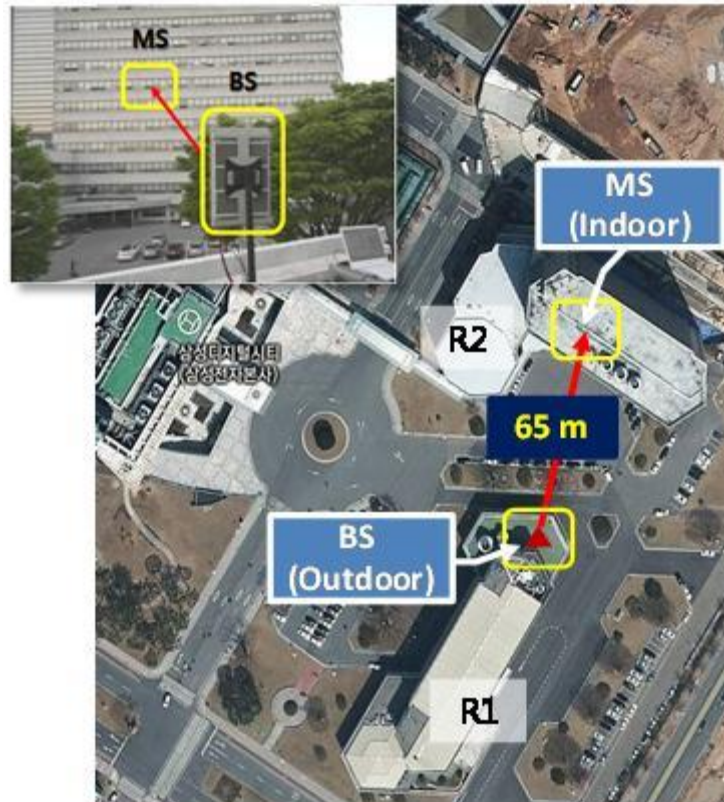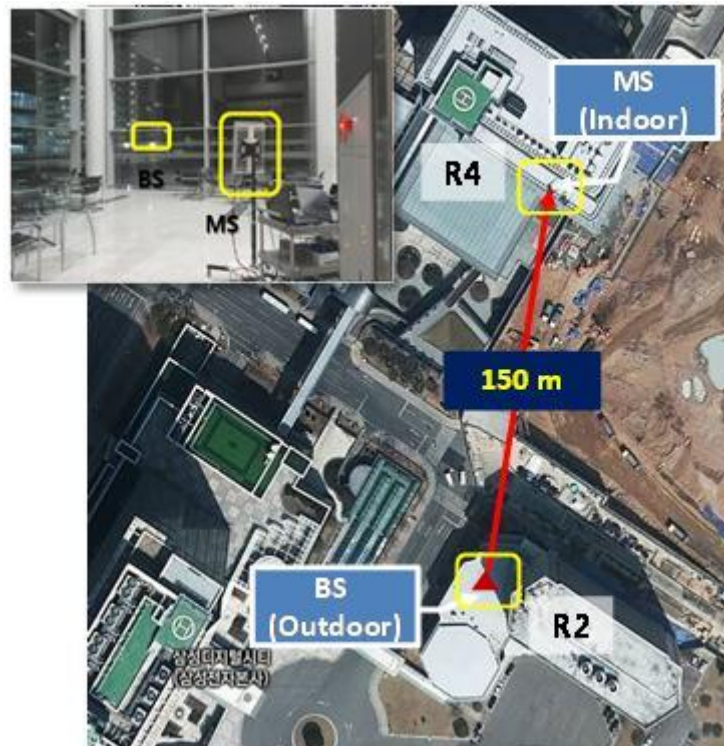**View of building penetration environments – Case 1**

FIGURE A2.1-7

View of building penetration environments – Case 2

Summary

A prototype millimetric wave system using pencil beamforming has been developed and various tests were conducted with real-time processing. Initially, the maximum range in LoS environments was provided as 1.7 km, but it is evident that using higher power will result in lengthened distances of more than 2 km.

Mobility test results were also provided in NLoS environments. With a speed of the MS of around 8 km/h, it was verified that a stable communication link was maintained with a fast beam-tracking algorithm. Final results show that the signal is still pretty well received and some coverage for a communication link can be retained even inside a building with window glass.

All test results point out the possibility of using millimetric wave frequency bands for IMT systems.

A2.2 Coverage test results

In this section, a coverage map based on the prototype IMT system is provided to demonstrate the service availability in typical IMT environments, including LoS, NLoS and window penetration links.

The prototype IMT system used to carry out coverage tests included the following key system features:

– Operating frequency: 27.925 GHz
– Bandwidth: 500 MHz
– Tx power: 31 dBm for case 1, 24 dBm for case 2
– Half power beam width: 10 degrees
– Duplexing: TDD
– Channel coding: LDPC, 1/2
– Modulation: QPSK
– Supported data rates: 264 Mbit/s.

Note that the Tx power used for tests is as more than ten times smaller than the conventional BS Tx power in urban environments, while the system bandwidth is more than 25 times wider. It is obvious that the same level of Tx power as conventional IMT systems will give enlarged service coverage.

Coverage test results

1) Case 1: Outdoor environments

Firstly, coverage test results in outdoor environments are provided to demonstrate the service availability in Fig. A2.2-1, which covers a typical urban outdoor environment including both LoS and NLoS links. The BS is located at the 4th floor rooftop and the MS is located on the roads along various streets. More specifically, the tests were performed at various sites surrounded by tall buildings where different channel propagation effects such as reflection, diffraction, or penetration are expected to occur, as shown in Fig. A2.1-2.

As can be seen from the test results in Fig. A2.2-1, satisfactory communications links are maintained even in NLoS sites more than 200 m away, which is mostly due to reflections off neighbouring buildings(Locations 2, 4, 5, and 12).

On the other hand, there are NLoS locations where a proper link could not be established, i.e. coverage holes (Locations 1 and 13). These locations are expected to be covered well if the transmission power is increased up to the conventional level. Of course there are other solutions for coverage improvement techniques such as optimized cell deployment, intercell coordination, relays, or repeaters.

From Figs A2.2-3 to A2.2-5, various views from the MS receiver toward the BS transmitter are provided. Not only LoS links like Fig. A2.2-4, but also NLoS links like Figs A2.2-3 and A2.2-5 satisfy the target error rate (block error rate (BLER) < 10%).

FIGURE A2.2-1

Outdoor coverage test results of bands above 6 GHz beamforming prototype

FIGURE A2.2-2

A view from the transmitter side

FIGURE A2.2-3
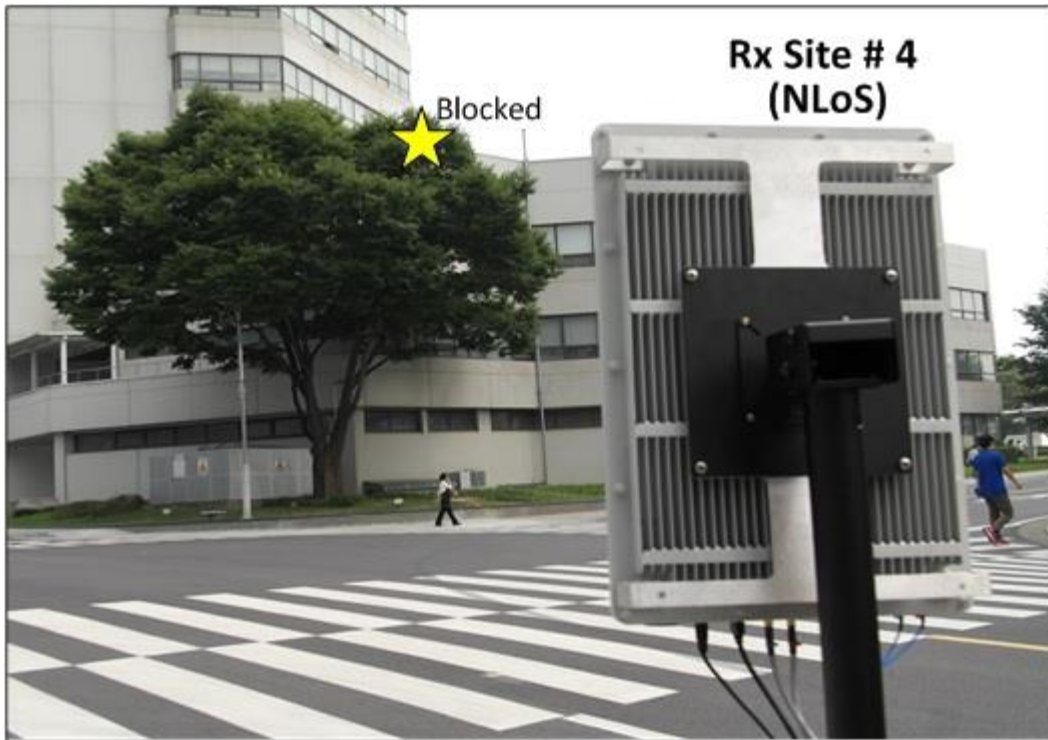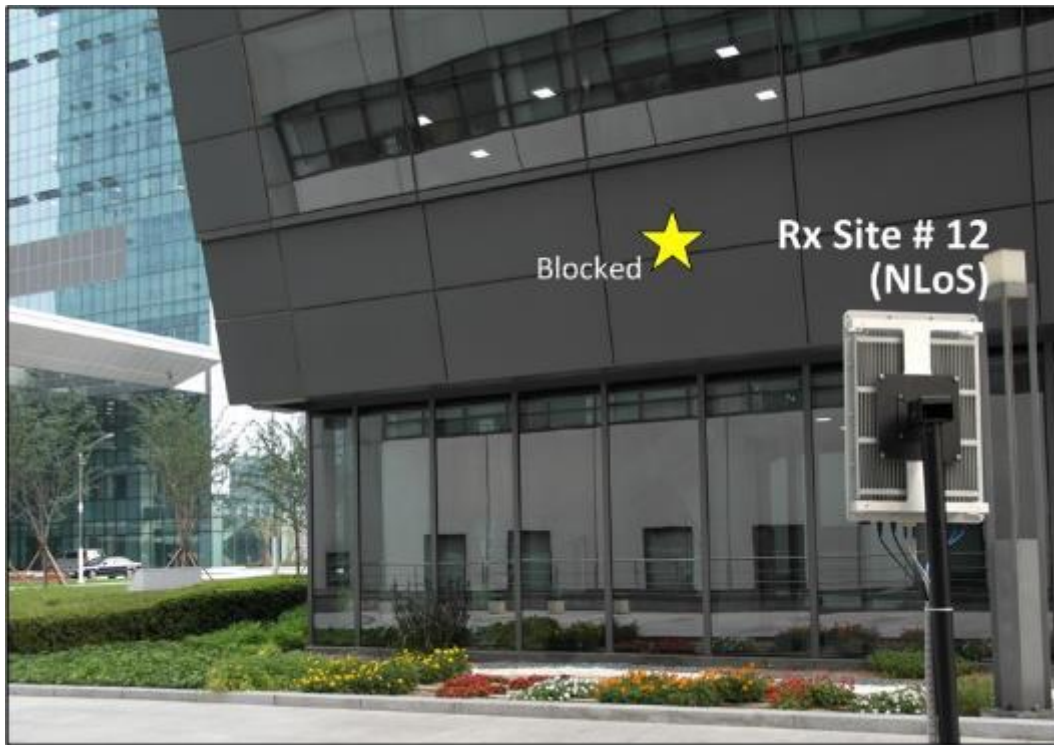
A view from the receiver side toward the transmitter at location 4

FIGURE A2.2-4

A view from the receiver side toward the transmitter at location 6

FIGURE A2.2-5

A view from the receiver side toward the transmitter at location 21

2)   Case 2: Window penetration environments

One of the important operation scenarios in practical cellular networks is communication between an outdoor BS and an indoor MS. The test scenario is shown in Fig. A2.2-6 where the BS is located outdoor on the 4th floor rooftop of a building, and the MS is located in the 1st lobby of another modern office building, which is 150 m away from the BS. The building windows surrounding the MS have heavily tinted glass. These types of building windows present highly unfavourable propagation (penetration) conditions even for current cellular frequency bands below 6 GHz.

Considering very low Tx power (only 24 dBm), as can be seen in Fig. A2.2-7, surprisingly amicable in-building coverage results were obtained, with only the totally obstructed, farthest side of the building resulting in lost connections. Therefore the spots showing block error rates around 10-50% can be easily improved just by having a BS equipped with the conventional Tx power. Furthermore there are many link quality enhancement techniques such as hybrid automatic repeat request (HARQ) and adaptive modulation/coding (AMC). Also, alternative ways can be considered to overcome coverage holes, such as repeaters and indoor femto cells, which are widely used in traditional cellular systems.

FIGURE A2.2-6

**A satellite view for outdoor-to-indoor penetration test (left) and a view
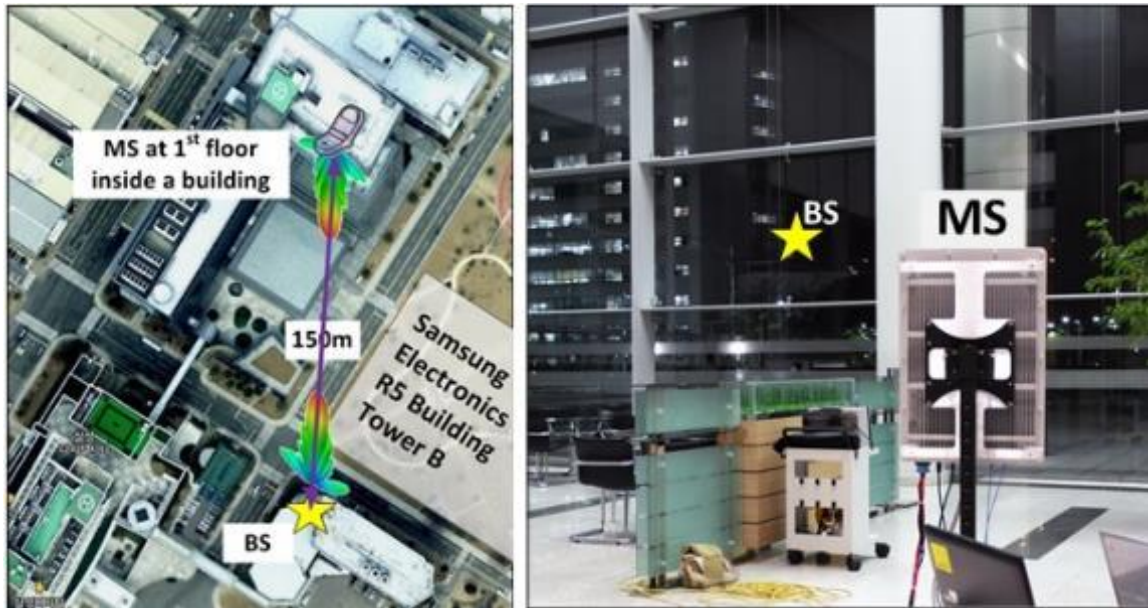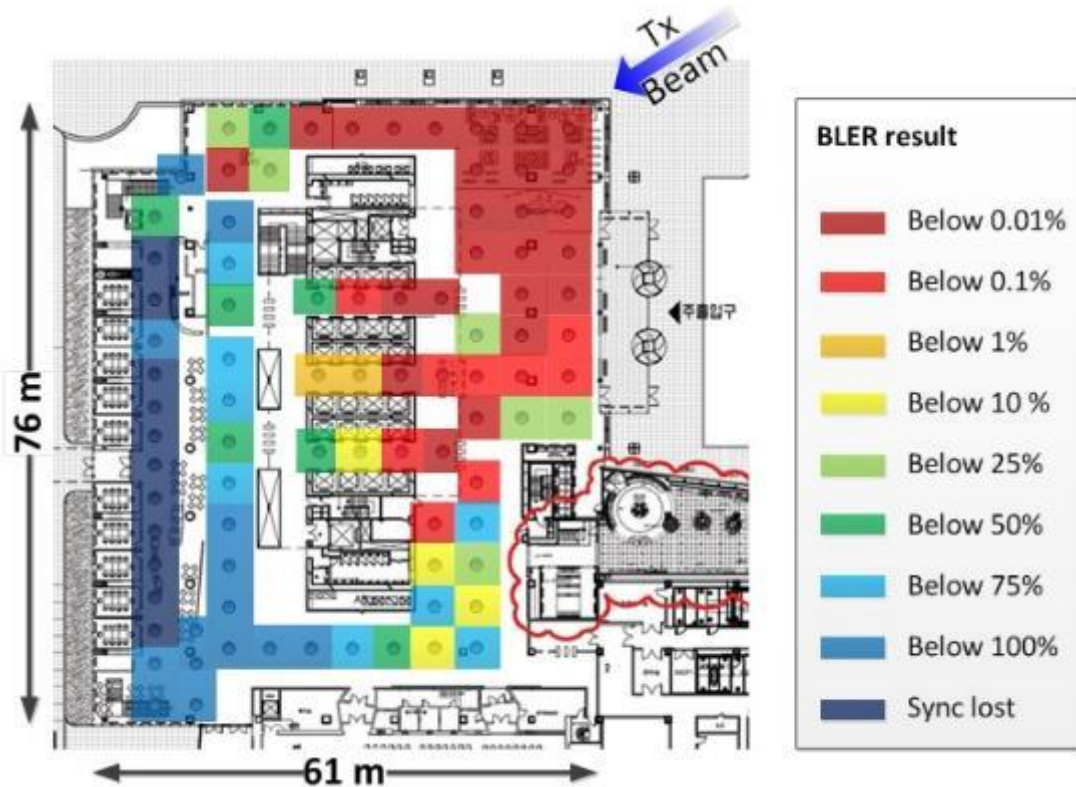from the receiver side toward the transmitter (right)**

FIGURE A2.2-7

Outdoor-to-indoor penetration test results of bands above 6GHz beamforming prototype

Summary

Coverage test results are provided for millimetric wave prototype IMT systems with a large system bandwidth in excess of 500 MHz at 28 GHz, and with tens of antennas placed in planar arrays at both of the communicating ends. The system incorporates a real-time baseband modem, full millimetric wave RF circuitry, and relevant software. This system successfully demonstrated that the millimetric

wave frequency band is capable of supporting radii of a few hundred meters in typical urban environments.

A2.3   High mobility test results

In this section, the mobility test result on the prototype system at 28 GHz is presented. It is very important to support users with high throughput in mobility because mobile services want to provide seamless connectivity even in moving scenario. To model a fast moving environment, the experiment was conducted in moving vehicle. In Fig. A2.3-1, the mobile unit including RF unit and baseband model is shown equipped on the roof of the mini-van vehicle. The prototype system is designed with the following the key parameters:

–   Operating frequency: 27.925 GHz
–   Bandwidth: 800 MHz
–   Half power beam width (BS) :   10 degrees
–   Half power beam width (MS) :   20 degrees (Azimuth) / 140 degrees (Elevation).

FIGURE A2.3-1

Mobile unit equipped on the roof of the mini-van

The test was conducted with the speed of a vehicle racing (more than 100 km/h) on a 4.35 km professional outdoor race track in safe condition as shown in Fig. A2.3-2. The base station is placed on the building in the track, and covers the area where the vehicle is moving with 110 km/h speed. Figures A2.3-3 and A2.3-4 show the views of the point at the base station and the point at the mobile station, respectively, while the experimental test performed. The vehicle moves fast along the track which is much curved.

FIGURE A2.3-2

A satellite view of the Everland Speedway for mobility test

FIGURE A2.3-3

View from the point at Base Station

FIGURE A2.3-4

Mobile Unit on moving in Speedway track

As the results shown in Fig. A2.3-5, the peak data rate reached to 1.2 Gbit/s in the vehicle travelling over 112 km/h speed. The diagnostic monitor in Fig. A2.3-5 shows the status of transmission including beam directions and the constellations of received data while the mobility test conducted. More details including the movie clip of the experiment test can be found at the link below: http://global.samsungtomorrow.com/samsung-electronics-sets-5g-speed-record-at-7-5gbps-over-30-times-faster-than-4g-lte.

FIGURE A2.3-5

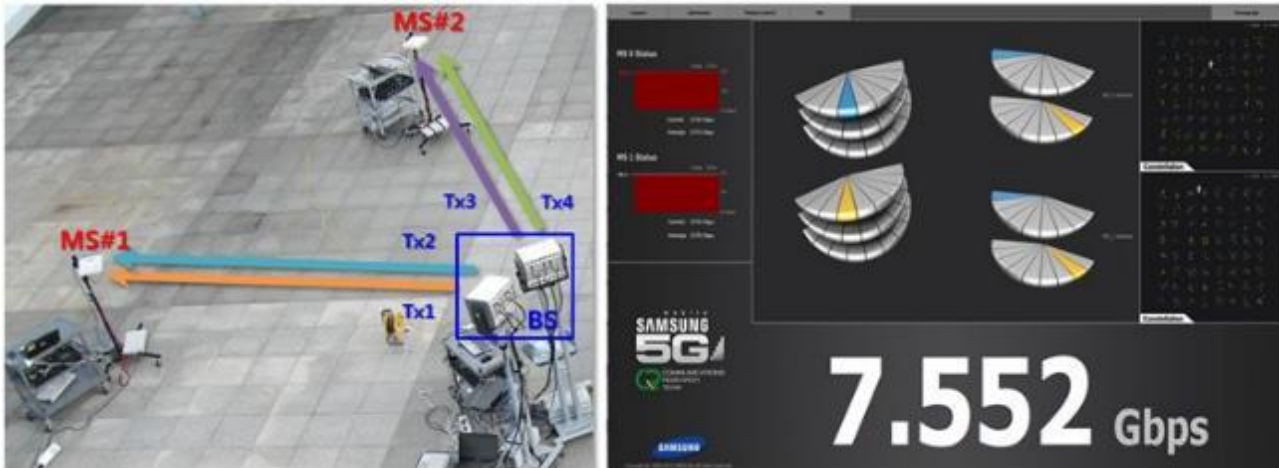**Test results on data rate achieved 1.2 Gbit/s**

A2.4 Multi-user MIMO test results

As an extension of the point-to-point transmission, the multi-user transmission experiment was performed. The transmission test is designed that one base station supports two mobile stations at same time while stationary. As you can see in Fig. A2.4-1 below, each link between base station and mobile station supports 2×2 MIMO achieving 3.77 Gbit/s throughput per user. The total transmission throughput from the base station point of view is achieved up to 7.552 Gbit/s in a stationary condition.

FIGURE A2.4-1

**A view for multiple user transmission experiment (left) and
the result of diagnostic monitor on test achieving 7.552 Gbit/s (right)**

A2.5 Test results in 70 GHz bands

The 70 GHz measurements were conducted in downtown New York City around the New York University (NYU) campus, which offers a very rich multipath environment. Measurements consisted of both backhaul-to-backhaul and base-station-to-mobile scenarios, with transmitter (TX) and receiver (RX) intersite distances between 30 and 200 m. Two TX locations were on top of NYU Coles Sports Center at heights of 7 m, two TX locations were on the 2nd floor balcony of the Kimmel Center at heights of 7 m, a final TX location was on the 5th floor balcony of the Kaufman building at a height of 17 m, and 27 RX locations were located in the surrounding campus at heights of 2 m (mobile) and 4.06 m (backhaul). Figure A2.5-1 shows the measurement locations.

A majority of the measurements were in NLoS conditions, as LoS conditions are less common in dense-urban environments. Also, RX locations were pseudo-randomly selected around campus based on AC outlet access and prior NYU Public Safety approval.

FIGURE A2.5-1

Map of TX and RX measurement locations around NYU campus

The TX and RX antennas used for the 70 GHz measurements were rotatable 27 dBi horn antennas with a 7° 3dB-beamwidth. For each TX-RX location scenario, the TX and RX antennas were mechanically steered in both the azimuth and elevation planes to exhaustively search for the strongest receive power angle combinations. For the strongest TX-RX angle combinations, the RX antenna was then incrementally swept in 8° increments in the azimuth plane for NLoS environments (10° increments for LoS) with the TX antenna fixed in both the azimuth and elevation plane. At each incremental step along the sweep in the azimuth plane, a power delay profile (PDP) was recorded at the receiver (PDPs were not recorded for angles which did not produce a detectable signal). Variations in the elevation plane for the TX and RX were also sampled for RX azimuthal sweeps; that is, the RX antenna elevation was fixed to +/− one beamwidth from the horizon in the elevation plane for two azimuth sweeps and the TX antenna elevation was fixed to +/− one beamwidth from the horizon in the elevation plane for two RX azimuth sweeps. This procedure resulted in five initial RX sweeps using a fixed TX orientation that provided the strongest initial received power. TX azimuth sweeps were then conducted with the RX antenna fixed in the two strongest azimuth and elevation angle settings, using the pointing angle combinations determined during the first five RX sweeps.

Upon completion of the two TX azimuth sweeps, a different main angle of departure at the TX was selected to perform five more similar RX sweeps, resulting in 12 possible measurement sweeps per TX-RX combination. Measurements from RX sweeps are used to develop angle-of-arrival (AOA) statistics and models, and angle-of-departure (AOD) models can be generated from the TX sweeps. The NYU WIRELESS research team conducted measurements for 36 base station-to-mobile and 38 backhaul-to-backhaul combinations; however, there were outages at various locations for each scenario.

The measurements at 70 GHz show very comparable path loss behaviour for the base-station-to-mobile scenarios measured at 28 and 38 GHz [1][2][3], thus indicating that propagation in many different bands above 20 GHz will be quite comparable and quite viable with directional, high-gain antennas used at both the mobile device and base station.

In the first step, omnidirectional large-scale path loss models at 70 GHz for backhaul and mobile access in an urban environment were studied. These new omnidirectional path loss models are suitable for use by standards bodies and academicians who may wish to study arbitrary antenna patterns or MIMO approaches. The omnidirectional path loss models were developed by considering the measured PDPs at every individual pointing angle for each TX and RX location, and integrating each of the PDPs to obtain received power as a function of pointing angle, and then subtracting the TX and RX antenna gains from every individual power measurement. All of the received powers at unique pointing angles (taking care not to double-count for replicated antenna pointing angles) were summed to obtain the omnidirectional path loss models given here. Results of the 70 GHz omnidirectional measurements from New York City are shown in Figs A2.5-2 and A.2.5-3, where best-fit path loss exponents (PLEs) are shown for omnidirectional backhaul-to-backhaul and omnidirectional base-station-to-mobile access scenarios, respectively. Path loss and shadow factors (i.e. the standard deviation about the distance-dependent mean path loss model) were computed for both LoS and NLoS measurements for each scenario. Two path loss models are considered: the first model, the free-space path loss (FSPL) reference distance model, provides a path loss exponent which has physical relevance since the path loss is tied to the FSPL at a specific close-in reference distance (1 m is convenient and practical at millimetric wave frequencies). In equation form, this path loss is given by:

$$PL[\text{dB}](d) = 20\log_{10}\left(\frac{4\pi d_0}{\lambda}\right) + 10n\log_{10}(d/d_0) + X \tag{1}$$

where

d_0 : reference distance (1 m in this paper)

λ : wavelength

n : path loss exponent

d : distance between TX and RX (m) and

X : shadow fading term which is a zero-mean Gaussian variable with a given standard deviation (i.e. the shadow fading) (dB).

For the large-scale propagation model in (1), the path loss exponent and shadow fading standard deviation are chosen to give the best fit to the data. The second path loss equation considered is the traditional one used in industry (e.g. by 3GPP) referred to as an *alpha plus beta* model. This model has the following form:

$$PL[\text{dB}](d) = \alpha + 10\beta \log_{10}(d) + X \tag{2}$$

where α and β are determined with a least-squares fit to the measured data and X is the shadow fading term. Note that this path loss formula is limited to only the range of distances measured in the field [6].

In equation (2), β cannot be considered to be a true path loss exponent because it is floating and is only chosen to optimize the fit to the data along with the y-intercept, α. Also, since the path loss formula in (2) is only valid over the range for which the measurements were taken, it is inaccurate and often misleading for distances where the physical model of (1) will still hold [4] [6]. The advantage of the alpha plus beta model is that it minimizes the standard deviation (minimizes the mean square error fit to data) with an improvement of about 0.5 to 1 dB to a FSPL model, but the disadvantage is that there is no physical basis for the model and it does not fit real world data well beyond the specific range of data for which it is created.

Figures A2.5-2 and A2.5-3 show that the measured omnidirectional LoS path loss is very close to the free-space path loss with an exponent of 2 in both the backhaul and access (base-to-mobile) cases. Also shown is how the alpha plus beta model compares to the FSPL reference distance model. Over the range of distances of the measured data (30 to 200 m in [4][5]), both models produce similar path loss values, but outside of that range the two models would deviate quite significantly. Table A2.5-1summarizes the results found for the omnidirectional 1 m FSPL reference distance model for the case of both backhaul-to-backhaul and base-station-to-mobile, and Table A2.5-1 summarizes the path loss models for the alpha plus beta model. These results show that the omnidirectional NLoS PLEs for the backhaul-to-backhaul and base-station-to-mobile scenarios are comparable to one another, and are also quite comparable to urban path loss observed at 28 GHz [4] [5].

FIGURE A2.5-2

Measured omnidirectional antenna path loss computed relative to 1 m free-space path loss for 70 GHz

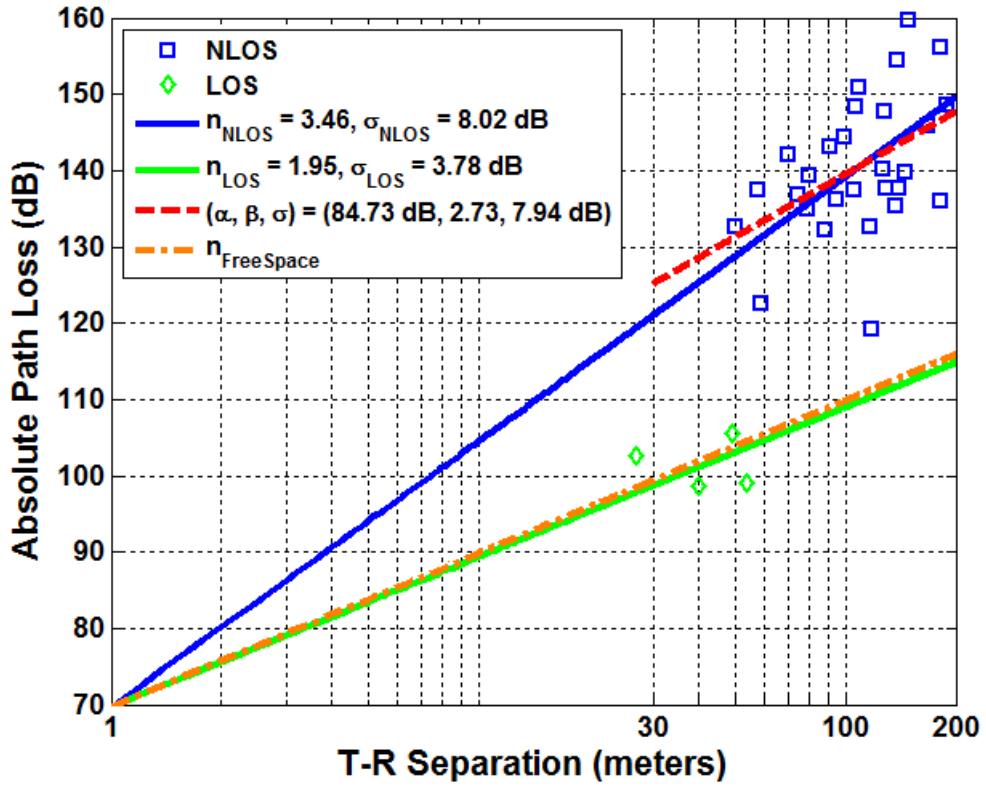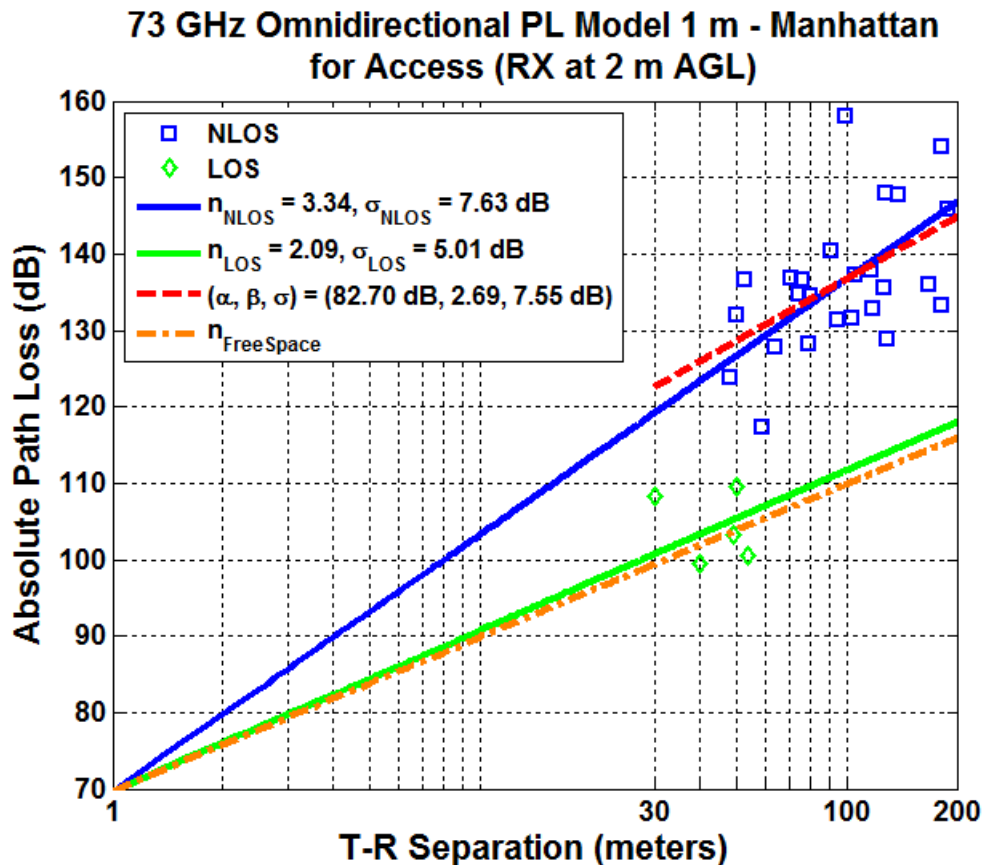73 GHz Omnidirectional PL Model 1 m - Manhattan for Backhaul

FIGURE A2.5-3

Measured omnidirectional antenna path loss computed relative to 1m free-space path loss for 70 GHz base-station-to-mobile access (TX height was 17 m and 7 m and the RX height was 2 m)

These recent 70 GHz measurements in New York City show that the propagation channel is rich in multipath, both in terms of time delays and angular arrivals. This diversity provides ample signal paths that will be exploited to provide multi-Gigabit per second data transmissions in the vast millimetric wave spectrum bands. Figure A2.5-4 shows typical measured PDPs that have a large number of strong multipath components when using highly directional antennas at the TX and RX. Figure A2.5-5 compares the angles of arrival at 28 and 70 GHz, and shows that distinctive lobes of energy arrive in a similar manner at a wide array of different angles in both LoS and NLoS environments. Figure A2.5-5 suggests that multipath "lobes" may be used to statistically describe the arrival of energy when using directional antennas, where the lobe size may be a function of the particular antenna gain used at the receiver.

Table A2.5-1 shows the path loss exponents (relative to a free-space reference distance of 1 m) and shadow factors for the FSPL reference distance model for New York City at 70 GHz with TX heights of 17 m and 7 m and backhaul-to-backhaul RX heights of 4.06 m, and base-station-to-mobile scenarios with RX heights of 2 m. PLEs and shadow factors are shown for omnidirectional antennas at the RX and TX.

TABLE A2.5-1

Path loss exponents (relative to a free-space reference distance of 1 m) and shadow factors for the FSPL reference distance model for New York City at 70 GHz

	70 GHz backhaul-to-backhaul		70 GHz base station-to-Mobile	
	PLE	*SF* (dB)	*PLE*	*SF* (dB)
LOS	1.95	3.78	2.09	5.01
NLoS	3.46	8.02	3.34	7.63

Table A2.5-2 shows alpha, beta, and shadow factors for the alpha plus beta model for New York City at 70 GHz with TX heights of 17 m and 7 m with backhaul-to-backhaul RX heights of 4.06 m, and base-station-to-mobile scenarios with RX heights of 2 m. PLEs and shadow factors are shown for omnidirectional antennas at the RX and TX. Also shown is a hybrid model from that combines the powers at each RX location for both mobile and backhaul heights.

TABLE A2.5-2

Alpha, beta, and shadow factors for the alpha plus beta model for New York City at 70 GHz

	70 GHz backhaul-to-backhaul			70 GHz base station-to-mobile		
	α	β	*SF* (dB)	α	β	*SF* (dB)
NLoS	84.73	2.73	7.94	82.70	2.69	7.55
NLoS Hybrid [14]	86.6	2.69	8.0	86.6	2.69	8.0

FIGURE A2.5-4

Two PDPs measured in nearly identical locations in New York City (one year apart) at 28 GHz (left) and 70 GHz (right)
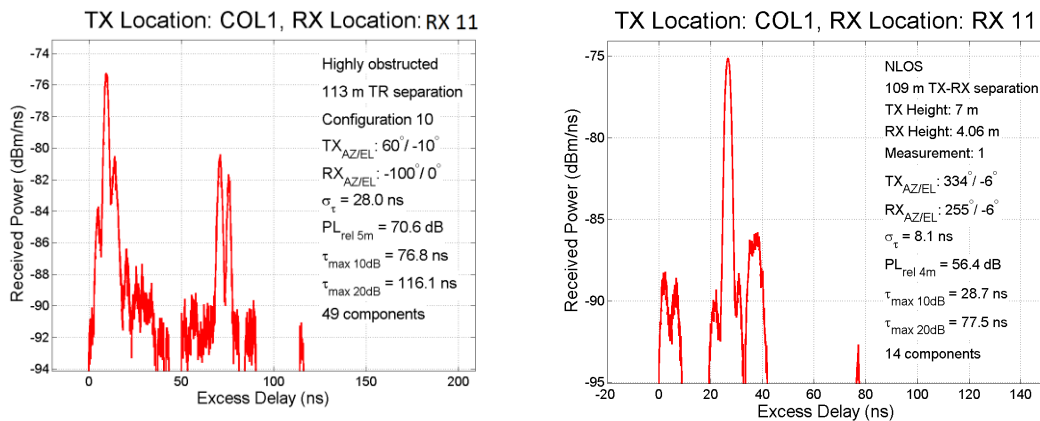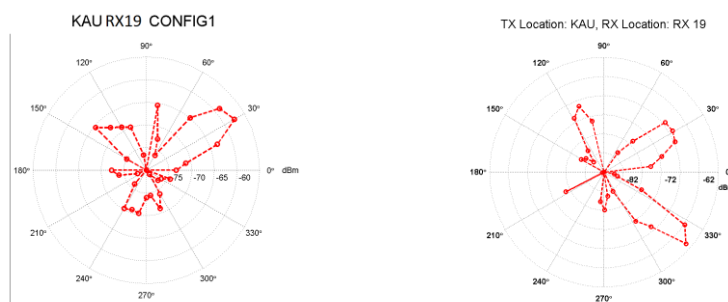
FIGURE A2.5-5

Two polar plots measured at similar locations at 28 GHz and 70 GHz (one year apart).

List of references

[1]   Rappaport, T.S., Sun, S., Mayzus, R., Zhao, H., Azar, Y., Wang, K., Wong, G.N., Schulz, J.K., Samimi, M., and Gutierrez, F., "Millimeter Wave Mobile Communications for 5G Cellular: It Will Work!" *IEEE Access Journal*, Vol 1, No. 1, May 2013.

[2]   Rappaport, T.S., Sun, S., Mayzus, R., Zhao, H., Azar, Y., Wang, K., Wong, G.N., Schulz, J.K., Samimi, M., and Gutierrez, F., "Millimeter Wave Mobile Communications for 5G Cellular: It Will Work!" *IEEE Access Journal*, Vol 1, No. 1, May 2013

[3]   Y. Azar, G. N. Wong, K. Wang, R. Mayzus, J. K. Schulz, H. Zhao, F. Gutierrez, D. Hwang and T. S. Rappaport, "28 GHz Propagation Measurements for Outdoor Cellular Communications Using Steerable Beam Antennas in New York City," *2013 IEEE International Conference on Communications (2013 ICC)*, June 9–13 2013.

[4]   S. Rangan, T. S. Rappaport andE. Erkip, "Millimeter-wave cellular wireless networks: Potentials and challenges," *Proc. of the IEEE*, Vol. 102, No. 3, March 2014.

[5]   Samimi, M., Wang, K., Azar, Y., Wong, G.N., Mayzus, R., Zhao, H., Schulz, J.K., Sun, S., Gutierrez, F., and Rappaport, T.S., "28 GHz Angle of Arrival and Angle of Departure Analysis for Outdoor Cellular Communications using Steerable Beam Antennas in New York City," *IEEE Vehicular Technology Conference (VTC)*, 2013

[6]   MacCartney, G.R., Zhang, J., Nie, S., and Rappaport, T.S., "Path Loss Models for 5G Millimeter Wave Propagation Channels in Urban Microcells," *IEEE Global Communications Conference, Exhibition & Industry Forum (GLOBECOM)*, Dec. 9~13, 2013.

[7]   A. Ghosh et al., "Millimeter wave enhanced local area systems: A high data rate approach for future wireless networks,"*IEEE Journal on Selected Areas in Communications, vol*. 32, no. 6, pp. 1152-1163, June, 2014.

Annex 3

Simulation results above 6 GHz

The propagation models contained in this Annex are the ones that have been used in the studies that are described[8].

A3.1 Simulations at 10 GHz, 30 GHz, and 60 GHz

A3.1.1 Introduction

This section contains evaluations of the performance of outdoor-deployed small cells used for covering a single building indoors(i.e. base station(s) located outdoors to serve indoor users) at frequencies above 6 GHz. Simulations have been performed for a range of frequencies up to 60 GHz, and results are presented in terms of propagation gain maps as well as user throughput. The specific frequencies used in the simulations (10 GHz, 30 GHz, and 60 GHz) are selected as examples to illustrate the general trends of how coverage varies across the frequency range.

The outline of § A3.1 is as follows: § A3.1.2 introduces the channel model used, § A3.1.3 gives a description of the scenario and the simulation setup, § A3.1.4 presents the simulation results, and finally, conclusions are given in § A3.1.5.

A3.1.2 Propagation models used in this study

The channel models used in this section are based on Refs. [1]-[9]. The basis is the site-specific propagation model [1], where LoS propagation is based on equation (3) of [9] and NLoS propagation is based on the model in Reference [1]. This model has been further updated to include frequency-dependent building-penetration and indoor wall-loss models presented in the following subsections.

Building penetration loss

The building penetration loss was calculated based on the assumed material percentages for different building types (A) the "old building" assumption corresponds to a composite model with 30% standard glass and 70% concrete wall, and (B) the "new building" composite model corresponds to 70% infrared reflective glass (IRR) glass and 30% concrete wall.

The total loss through the standard glass and the coated (IRR) glass windows was estimated according to the equations

$$\textbf{Lossthroughastandardglasswindow (dB)} = \textbf{0.2} * \textbf{\textit{f}} + \textbf{2} \tag{A3-1}$$

$$\textbf{Lossthroughacoatedglasswindow (IRR) (dB)} = \textbf{0.3} * \textbf{\textit{f}} + \textbf{23} \tag{A3-2}$$

and the concrete wall loss was calculated based on

$$\textbf{Lossthroughaconcretewall (dB)} = \textbf{4} * \textbf{\textit{f}} + \textbf{5} \tag{A3-3}$$

where f is the frequency in GHz.

The overall building penetration loss was then obtained based on a weighted average (with gains in linear scale) according to the percentage of glass and concrete for the respective building type. The resulting models are illustrated in Fig. A3.1-1.
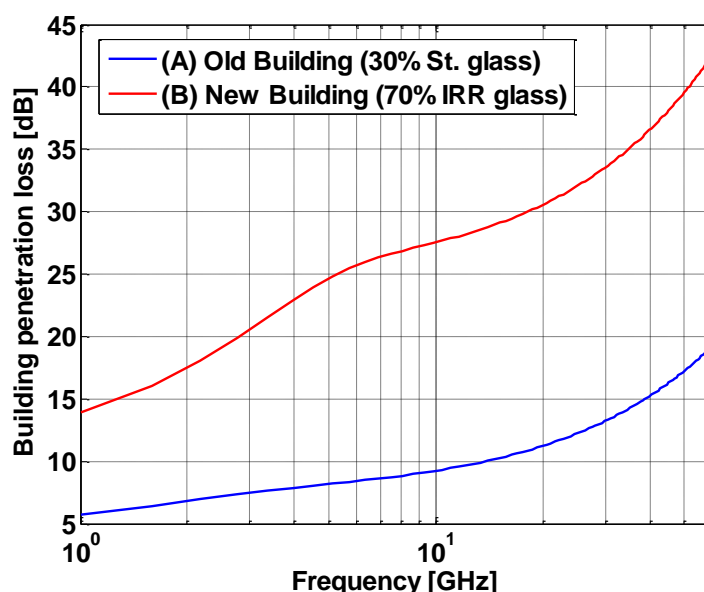
---

[8] In some cases, propagation models may have been applied beyond the frequency range for which they were developed. For future studies, it is recommended that propagation models contained in ITU-Recommendations should be used where these are available.

There are several factors motivating the averaging over different wall materials:

- The DL beams in this study are wide enough to cover multiple windows and concrete wall sections of the targeted building.
- The terminals have wide receiving beams (omnidirectional in this study), resulting in even further averaging.
- Scattering at window frames will distribute substantial power also to terminals behind wall sections with large penetration loss.
- Since the building in the present study is quite large (deep), many terminals (not least those in the worst percentiles) will only receive signals that have been scattered one or more times against indoor walls or floors. Indoor penetration is further discussed under the header "Analysis of the different indoor models" below.

It should also be noted that the channel model used includes a statistical distribution of the shadow fading to account for remaining variations in path loss.

FIGURE A3.1-1

Building penetration loss – combined models

In addition to the loss illustrated above, an angular wall loss model is available to account for the additional loss that can be experienced depending on the incident angle according to [1]

$$\text{Angularwallloss (dB)} = 20 * (1 - \cos\theta)^2 \tag{A3-4}$$

where θ, the angle of incidence, is set to $\pi/3$ radians for NLoS propagation i.e. the angle of incidence corresponding to an average angular loss.

Indoor wall loss

The indoor environment is assumed to be open, with standard glass, alternatively plaster, indoor walls. The loss model per wall is calculated as a function of the carrier frequency, with an average wall distance of 4 m. The approach is similar to [10], but instead of the $N\log_{10} d$ distance dependence with an empirical frequency dependence for N, the model αd is used, where $\alpha(f)$ is derived from physical considerations of the impact of interior walls, and calibrated against measurements. Two indoor loss models are considered, model 1 and model 2.

Model 1 assumes a wall loss equal to that of a single standard glass layer,

$$\text{Indoor wall loss, model 1 (dB)} = 0.1 * f + 1 \tag{A3-5}$$

where f is the frequency in GHz.

Indoor loss model 2 is based on measurements in [3]. The indoor wall loss is estimated as

$$\text{Indoor wall loss, model 2 (dB)} = 0.2 * f + 1.7 \tag{A3-6}$$

where f is again the frequency in GHz.
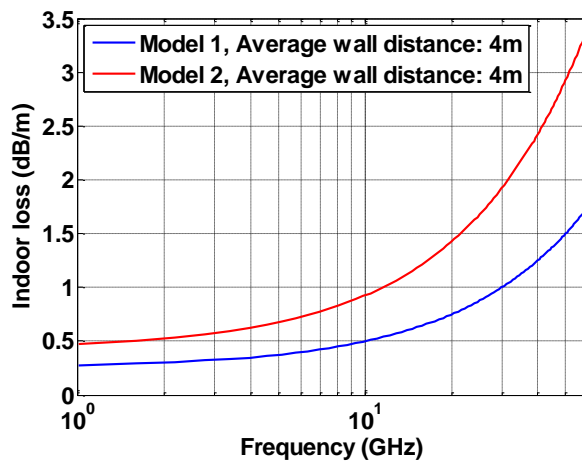
Analysis of the different indoor models

Indoor wall-loss model 1 (equation (A3-5)) may tend to underestimate the indoor loss at high frequencies, as well as the loss corresponding to the first X meters inside the building. For instance, it can be observed from the measurements performed in [3] that after passing the first X m inside the building, the signal tends to find a relatively better path to the receiver (e.g. through open doors, corridors, etc.) than in the case of a receiver standing right behind the exterior wall (or within the first X m).

On the other hand, model 2 (equation (A3-6)), might be pessimistic as we interpolate the dB/m indoor loss to provide an estimated loss deep inside a large building, especially as the measurements in [3] provide an indication of the indoor loss for up to 10 m.

As will be shown in the simulations in § A3.1.4, the assumptions for the indoor loss model will have a significant impact on the results. Thus, both models are considered in this study, which in turn provides an insight into the sensitivity of the results towards the assumptions made on indoor loss models. Figure A3.1-2 illustrates the two different models.

It should be noted that inner walls may be the glass/plasterboard ones that we consider, but also the thick concrete load-bearing ones, which have a loss in the order of an outer wall. The latter case would result in a totally different indoor loss pattern. In addition, other obstructions such as metal white boards could be mounted on the walls causing a higher loss.

FIGURE A3.1-2

Indoor loss models for different frequencies

A3.1.3 Scenario

A single building deployment is considered in this study in order to give an indication of the deployment density that is needed to be able to provide indoor coverage in the entire building, given a minimum achievable bit rate threshold.

As depicted in Fig. A3.1-3, an outdoor-deployed base station is placed at a certain height and distance from the targeted building, which may correspond to the case where a base station is mounted on the exterior wall of another building.

The main deployment and simulation parameters are available in Table A3.1-1.

FIGURE A3.1-3
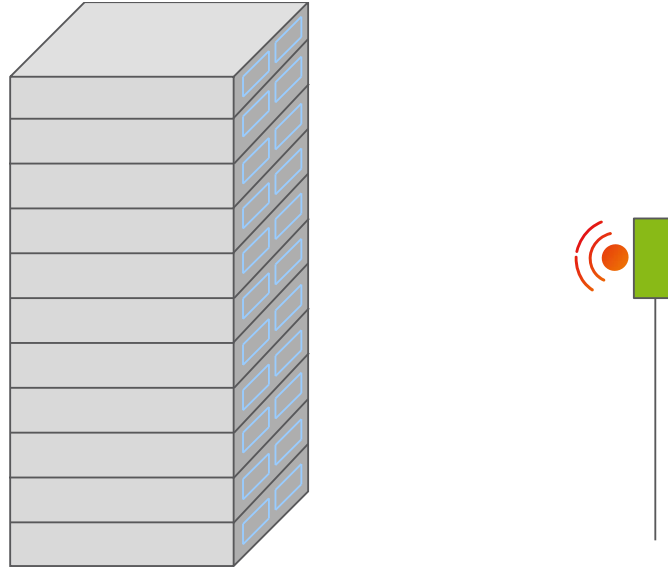
Single building deployment

TABLE A3.1-1

Deployment and simulation parameters

Deployment/simulation parameters	Parameter value
Number of buildings	1
Building height (m)	63
Number of floors	21
Number of base stations	1
Distance between BS and building (m)	35
BS height (m)	31.5
BS output power (dBm)	33
BS antenna	Wall-mounted HV antennas (Hv1, Hv2)[9]
BS antenna gain (dBi)	8 (Hv1) and 16.3 (Hv2)
BS antenna horizontal beam width (degrees)	60 (Hv1 and Hv2)
BS antenna vertical beam width (degrees)	84 (Hv1) and 33.4 (Hv2)
UE antenna	Omni-directional
Carrier frequencies (GHz)	10, 30, 60
System bandwidth	100 MHz
Total system offered load (Mbit/s)	Selected from set [0.625 1.25 2.5 3.75 7.5] (see "User throughput" under § A3.1.4)

A3.1.4 Simulation results

Results based on simulations in a static system level simulator are presented in terms of propagation gain (under the header "Indoor gain maps") and throughput (under the header "User throughput").

Indoor gain maps

1 Building type A (old building)

Figures A3.1-4, A3.1-5, and A3.1-6 illustrate the gain map in the target building at 10, 30 and 60 GHz, respectively, using antenna Hv1. Building size scales are in meters. It can be noticed that the different indoor models have a significant impact on the coverage and on the achievable bit rate levels, especially as the user moves deep inside the building. This observation becomes more and more crucial as we increase the carrier frequency since covering the building may already be challenging even with an optimistic indoor loss model.

The average indoor loss at 10, 30 and 60 GHz can be extracted from Fig. A3.1-2 and is respectively 0.5, 1, and 1.75 dB/m in case of indoor model 1, whereas the corresponding loss values in case of indoor model 2 are 0.9, 1.9 and 3.4 dB/m, which explains the challenges in providing coverage as the indoor distance increases (i.e. up to 40 m in this case).

---

[9] The HV antenna model uses Gaussian-shaped main lobe and flat side lobes, with the principal axes of the (elliptical) Gaussian in the horizontal and vertical directions.

FIGURE A3.1-4

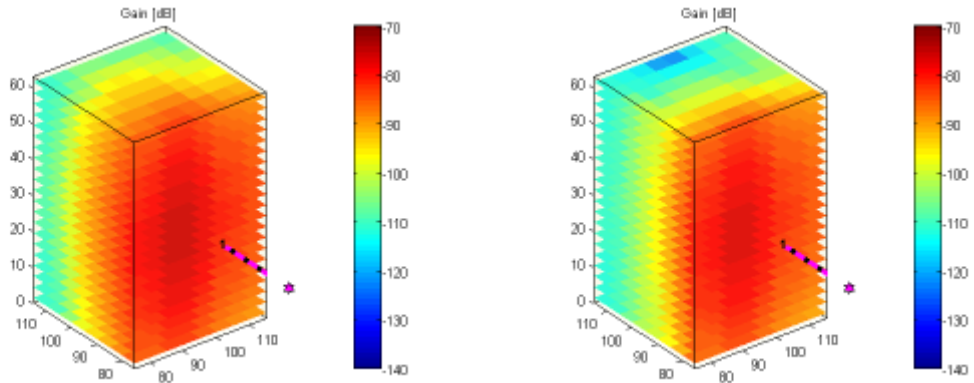**Gain map for building type A at 10 GHz with indoor model 1 (left) and model 2 (right), Hv1**

FIGURE A3.1-5

Gain map for building type A at 30 GHz with indoor model 1 (left) and model 2 (right), Hv1
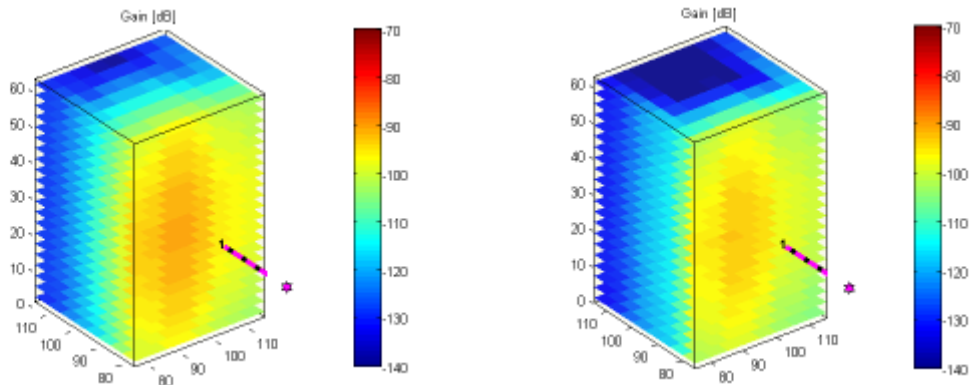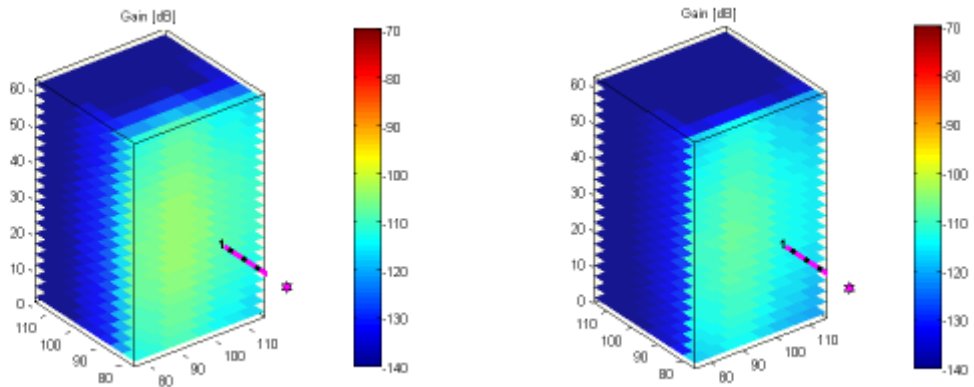

FIGURE A3.1-6

Gain map for building type A at 60 GHz with indoor model 1 (left) and model 2 (right), Hv1

2   Building type B (new building)

Gain maps for building type B are presented in Figs A3.1-7, A3.1-8 and A3.1-9.

FIGURE A3.1-7

Gain map for building type B at 10 GHz *with* indoor model 1 (left) and model 2 (right), Hv1
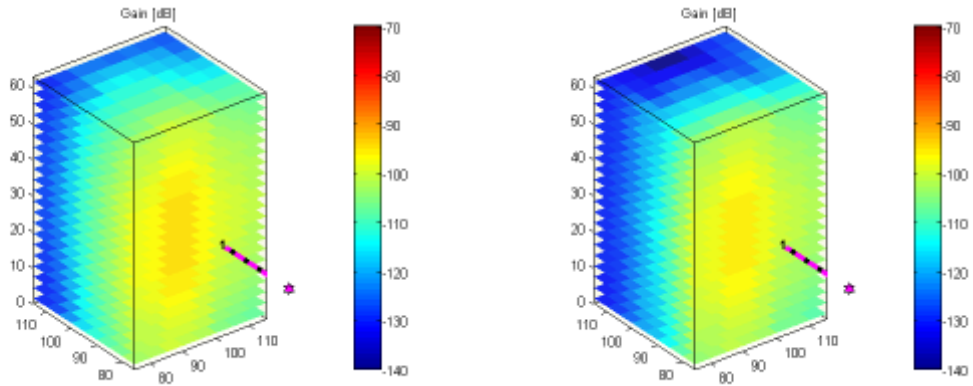

FIGURE A3.1-8

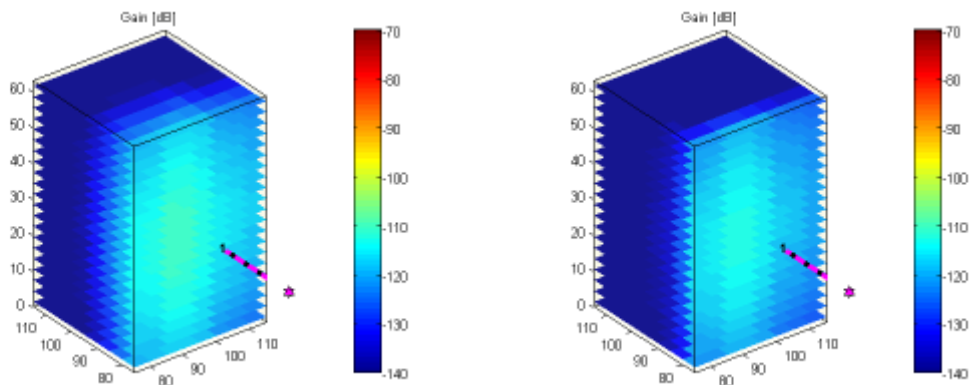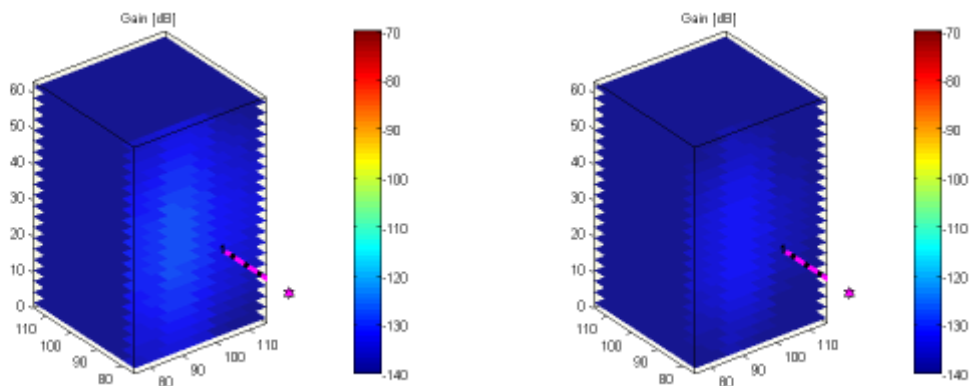**Gain map for building type B at 30 GHz with indoor model 1 (left) and model 2 (right), Hv1**

FIGURE A3.1-9

Gain map building type B at 60 GHz with indoor model 1 (left) and indoor model 2 (right), Hv1

User throughput

In this section, performance results are presented in terms of downlink (DL) user throughput. The throughput is calculated from path loss based on throughput-versus-SINR curves obtained in a detailed link-level simulator.

As we are primarily interested in coverage, the focus has been on simulating lowest-load case (0.625 Mbits/s, cf. Table A3.1-1). However, in the less challenging case of building type A, also four higher loads (i.e. in total all five loads from Table A3.1-1) are considered in order to get insight into the achievable capacity. The higher-gain antenna Hv2 is used in all cases unless Hv1 is explicitly stated in figure caption.

1 Building type A

1.1 10 GHz carrier frequency

Figure A3.1-10 shows that DL user throughput with indoor model 1. The five squares represent the building as seen from above for five different load cases according to Table A3.1-1. The colours of the dots in each square (in this as well as in subsequent figures) indicate the achievable throughput in the corresponding part of the building, according to the colour scale to the right in the figure. As can be seen, the top floor is all green in Fig. A3.1-10, indicating full coverage for at least 100 Mbits/s. The same holds also for all lower floors in this case (not visible in the figure).

In this simulation the total system offered load is less than the full system capacity. Most of the time there is no traffic in the system, but when there is the data to be sent is consistently delivered with a rate exceeding 100 Mbit/s. The system simulations need to operate in < 100% capacity to avoid queue build-up.

Indoor model 2 makes reaching high data rates more challenging, but as can be seen from Fig. A3.1-11, with the considered output power (33 dBm) and bandwidth (100 MHz), a user throughput above 100 Mbits/s can still be reached.

FIGURE A3.1-10

DL user throughput for building type A at 10GHz for different loads, indoor model 1, Hv1
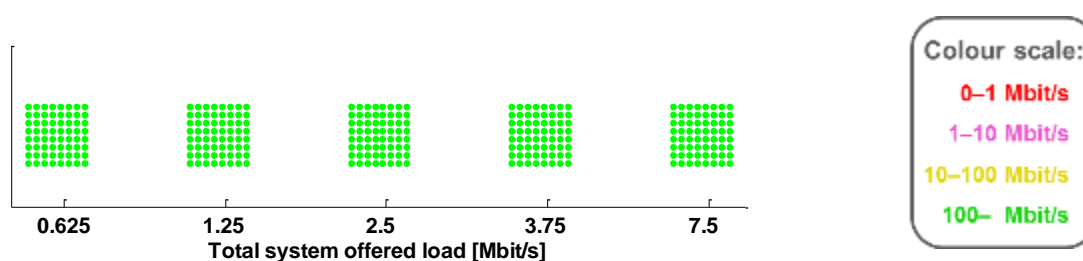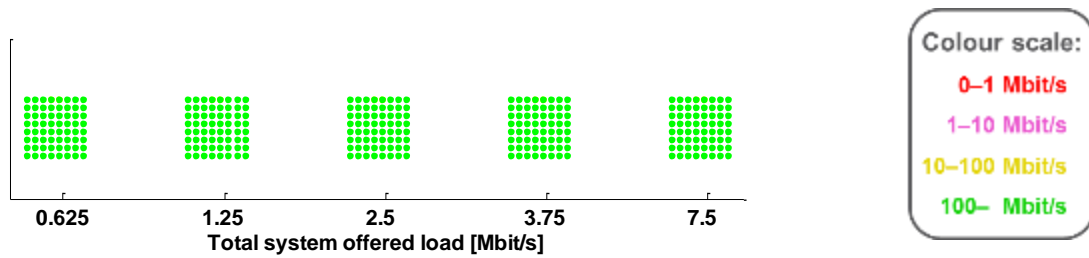
FIGURE A3.1-11

DL user throughput for building type A at 10 GHz for different loads, indoor model 2
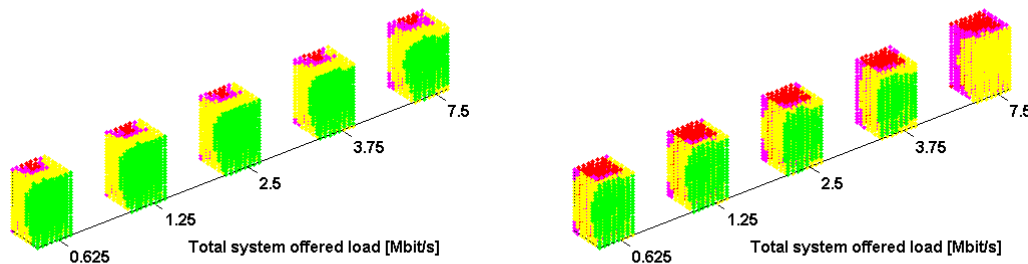

1.2   30 GHz carrier frequency

Results with indoor models 1 and 2 are shown in Fig. A3.1-12. The colour scale in these and all subsequent figures is the same as in Figs A3.1-10 and A3.1-11. The results with model 1 (left panel) indicate that more base stations may be needed to be able to reach the desired user throughput especially in the other side of the building. With indoor model 2 (right panel), high user throughput becomes even more difficult to reach as the indoor distance increases; however, covering the entire building may still be manageable with a reasonable number of base stations.

FIGURE A3.1-12

DL user throughput for building type A at 30GHz for different loads, indoor models 1 (left) and 2 (right)
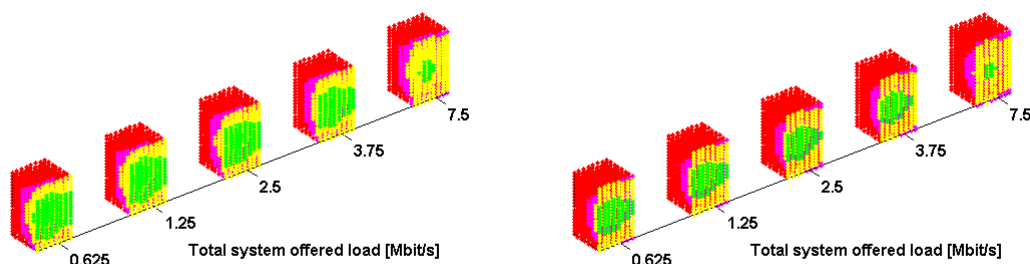**See Fig. A3.1-11 for colour scale**

1.3   60 GHz carrier frequency

At 60 GHz both outdoor-to-indoor penetration loss and indoor propagation loss become too high to be overcome using reasonable assumptions on output power, bandwidth, and antenna gain. As can be seen for indoor model 1 (left panel of Fig. A3.1-13), a high deployment density is required at such high frequencies.

The same observation can be made for indoor model 2 (right panel of Fig. A3.1-13). In addition, it can be noticed that higher antenna gain than what is considered in this study would be needed in order to achieve 10 Mbits/s user throughput in the entire building.

FIGURE A3.1-13

DL user throughput for building type A at 60 GHz for different loads, indoor models 1 (left) and 2 (right)
See Fig. A3.1-11 for colour scale

2 Building type B

For building type B, with its larger indoor-to-outdoor penetration loss, only the lowest load (0.625 Mbit/s) has been simulated.
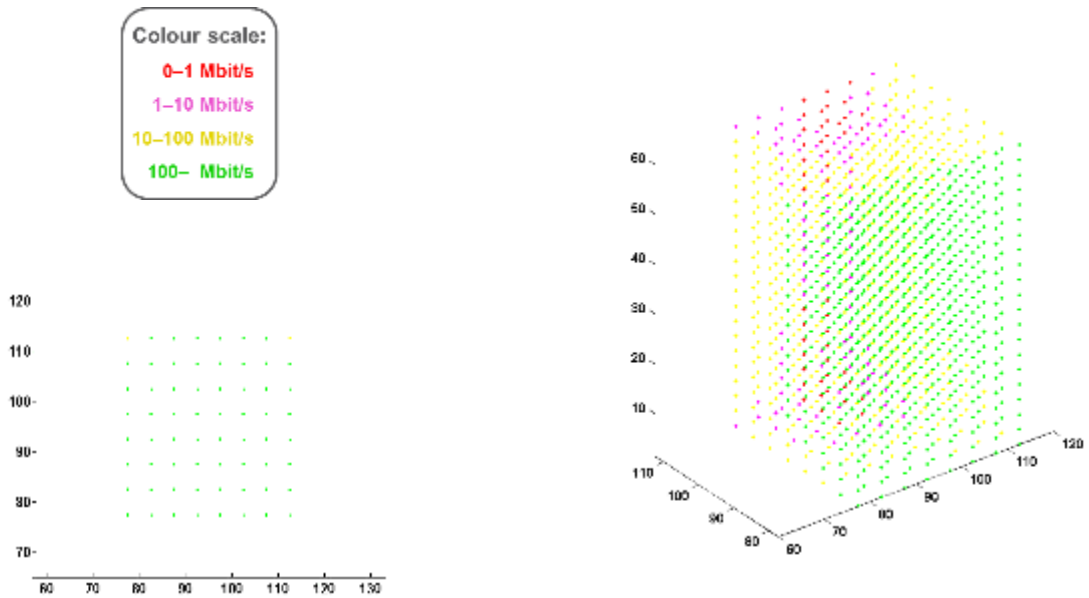
2.1 10 GHz carrier frequency

For building type B and at 10 GHz carrier frequency, the outdoor-to-indoor penetration loss is ~18 dB higher in average compared to that of building type A. As a result, user throughput higher than 100 Mbit/s cannot be guaranteed in the entire building, in contrast to the case of building type A.

On the other hand, the left panel of Fig. A3.1-14 (top view of building) shows good coverage using indoor model 1 with at least 10 Mbit/s user throughput (and in most parts of the building even >100 Mbit/s). In case indoor model 2 is considered, a slightly denser deployment would be needed to provide a similar coverage, as can be seen in the right panel of panel of Fig. A3.1-14.

FIGURE A3.1-14

DL user throughput for building type B at 10 GHz, indoor model 1 (left) and indoor model 2 (right)
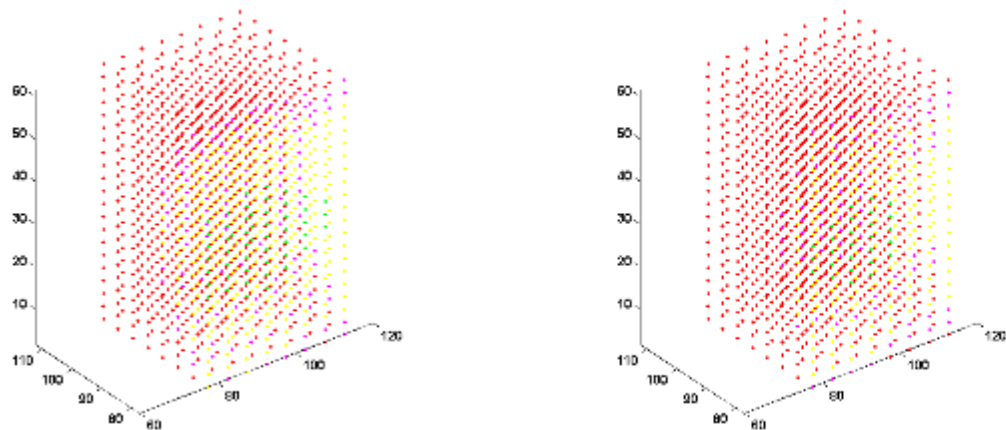

2.2   30 GHz carrier frequency

Outdoor-to-indoor penetration loss at this carrier frequency is ~20 dB higher in average than the corresponding value for building type A, which makes the overall coverage worse than that of building type A at 60 GHz. Hence, even with indoor model 1, there might be a need for a quite dense deployment of small base stations with a relatively high power, large bandwidth allocation, and high antenna gain, which can be noted in the left panel of Fig. A3.1-15 (using the same colour scale as in Fig. A3.1-14).Similar conclusion holds for the case with indoor model 2 as shown in the right panel of Fig. A3.1-15.

FIGURE A3.1-15

DL user throughput for building type Bat 30 GHz, indoor model 1 (left) and indoor model 2 (right)
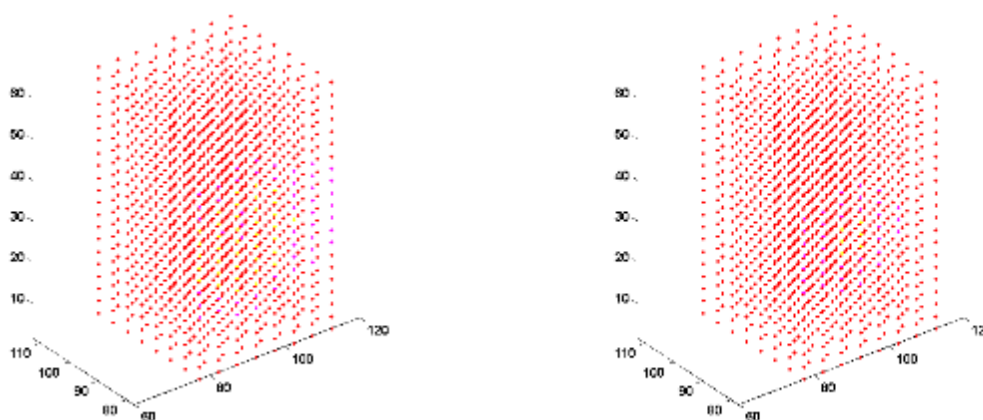**See Fig. A3.1-14 for colour scale**

2.3 60 GHz carrier frequency

Around 23 dB higher building penetration loss should be accounted for in this case compared to building type A, mainly because of the high loss caused by IRR glass. As a result, covering this type of buildings at such high frequencies and with an outdoor deployment of the small bases stations is really difficult, if not impossible, which can be seen in Fig. A3.1-16.

For instance, even with highly directive antennas where narrow beams penetrate the building through the window, this would still be extremely challenging since the IRR glass loss is comparable of that of the concrete wall (i.e. ~40 dB).

FIGURE A3.1-16

DL user throughput for building type Bat 60 GHz, indoor model 1 (left) and indoor model 2 (right).
See Fig. A3.1-14 for colour scale

A3.1.5 Conclusions

The indoor DL coverage at a range of frequencies above 6 GHz (up to 60 GHz) has been analysed in the context of a single-building scenario with an outdoor-deployed base station and low load conditions. The specific frequencies used in the simulations (10 GHz, 30 GHz, and 60 GHz) are arbitrarily selected and intended as examples to illustrate the general trends of how coverage varies across the frequency range. Table A3.1-2 summarizes the presented results for the different building types, indoor models, and operating frequencies.[10] In the cases where 1 BS was not enough to reach 100 Mbit/s, rough estimates of how many BSs would have been needed to reach at least 10 Mbit/s are given.

A main observation, also subject to the assumptions made on propagation, antenna pattern and bandwidth size, is that outdoor-to-indoor coverage with DL user throughput higher than 10 Mbit/s, and in certain cases higher than 100 Mbits/s, is possible at 10 GHz and above. The case with carrier frequencies up to 30 GHz is more challenging but still manageable, whereas providing outdoor to indoor coverage at 60 GHz may be quite difficult for some building types. It has also been seen that the use of high gain antennas is crucial at high frequencies (30 GHz and above).

In addition, it has been shown that the required site count per building, in other words the deployment density, depends on the type of the building (i.e. exterior wall material, interior layout and wall material, building size, etc.).

---

[10] It should be noted that the allowed e.i.r.p. puts a limit on the maximum antenna gain that can be assumed. For instance, if an output power of 33 dBm is to be considered, the allowed additional gain from the antenna is in the order of 27 dB for narrow street.

TABLE A3.1-2

Summary of simulation results

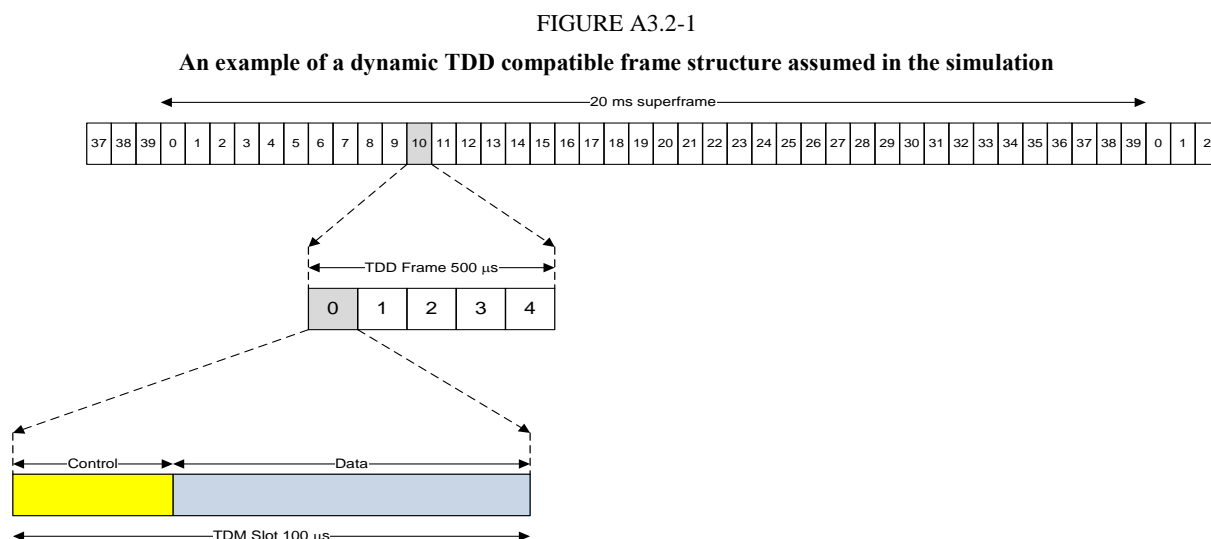|	Building A		Building B	
	Indoor Model 1	**Indoor Model 2**	**Indoor Model 1**	**Indoor Model 2**
10 GHz	1 BS >100 Mbit/s	1 BS >100 Mbit/s	>1 BS >10 Mbit/s	>2 BSs >10 Mbit/s
30 GHz	>1 BS >10 Mbit/s	>2 BSs >10 Mbit/s	>6 BSs >10 Mbit/s	>6 BSs >10 Mbit/s
60 GHz	>6 BSs >10 Mbit/s	>6 BSs >10 Mbit/s	>10 Mbit/s: Not achievable even with narrow beam entering through the window as the IRR glass loss is comparable to that of the concrete wall (~40 dB)	>10 Mbit/s: Not achievable even with narrow beam entering through the window as the IRR glass loss is comparable to that of the concrete wall (~40 dB)

References

[1]   E. Semaan, F. Harrysson, A. Furuskär, H. Asplund, "Outdoor-to-Indoor Coverage in High Frequency Bands", The First International Workshop on Mobile Communications in Higher Frequency Bands, IEEE GLOBECOM December 2014, Austin, TX, USA, pp. 393-398. DOI: 10.1109/GLOCOMW.2014.7063463
http://ieeexplore.ieee.org/stamp/stamp.jsp?tp=&arnumber=7063463

[2]   COST 231 "*Ericsson micro-cell model*", Section 4.5.2, COST 231 Final Report, Link.

[3]   "An Outdoor-to-Indoor Propagation Scenario At 28 GHz", Christina Larsson, Fredrik Harrysson, Bengt-Erik Olsson, Jan-Erik Berg, 8th European Conference on Antennas and Propagation (EuCAP 2014), pp. 3301–3304.

[4]   "Measurements to Support Modulated-Signal Radio Transmissions for the Public-Safety Sector", National Institute of Standards and Technology Technical Note 1546, April 2008.

[5]   "Building penetration measurements from low-height base stations at 912, 1920, and 5990 MHz", NTIA Technical Report TR-95-325, Lynette H. Loew, Yeh Lo, Michael Laflin, Elizabeth E. Pol, October 1995.

[6]   "Propagation Losses Through Common Building Materials, 2.4 GHz vs 5 GHz, Reflection and Transmission Losses Through Common Building Materials", Robert Wilson, University of Southern California, August 2002.

[7]   "EMF shielding by building materials. Attenuation of microwave band electromagnetic fields by common building materials", Link.

[8]   "Radar Surveillance through Solid Materials", Lawrence M. Frazier, Hughes Advanced Electromagnetic Technologies Center, Hughes Missile Systems Company, Rancho Cucamonga, CA.

[9]   "Calculation of free-space attenuation", Recommendation ITU-R P.525-2, Link.

[10]   "Propagation data and prediction methods for the planning of indoor radiocommunication systems and radio local area networks in the frequency range 900 MHz to 100 GHz", Recommendation ITU-R P.1238-7, Link.

Abbreviations

BS	Base station
DL	Downlink
E.I.R.P.	Effective isotropic radiated power
IRR	Infrared reflective glass
LOS	Line-of-sight
MMW	Millimetric waves
NLoS	Non-line-of-sight
SINR	Signal-to-interference-plus-noise ratio
UE	User equipment

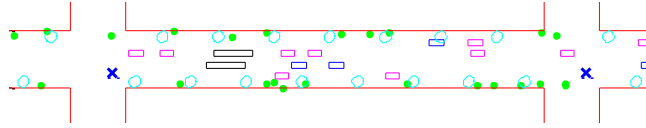**A3.2   System simulations at 72 GHz – Example 1**

Details of system-level simulations for outdoor local area access systems employing very high frequencies are presented in [3]. LoS blocking probability models were developed from a ray-tracing environment which can be used to add more realism to system-level simulations. System-level simulation results were presented using a newly developed very high frequencies channel model. The full details of the channel can be found in [2]. In the simulation setup, a low-latency dynamic TDD, device-to-device and self-backhauling compatible frame structure shown in Fig. A3.2-1 was assumed, where a 20 ms super frame is broken into 500 μs subframes, which in turn contain 10 slots of length 50 μs.

FIGURE A3.2-1

An example of a dynamic TDD compatible frame structure assumed in the simulation

At very high frequencies objects such as vehicles, trees, and people, will block the LoS signal from the radio node to the mobile if they are between the radio node and mobile. This blockage was modeled in [3] to reasonably assess the capacity gains as well as outage probabilities. Figure A3.2-2 shows one block of the simulated environment which includes cars, trucks, sport-utility vehicles (SUVs), trees, people, and radio nodes. One hundred users are dropped along 3 m wide sidewalks which are on both the north and south sides of the street and the users are assumed to be walking east or west (randomly determined). The users hold the mobile 0.4 m in front of them and 1.5 m above the ground at shoulder height. The user is modeled as a 1.5 m high and 0.5 m wide cylinder topped with a head which is a 0.3 m high and 0.3 m wide cylinder.

FIGURE A3.2-2

Example ray-tracing environment for determining LoS probability.
Green dots are users, cyan circles are trees, blue x's are radio nodes, magenta rectangles are cars,
blue rectangles are SUVs, and black rectangles are trucks

Four different radio nodes layouts are considered as shown in Fig. A3.2-3 and Fig. A3.2-4 where all radio nodes are 5 m above the ground. In all cases the radio nodes have four sectors pointing north, east, south, and west. In layout A, there are radio nodes located at the southeast building corner in every intersection. Layout B has the same radio nodes locations as layout A but with an additional radio node in each intersection located at the northwest building corner in an intersection.

The additional radio nodes give a second chance for a user to have a LoS link if the user is blocked to one of the radio nodes. In layout C an additional set of radio nodes over layout A are added in the middle of the blocks of the north-south running streets. In layout D, an additional set of radio nodes over layout C are added in the middle of the blocks of the east-west running streets. The radio nodes density is 75/km^2 for layout A, 150/km^2 for layouts B and C, and 187/km^2 for layout D.

FIGURE A3.2-3

Radio node layouts A with a density of 75/km2 (left) and B with a density of 150/km^2 (right).
Radio nodes locations are marked with an x and the red area demarcates the data collection area

Radio nodes layouts C with a density of 150/km² (left) and D with a density of 187/km² (right).
Radio nodes locations are marked with an x and the red area demarcates the data collection area

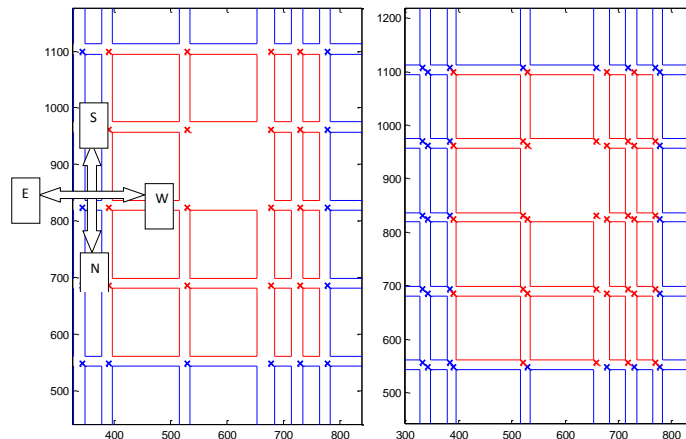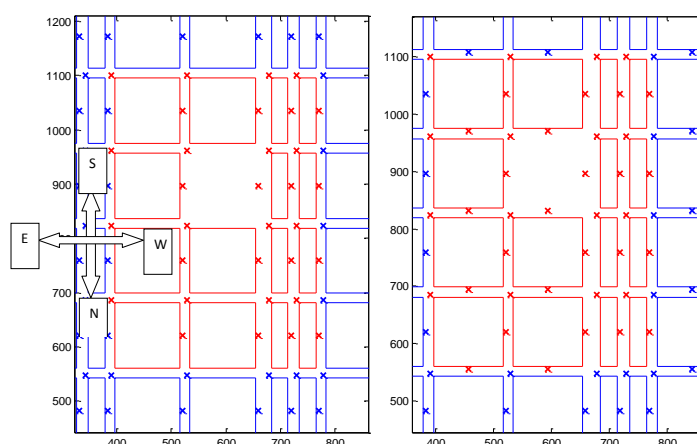The general system-level parameters are given in Table A3.2-1.

TABLE A3.2-1

System simulation parameters

Parameter	Value
Carrier frequency	72 GHz
Bandwidth	2.0 GHz
Traffic type	Full buffer
Radio node array	4 sectors, each sector has two 4 × 4 RF arrays (one vertically polarized, one horizontally polarized) with 0.5λ spacing in both dimensions
Mobile antennas	2 omni-directional antennas, one with vertical polarization, one with horizontal polarization
Radio Node Tx power	30.8 dBm/sector (split between the two arrays in each sector)
Maximum rank	2 (single-user MIMO only)
Beamforming	Eigen beamforming using the uplink signal to point Radio Node RF beams
Modulation levels	LTE MCS levels
Channel estimation	Ideal
Scheduler	Proportional fair
HARQ	None, but retransmissions are allowed

The overall system-level results including average user throughput, cell-edge throughput (i.e. the 5% throughput point), and outage probability (as determined as the percent of users which do not obtain 100 Mbit/s) is shown in Table A3.2-2.

TABLE A3.2-2

Summary of system-level results

Layout	Radio node density	Average user throughput	Cell edge throughput	Outage probability
A (no foliage)	75/km^2	2.10 Gbit/s	18.3 Mbit/s	6.6%
B (no foliage)	150/km^2	3.80 Gbit/s	456 Mbit/s	1.0%
C (no foliage)	150/km^2	3.93 Gbit/s	375 Mbit/s	1.75%
D (no foliage)	187/km^2	4.82 Gbit/s	707 Mbit/s	0.33%
A (foliage)	75/km^2	2.07 Gbit/s	0 Mbit/s	16.4%
B (foliage)	150/km^2	4.06 Gbit/s	222 Mbit/s	3.2%
C (foliage)	150/km^2	4.15 Gbit/s	173 Mbit/s	4.4%
D (foliage)	187/km^2	5.12 Gbit/s	552 Mbit/s	1.0%

As can be seen, very high average user throughputs of between 2.07 Gbit/s to 5.12 Gbit/s are obtained in all layouts. The cell-edge throughput of layout A is 18.3 Mbit/s without foliage and 0 Mbit/s with foliage due to coverage holes deriving from inadequate radio node density, but when the radio node density is increased as in layouts B-D then the cell-edge throughputs are an impressive 173 to 707 Mbit/s.

The system simulation results show that low outage probability is possible with a high enough radio nodes density and that average mobile throughputs of up to 5.12 Gbit/s and cell edge rates of up to 707 Mbit/s are possible. Also the results showed the impact of foliage on the system capacity where foliage helps average user throughput by decreasing the interference seen by strong links but hurts cell-edge throughput and coverage by creating more NLoS links.

[1]   A. Ghosh, et al., "Millimeter wave enhanced local area systems: A high data rate approach for future wireless networks," *IEEE Journal on Selected Areas in Communications, vol*. 32, no. 6, pp. 1152-1163, June, 2014.

[2]   T. A. Thomas, et al., "3D mmWave Channel Model Proposal," *in Proc. IEEE VTC-Fall/2014*, Vancouver, Canada, September 14-17, 2014.

[3]   Timothy A. Thomas, Frederick W. Vook, "System Level Modeling and Performance of an Outdoor mmWave Local Area Access System", *IEEE PIMRC 2014, Washington, DC, USA, September 2-5, 2014*

A3.3   System simulation results on 72 GHz – Example 2

A3.3.1 Introduction

This section contains evaluations of the performance of outdoor-deployed millimetric wave cells with different distributions at 72 GHz. Simulations have been performed and results are presented in terms of the propagation models at 72 GHz and the pre-defined beam patterns.

The outline of Section A3.3 is as follows: § A3.3.2 introduces the channel model used, § A3.3.3 gives a description of the scenario and the system parameters, § A3.3.4 presents the simulation results, and finally, conclusions are given in § A3.3.5.

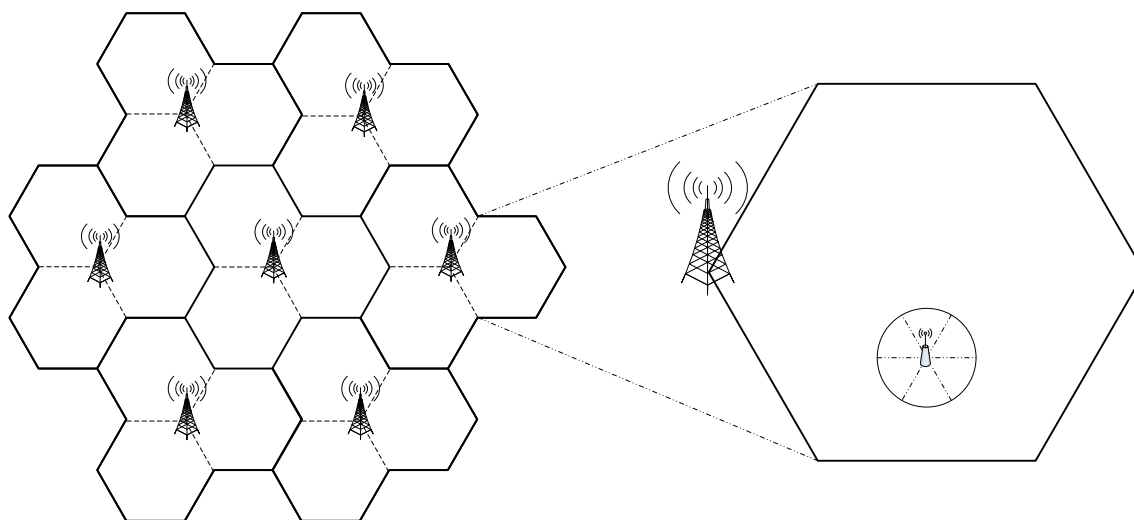### A3.3.2 Propagation models used in this study

In order to simulate a heterogeneous structure as detailed in § A3.3.3, the pathloss model for 72 GHz used in this section is based on § A4.4.

The fast fading model for 72 GHz band used in this section is the double-directional geometry-based stochastic model, which has been officially used for IMT-Advanced Self Evaluation Report [1], and this model is a system level model in the sense that is employed e.g. in the spatial channel model (SCM). The channel model parameters of urban micro cell scenario in Report ITU-R M.2135 are chosen for the evaluations in this section. For detailed parameters, refer to § 1.3.2 in Report ITU-R M.2135.

A3.3.3 Simulation scenario and system parameters

In this section, the capacity performance of outdoor-deployed millimetric wave cells is studied via system level simulations. A HetNet configuration is considered, where the macro cells are operating at 2 GHz band and pico millimetric wavecells operating at 72 GHz band. Macro stations are deployed to ensure network coverage, while pico stations are dedicated to high-data-rate communications at close distances between pico cells and UEs. The simulations are performed in the typical 3GPP HetNet scenarios. The system configuration largely follows the system simulation methodology in [2] at 2GHz band and some new features, in particular the 72 GHz pathloss characteristics and high antenna beamforming gain capabilities, are introduced for millimetric wave communications.

FIGURE A3.3-1

Simulation scenario

In the simulation scenario, macro sites with intersite distance of 500 m are deployed and millimetric wavepico stations are uniformly distributed within each macro cell with minimum intersite distance of 90 m. Each macro station adopts 3 macro cells and each pico station adopts 6 pico cells. A one-tier wrap-around model is used for the network layout in the simulation where total 147 macro cells exist. Three cases with 1, 2 and 3 pico stations dropped uniformly within each macro cell are simulated. On average 20 UEs are randomly distributed within one pico cell with the minimum distance of 5 m between pico station and UE. All UEs are considered to be the outdoor UEs.

The RSRP-based criterion is used for UE cell selection. According to the RSRP received from macro cells and pico cells, the cell with the maximum RSRP is selected as the UE serving cell.

Directional antennas with high beamforming gains are a beneficial feature for millimetric wave communications. In our simulations, there are 32×32 antenna elements mounted on a $10\,\text{cm} \times 10\,\text{cm}$

plate for one pico cell, and the maximum beam gain is 34 dBi with about 4º beamwidth on both horizon and elevation planes. On UEs, for 72 GHz operation, uniform linear array of 64 antenna elements are mounted, and the maximum beam gain is 21 dBi. Considering the minimum distance between a pico station and UE and the minimum intersite distance of pico stations, the maximum elevation angle of the pico cell antenna is about 50º. Thus the 3D space covered by one pico cell can be separated into 195 beams. The 195 beam patterns are produced beforehand as a table list for system-level simulator to look up.

More simulation parameters for pico cells are available in Table A3.3-1.

TABLE A3.3-1

Simulation parameters

Parameters	Value
Carrier frequencies	72 GHz
Downlink bandwidth	2.5 GHz
ISD of pico stations	90 m
Pico cells per pico station	6
Pico stations per macro cell	1, 2, 3
Height of pico station	10 m
Height of UE	1.5 m
Max. pico Tx power	22 dBm
Pico antenna config.	32×32
Channels per pico cell	4
UE antenna config.	1×64
Noise figure	11 dB
Thermal noise level	−174 dBm/Hz
UE mobility speed	3 km/h
Number of UEs per pico cell	20
Traffic model	Full buffer
Scheduling	Proportional fairness

A3.3.4 Simulation results

The system-level simulations are carried out for the 72 GHz band and the corresponding results are shown in Fig. A3.3-2 and Table A3.3-2. The detailed system parameters have been listed in Table A3.3-1. In Fig. A3.3-2, "pico/cell" refers to the number of pico stations dropped per macro cell. In HetNet deployment, the proportion of UEs communicating with pico stations is also an essential factor in evaluating the overall system quality. Hence, the pico UE proportions in respective cases are provided in Table A3.3-2.

FIGURE A3.3-2

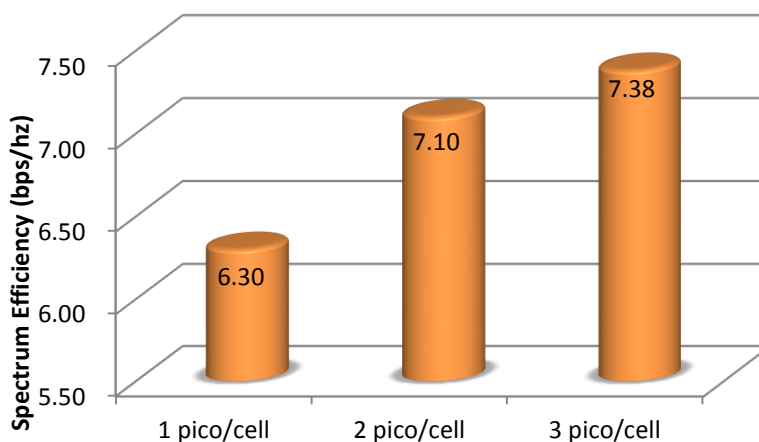**Spectrum efficiency of systems with various pico densities**

TABLE A3.3-2

Cell throughput comparison

Pico density	Throughput per macro cell	Average area throughput	Pico UEs/all UEs
1 pico/cell	94.45 Gbit/s	1 308.16 Gbit/s /km^2	58.26%
2 pico/cell	212.95 Gbit/s	2 949.42 Gbit/s /km^2	46.20%
3 pico/cell	332.20 Gbit/s	4 601.07 Gbit/s /km^2	41.13%

Observed from Table A3.3-2, close to 95 Gbit/s average throughput per macro cell can be achieved in a single pico station case. The overall throughput enables the spectrum efficiency of an average pico cell to reach 6.3 bps/Hz. In terms of area throughput, the value becomes 1308.16 Gbit/s/km^2. When increasing the pico density in each macro cell, the throughput ascends almost linearly with the number of pico stations. In case of 3 pico stations/macro cell, the throughput can reach as high as 332.20 Gbit/s, with an area throughput up to 4601.07 Gbit/s/km^2. Correspondingly, the spectrum efficiency in this case can rise above 7.1 bps/Hz, as depicted in Fig. A3.3-2. The reason is that the pico UE proportion reduces when pico density increases. A denser environment causes a lower coverage.

References

[1] "Spatial channel model for multiple input multiple output (MIMO) simulations," Tech. Rep., 3GPP 25.996.

[2] 3GPP TR 36.814, v9.0.0, "Further advancements for E-UTRA physical layer aspects", March 2010.

A3.4 Performance comparison of millimetric overlay HetNet

Following previous work such as those reported in [Ref A3.4-0], this section provides results of a system level simulator developed in MiWEBA project. Details of the developed system architecture, link level simulator of the access link between the base station and mobile terminal, parameters employed in the system level simulator, evaluation methods and factors showing the impact of the proposed millimetric wave Overlay HetNets can be found in MiWEBA Deliverable 4.1 [11]. Preliminary systematic evaluation results are summarized below.

A3.4.1 Full-buffer scenario

A3.4.1.1 Examples of millimetric wave overlay HetNet deployment in two scenarios

This Section compares performance of millimetric wave HetNet deployment in full-buffer model for two example scenarios. Assumptions for e.i.r.p. for the two scenarios are different, leading to denser millimetric wave small cell deployment for case 2 scenario under assumption of constant UE density. In order to achieve similar SNR for cell edge UEs, in the simulations small cell radius for case 2 scenario is reduced by factor 2.5 in comparison with case 1 scenario, as illustrated in Fig. A3.4-1.

FIGURE A3.4-1

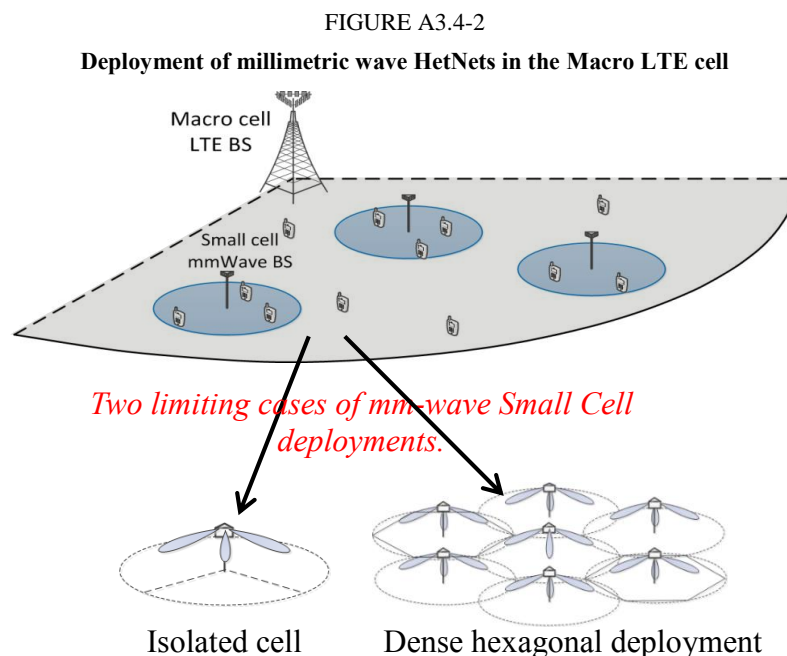**Deployment scenarios for case 1 and case 2**

A3.4.1.2 Deployment of millimetric wave small cells in the Macro LTE cell

In practical deployments millimetric wave small cells are randomly dropped in hotspots inside of Macro Cell area (see Fig. A3.4-2). But for initial performance evaluation the following two extreme cases are considered:

- "Isolated cell" – In this case small cells are dropped so rarely that interference between them can be neglected. The overlay millimetric wave network performance is estimated through simulating only one millimetric wave small cell.

- "Dense hexagonal deployment" – In this opposite extreme case millimetric wave HetNet deployment has maximal density and therefore the maximal inter-cell interference is achieved.

It should be noted that all other millimetric wave HetNet deployments will have performances between these two extreme cases.

---

[11] Work Package 4.1 "Radio Resource Management for mm-wave Overlay HetNets" http://www.miweba.eu/wp-content/uploads/2014/07/MiWEBA_D4-1_v10.pdf

FIGURE A3.4-2

Deployment of millimetric wave HetNets in the Macro LTE cell

Two limiting cases of mm-wave Small Cell deployments.

Isolated cell   Dense hexagonal deployment

A3.4.1.3 System level simulations results

The overlay millimetric wave HetNets parameters used for simulations are presented in Table A3.4-1. The parameters hereafter marked by (JP) and (EU) are for case 2 and case 1 scenarios, respectively.

TABLE A3.4-1

Millimetric wave simulation parameters

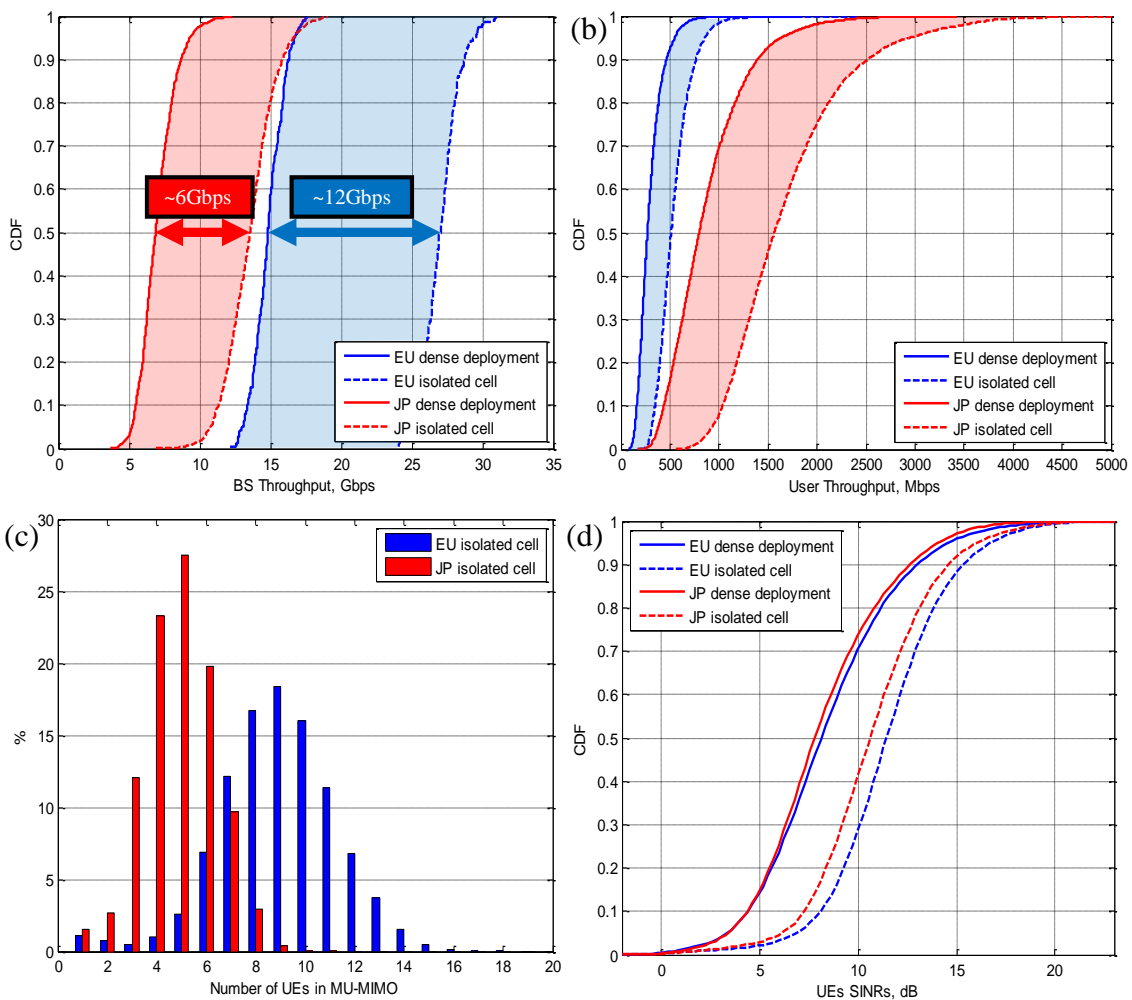| Parameters		Assumption
Deployment / Traffic load		Isolated single cell, Dense hexagonal / Full-buffer
Carrier frequency		60 GHz
Bandwidth / Frequency reuse		2 GHz / 3
Cell radius / Number of UEs per cell		20 m(JP), 50 m(EU) / 8(JP), 50(EU)
BS/UE antenna height		4 m / 1.5 m
Transmission scheme		MU-MIMO
Path loss model		LOS, Free space+O2 absorption (15 dB/km)
Link adaptation	Outer loop target FER	10 %
Scheduling	Type	Proportional-fair MU greedy scheduling
BS antenna element	Element gain/Front2Back	5 dBi/12 dB
	Horizontal/Vertical beamwidth	80°/80°
BS antenna array	Configuration/TX power	8 × 32 elements / 10 dBm(JP), 22 dBm(EU)
	Array model	Full adaptive antenna array
UE antenna		Single element, omni-directional

The main simulation results in full-buffer scenario obtained using the developed system level simulation platform are presented in Table A3.4-2 and Fig. A3.4-3.

TABLE A3.4-2

Full-buffer simulation results

Scenario	Small cell BS throughput (Gbit/s)	Avg. UE throughput (Mbit/s)	Cell edge UE throughput (Mbit/s)
Case 1 isolated cell	27.0	540	315
Case 2 isolated cell	13.6	1 695	927
Case 1 dense deployment	14.9	297	142
Case 2 dense deployment	7.0	876	379

FIGURE A3.4-3

Full-buffer simulation results. a) BS throughput CDF; b) UE throughput CDF; c) Number of Ues in MU-MIMO; d) Ues SINR CDF

The results presented in Table A3.4-2 show that densification of small cell BS in case 2 scenario by 5-6 times in comparison with case 1 scenario leads to 3 times higher average and cell edge UE throughputs for given area.

From comparison of two extreme cases: Isolated Cell, Dense Hexagonal deployment (see CDF BS throughput curves on Fig. A3.4-3(a)) the maximal inter-cell interference impact could be estimated: 6 Gbit/s in case 2 and about 12 Gbit/s in case 1 scenario. Therefore the implementation of modern interference mitigation schemes (e.g. CoMP, ICIC) may lead to substantial overlay millimetric wave system performance improvement (see for example [Ref A3.4-1]). More details about mmWave HetNet systems performance evaluations can be found in [Ref A3.4-2].

A3.4.2 Non-full-buffer scenario

Simulation execution parameters for the non-full-buffer scenario are shown in Table A3.4-3, noting that in order to alleviate the scheduler warming up effect, the first 100 ms results are discarded. In non-full-buffer scenario, Gamma and Poisson distributions are introduced to represent the traffic demand and traffic period of each user respectively.

Then, average traffic demand and traffic period are set to 62 Mbyte and 8s respectively, which corresponds to 1 000 times larger value than that of current value 62 kbyte per instruction measured in 2013 [Ref A3.4-0].

TABLE A3.4-3

Simulation Parameters

Parameter	Value
Evaluation period	1 000 ms (discard first 100 ms results)
Number of users (subscribers) per one macro cell	2 000
Number of smallcell BS per one macro cell	50
Average traffic demand	62 Mbyte
Average traffic period	8 s

The simulation results are summarized in Table A3.4-4.

TABLE A3.4-4

Simulation Results

Network	System rate	Average user rate	Cell edge (outage) user rate	System rate gain
HomoNet	121.46 Mbit/s	65.66 kbit/s	18.33 kbit/s	
HetNet (w/o MU-MIMO)	117 010 Mbit/s	63.25 Mbit/s	58.72 kbit/s	963
HetNet (w/ MU-MIMO)	153 580 Mbit/s	83.02 Mbit/s	126 kbit/s	1 264

In this realistic non-full-buffer simulation, about 1 000 times gain was obtained by installing 50 millimetric wave small cell BSs. By introducing MU-MIMO technology, a system rate gain of 1 264 times can be achieved since many users can obtain ultra-high speed transmission simultaneously. Also MU-MIMO can improve both the average user throughput and the outage user rate.

References

[Ref A3.4-0]   K. Sakaguchi, G. Khanh Tran, H. Shimodaira, S. Nanba, T. Sakurai, K. Takinami, I. Siaud, E. C. Strinati, A. Capone, I. Karls, R. Arefi, and T. Haustein, "Millimeter-wave Evolution for 5G Cellular Networks," IEICE Transactions on Communications, vol E.98-B, no. 3, pp. 388-402, March 2015.

[Ref A3.4-1]   G.V. Morozov, A.V. Davydov, A.A. Maltsev, "Analysis of the throughput of the cellular radio-communication systems using coordinated data transmission to suppress mutual unintended interference," *Radiophysics and Quantum Electronics,* vol. 57, no. 3, pp. 226-238, 2014.

[Ref A3.4-2]   A. Maltsev, A. Sadri, A. Pudeyev, R. Nicholls, R. Arefi, A. Davydov, I. Bolotin, G. Morozov, K. Sakaguchi and T. Haustein, "MmWave Smallcells is a Key Technology for Future 5G Wireless Communication Systems," in *European Conference on Networks and Communications (EuCNC'2014)*, Bologna, 2014.

Annex 4

Details of propagation channel measurements and modelling

A4.1   Description of a 10 and 18 GHz measurement campaign

The path loss models at 10 and 18 GHz are derived from a measurement campaign in 6 different scenarios listed in Table A4.1-1. They represent a typical European urban with transmitter and receiver antenna well below roof-top.

TABLE A4.1-1

Scenarios for obtaining 10 and 18 GHz path loss models

Scenario index	Street	LoS Range	NLoS Range
Scenario 1	NJV/NOVI	10-50 m	20-120 m
Scenario 2	Strandvej	10-80 m	20-90 m
Scenario 3	Bredegade / Nørregade	10-30 m	20-270 m
Scenario 4	Kennedy Arkaden	20-80 m	30-130 m
Scenario 5	Friis	10-80 m	10-120 m
Scenario 6	Salling	10-120 m	20-190 m

The channel measurements are performed in narrow band mode, i.e. continuous wave (CW) transmission, and the received power is recorded with R&S TSMW Radio Network Analyzer. The same antenna is used at both frequency bands, and it is compensated to achieve 'isotropic antenna' conditions. Figure A4.1-1 illustrates the measurement setup.

Figure A4.1-1+1 illustrates one of the measurement routes in the Scenario 1 around an office building. The GPS locations are recorded during the measurement to calculate the 3D distance from transmitter antenna (7 m height) to the current receiver antenna location (1.85 m height). Using the marker (in red line), the LoS and NLoS condition of each location is identified visually during the measurements. The LoS and NLoS measurements points are then fitted separately to derive the path loss model with respect to a close-in reference distance (d_0):

$$PL(d)[\text{dB}] = PL(d_0) + 10n\log 10(d/d_0) + X_0$$

where $PL(d_0)$ is reference path loss calculated using free space path loss model, d and d_0 are distance in meter, n is the path loss exponent and X_0 is a zero mean Gaussian distributed random variable (dB) with standard deviation σ. Figures A4.1-1+2, A4.1-1+3, A4.1-1+4 and A4.1-1+5 show the measurement points and fitting curve for both LoS and NLoS condition, with the rms error after fitting.

FIGURE A4.1-1

Measurement setup

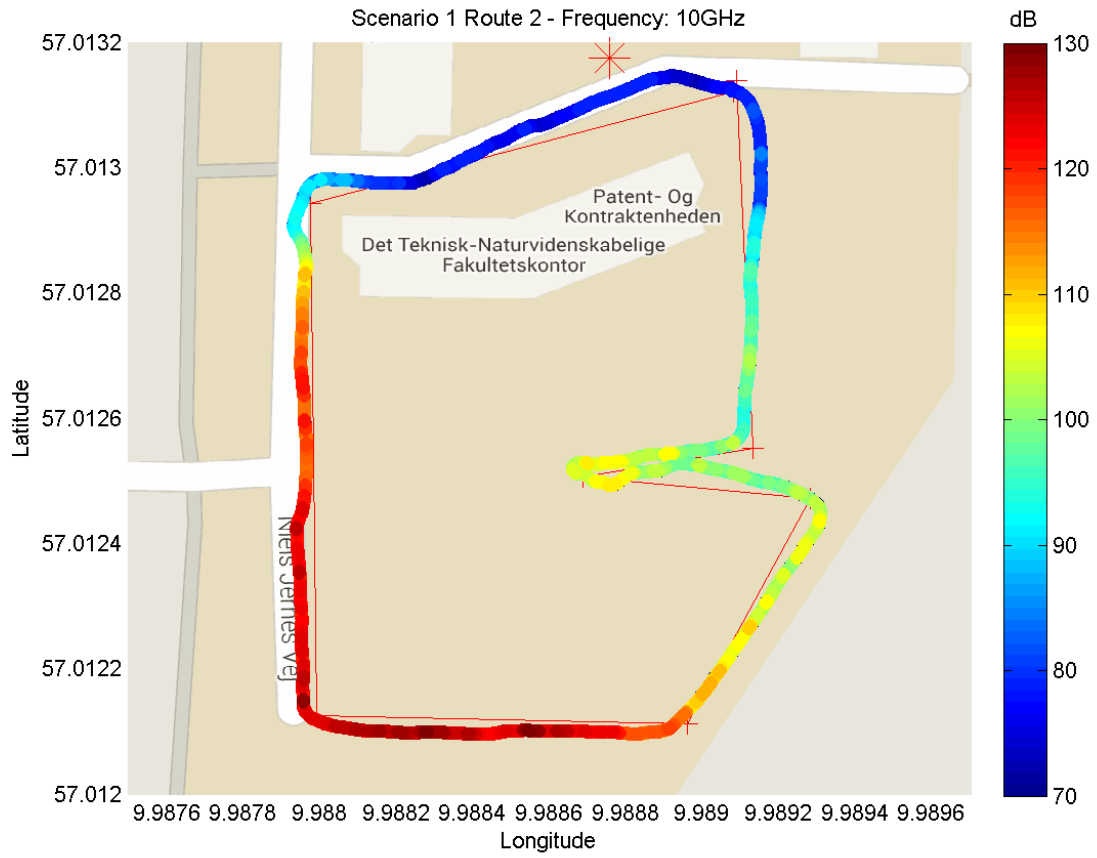FIGURE A4.1-1+1

One of the measurement routes

FIGURE A4.1-1+2

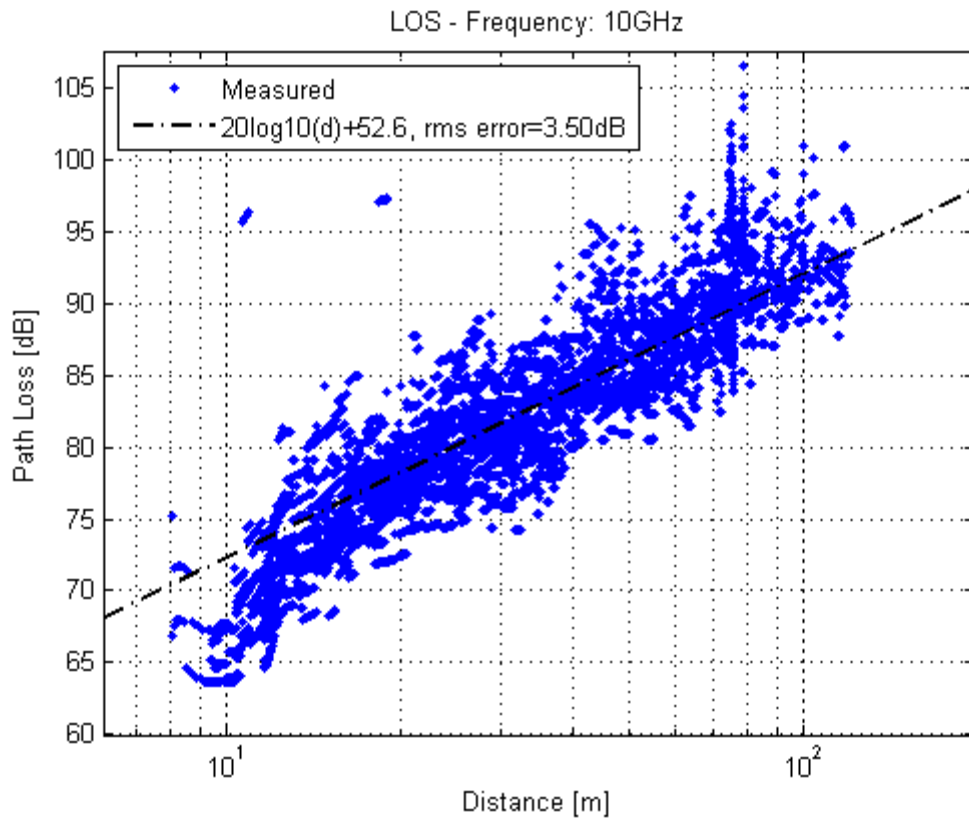**LoS measurement points and fitting curve at 10 GHz**

FIGURE A4.1-1+3

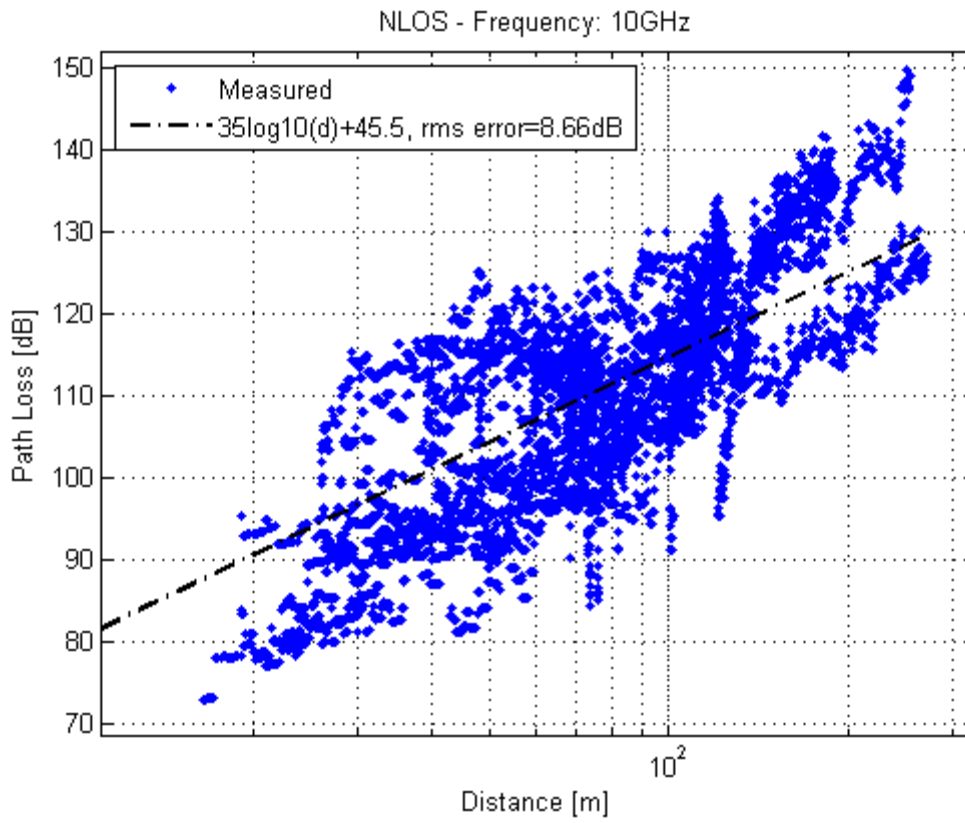**NLoS measurement points and fitting curve at 10 GHz**

FIGURE A4.1-1+4
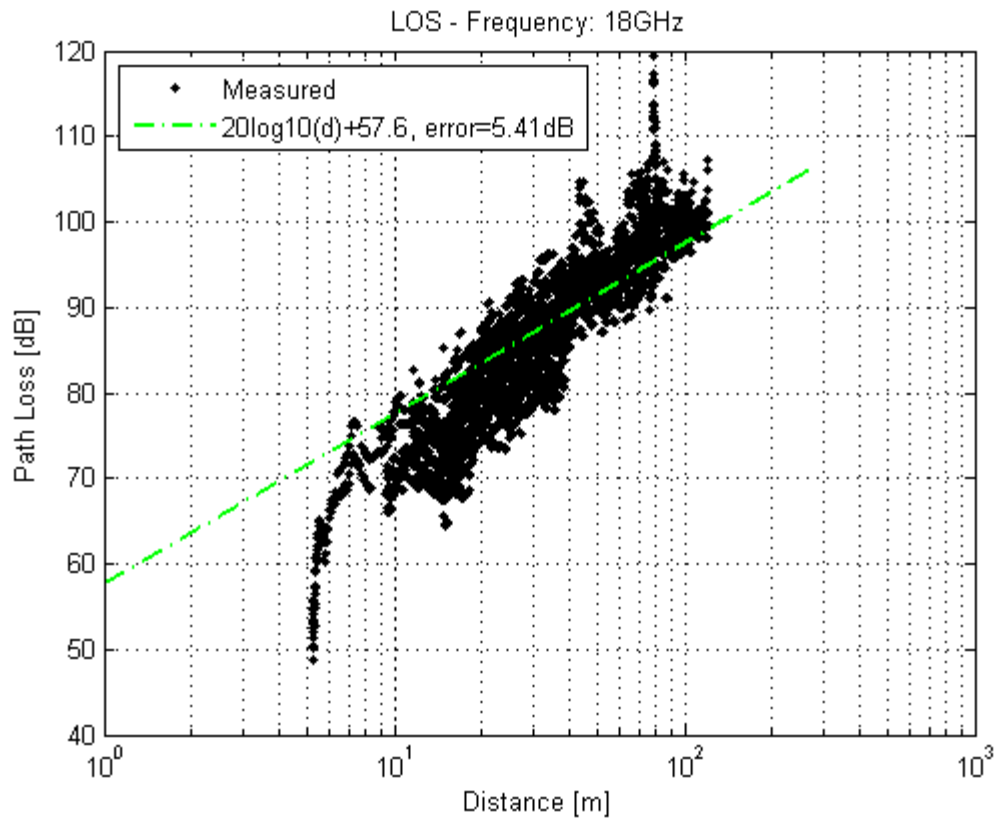
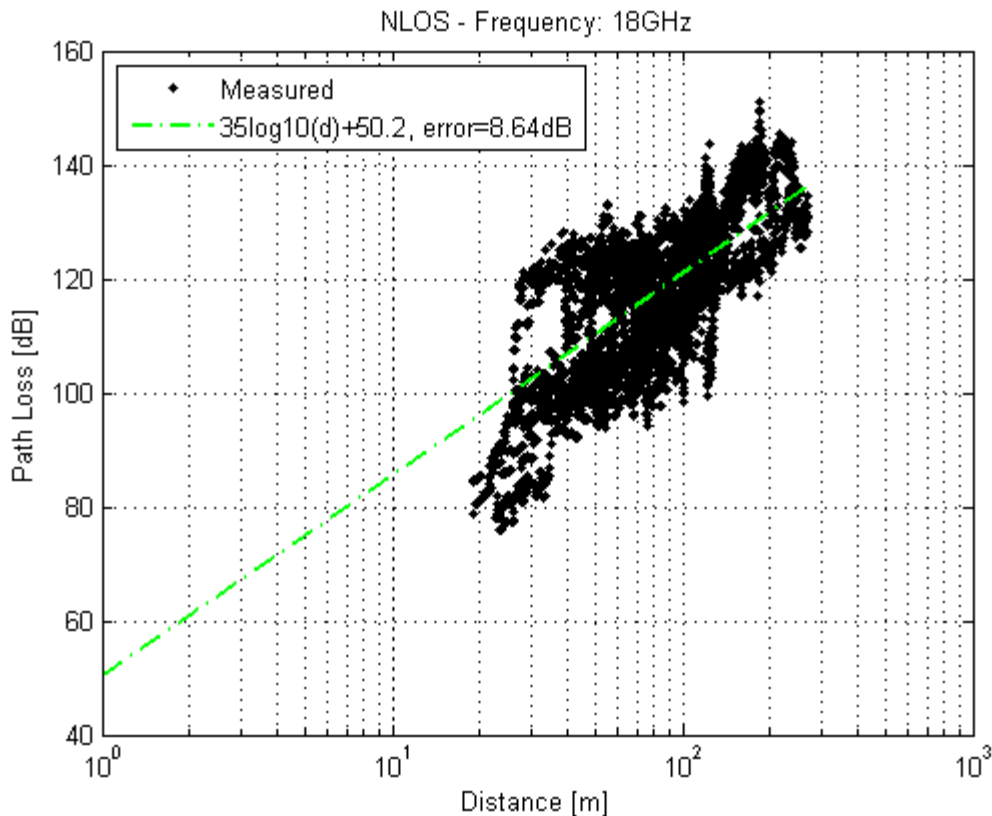**LoS measurement points and fitting curve at 18 GHz**

FIGURE A4.1-1+5

NLoS measurement points and fitting curve at 18 GHz

A4.2 Outdoor NLoS channel measurement results

Outdoor radio propagation

In order to investigate the feasibility of millimetric wave bands, channel measurement campaigns were conducted in various outdoor environments. This section shows measurement results obtained at the Univ. of Texas, Austin; in the Manhattan, New York, dense urban area, and at Samsung Electronics, Suwon Campus, Korea. It was expected that, since building surface walls are highly reflective in these bands, a radio communication link can be provided even through multiple NLoS paths. The measurement results confirm such expectations.

Campaign 1: University Campus (Univ. of Texas, Austin), 38 GHz [12] [13]
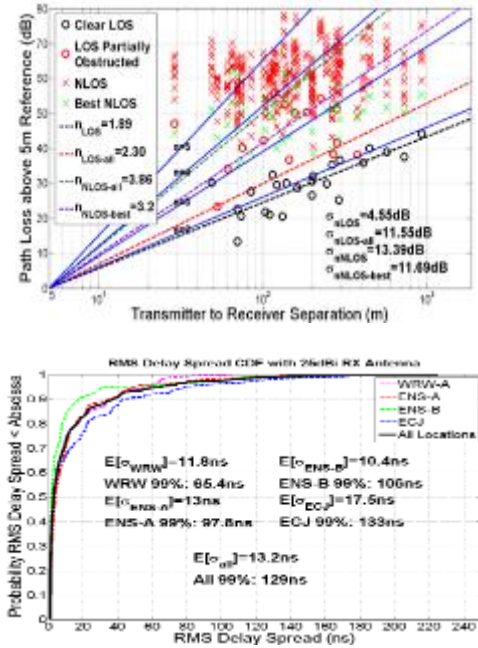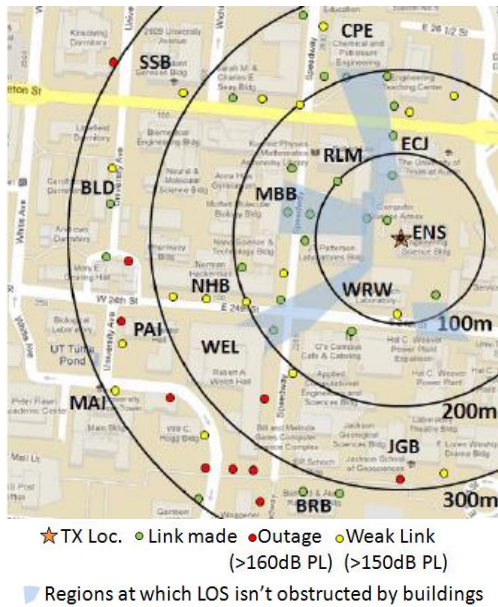
The first measurements were carried out in the 38 GHz band at the Univ. of Texas, Austin, campus. In this campaign, the channel bandwidth was 750 MHz, transmission power (at the amplifier) was 21 dBm, and horn antenna gain was 25 dBi for both transmitter and receiver.

For the given environments, communication links between transmitter and receiver were successfully made with distances of up to 200 m. Note that even at many locations beyond 200 m, the link could be made. Pathloss exponents calculated from the beamforming-based measurements are 1.89~2.3 for LoS links, and 3.2~3.86 for NLoS links.

Note that the subscript of 'NLoS-all' in the figure indicates a statistical value obtained from all NLoS results, while 'NLoS-best' represents the value obtained from the NLoS results only for the best matched Tx and Rx beams. We can see that radio propagation characteristics can be made more favourable by matching the best Tx and Rx beams.

FIGURE A4.2-1

Left: Measurement sites in UT Austin campus, Right: Pathloss and RMS delay spread results
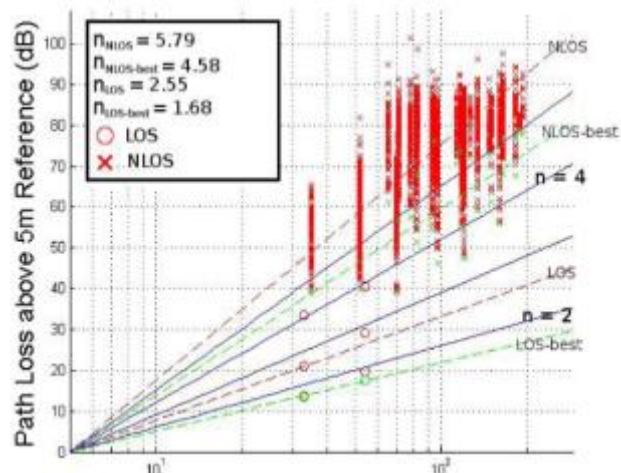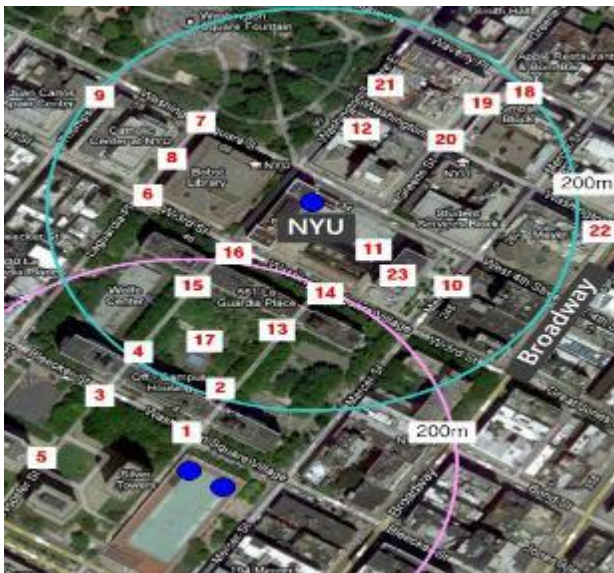
Campaign 2: Dense Urban (New York, Manhattan), 28 GHz [14][15]

The second step of measurements were carried out in the 28 GHz band in the Manhattan area. Channel bandwidth was 400 MHz, transmission power at the amplifier 30 dBm, and horn antenna gain was 24.5 dBi for both transmitter and receiver. Since these measurement environments are dense urban where buildings have brick and concrete walls, received signals are lower than at the UT Austin campus. For these measurements, the derived pathloss exponents are 1.68 in LoS and 4.58 in NLoS links, for the case of the best Tx and Rx beam matching.

FIGURE A4.2-2

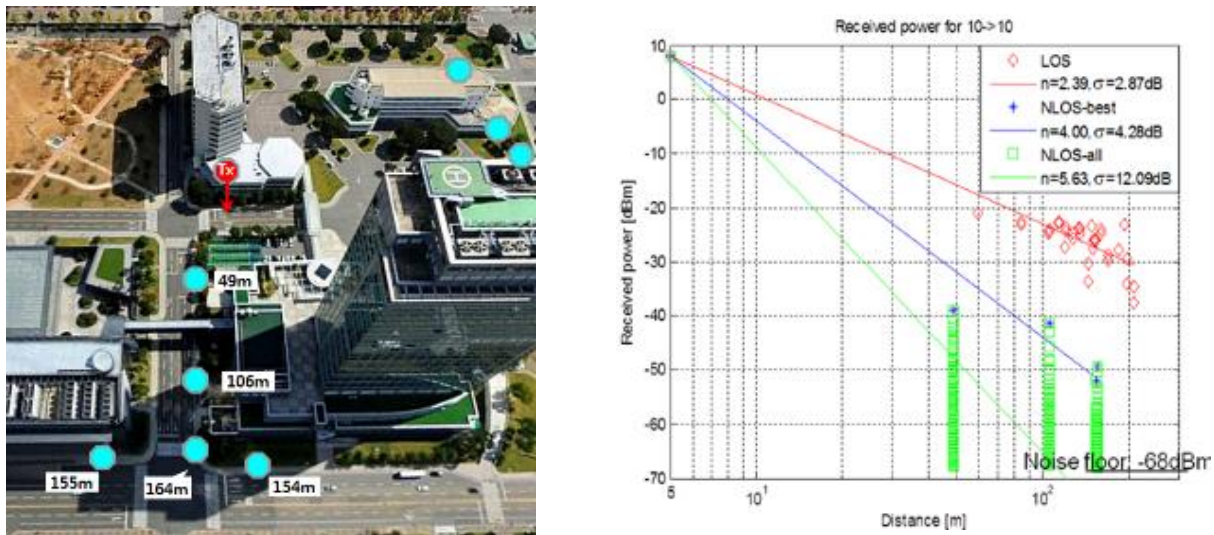**Left: Measurement sites in Manhattan, Right: Pathloss results**

Campaign 3: Research Campus (Samsung Electronics, Suwon Campus), 28 GHz [16]

The last measurements were performed in the 28 GHz band at the Samsung Complex, Suwon, Korea. Channel bandwidth was 500 MHz, transmission power at the amplifier was 18 dBm, and horn antenna gain was 24.4 dBi for both transmitter and receiver. These measurements show that the pathloss exponents are 2.39 for LOS conditions, and 4.0 for NLoS links with best matching of the Tx and Rx beams.

FIGURE A4.2-3

Left: Measurement sites of Samsung complex in Suwon, Korea, Right: Path loss exponent results

The results obtained from the three measurement campaigns in the 28/38 GHz bands yielded pathloss exponents for NLoS links of between 3.2 and 4.58. This range is not much discrepant from that in the existing bands identified for IMT (i.e. 3.67~3.91) [17].

Lastly, we would like to note that rain attenuation will place natural limits on radio propagation in bands above 6 GHz. In case of even heavy rain with rate of 60mm/hour, rain attenuations for 200 meter distance are only 2 dB and 3 dB in 27 GHz and 38 GHz, respectively [18] [19].

[12]   Murdock, J.N., Ben-Dor, E., Yijun Qiao, Tamir, J.I., Rappaport, T.S, "A 38 GHz cellular outage study for an urban outdoor campus environment,"Wireless Communications and Networking Conference (WCNC), 2012 IEEE.

[13]   Rappaport, T.S., Ben-Dor, E., Murdock, J.N., Yijun Qiao, "38 GHz and 60 GHz angle-dependent propagation for cellular & peer-to-peer wireless communications," International Conference onCommunications (ICC), 2012 IEEE.

[14]   Y. Azar, G. N. Wong, T. S. Rappaport, et al,"28 GHz Propagation Measurements for Outdoor Cellular Communications Using Steerable Beam Antennas in New York City,"submitted to IEEE International Conference on Communications (ICC), 2013. Jun.

[15]   H. Zhao, R. Mayzus, T. S. Rappaport, et al, "28 GHz Millimeter Wave CellularCommunication Measurements for Reflection and Penetration Loss in and around Buildings in New York City," submitted to IEEE International Conference on Communications (ICC), 2013. Jun.

[16]   RWS-120021, 3GPP Workshop, Jun, 2012.

[17]   ITU-R M.2135, "Guidelines for evaluation of radio interface technologies for IMT-Advanced".

[18]   Tom Rosa, "Multi-gigabit, MMW Point-to-point Radios: Propagation Considerations and Case Studies," Microwave Journal, August 8, 2007.

[19]   ITU-R P.838-3, "Specific attenuation model for rain for use in prediction methods", 2005.

A4.3 Measurements and quasi-deterministic approach to channel modelling at 60 GHz

A4.3.1 Introduction

Here, a quasi-deterministic (Q-D) approach for modelling outdoor and indoor millimetric wavechannels (Section III) is presented[12]. The 60 GHz band is exactly in the middle of the millimetric wave frequency range of 30-90 GHz and the measurement results may be extrapolated in both directions. The street canyon measurement campaign was performed with omnidirectional antennas in combination with supporting ray-tracing simulations. The feasibility of millimetric wavesmall cell has been shown, but at the same time, the high time variance of the propagation channel caused by movements of the UE and neighbouring objects has been discovered. The second measurement campaign was performed using directional and highly directional antennas on a university campus environment. The effects of ground reflection and scattering were investigated; the cross-polarization discrimination coefficients were estimated. An additional study was carried out to analyze the impact of UE movement on the channel transfer function.

As a result, the new Q-D approach has been developed for modelling outdoor channels at 60 GHz. This methodology is based on the representation of the millimetric wave channel impulse response by a few quasi-deterministic strong rays (D-rays) and a certain number of relatively weak random rays (R-rays).

Following the proposed Q-D modelling methodology, the channel models for open area (university campus), street canyon and hotel lobby scenarios have been developed. The appropriate model parameters for access links were selected on the base of experimental measurements and ray tracing simulations. The versatility of the Q-D methodology allows extending the developed channel model to other usage cases with the same environment geometries like Device-to-Device (D2D) and street-level backhaul links. The explicit introduction of the deterministic (D-rays) and random (R-rays) within the Q-D channel modelling approach have allowed the proper description of the real dynamic outdoor environment with taking into account the mobility and blockage effects.

There is increasing interest in using millimetric wavebands for next-generation mobile wireless networks [1], [2]. The development of new communication systems and standards requires adequate millimetric wavechannel models applicable to multiple usage cases and a wide frequency range from 30 GHz up to 90 GHz. However, despite a number of experimental measurement campaigns and results ([3], [4], [5], [6], [7], [8], [9], [10]), there are few millimetric wavechannel models available. One of the released millimetric wave channel models ([11], [12]) was developed for the IEEE 802.11ad standard in the 60 GHz band (57-64 GHz) [13]. It is based on experimental measurements and ray-tracing studies and focused on a limited number of indoor scenarios with site-specific parameterization. The most recent METIS 2020 intermediate deliverable D1.2 [14] suggests exploiting different channel modelling approaches including both stochastic (generic) and map-based (site-specific) models with parameterization from measurement results.

Signal propagation in the bands lower than 6 GHz is rather well studied; a number of accurate and realistic modelling approaches exist as basis for both link and system level evaluations. The millimetric waveband needs to be thoroughly investigated for wireless communication, since the about 10x increase of carrier frequency leads to qualitative changes of the propagation properties.

Firstly, the short wavelength results in a significantly higher propagation loss according to Friis' equation. To support high-gain antennas, the channel model shall take into account spatial (angular)

---

[12] This approach was developed in the framework of the FP7 MiWEBA project (MiWEBA Project homepage http://www.miweba.eu/project.html (FP7-ICT-2013-EU-Japan, project number: 608637), 2013) on the basis of two independent experimental measurement campaigns at 60 GHz. The project deliverable document D5.1 is available online (MiWEBA project deliverable D5.1, 2014).

coordinates of the channel rays at TX and RX and also support the entire spectrum of antenna technologies, from RF beamsteering to baseband MIMO processing.

Secondly, as confirmed by a number of works [11], [15], [16], [17], the 60 GHz propagation channel has a quasi-optical nature. The fraction of power arriving at the receiver due to diffraction and transmission through objects is practically not usable. Most of the transmission power is propagated between the transmitter and the receiver through the LoS and a few low-order reflected paths. To establish a communication link, steerable highly-directional antennas have to be used, pointing along the LoS path (if available) or one of the reflected paths. An additional consequence of the quasi-optical propagation nature is that the channel model should be fully 3-dimensional, taking into account signal propagation in a real environment. For example, map-based ray tracing can be an effective means for prediction of spatial and temporal properties of the channel paths and may be used to assist the channel modelling.

Thirdly, it should be noted that with ideal reflections, each propagation path would include only a single ray. However, as demonstrated by experimental investigations [18], [19], [20] each reflected path actually may consist of a number of rays closely spaced to each other in the time and angular domains due to roughness and structure of the reflecting surfaces. Hence, the clustering approach is directly applicable to channel models for millimetric waveindoor and outdoor systems with each cluster of the model corresponding to the LoS or a few reflected paths.

Fourthly, another important aspect of millimetric wave propagation is polarization. As demonstrated by experimental studies with millimetric wave prototypes [21], the power degradation due to polarization mismatch between the antennas and depolarization caused by the channel can be as high as 10-20 dB.

Thus, a proper 3D channel model for millimetric wave bands requires in particular an accurate representation of space-time characteristics of the propagation channel (basic requirement) for main usage models of interest; beam forming with steerable directional antennas support at TX and RX without limitation on the antenna technology; inclusion of polarization characteristics of antennas and signals, and support of non-stationary characteristics of the propagation channel in mobile environments.

State-of-the-art mobile communications channel models describe path loss (PL) and spatial channel characteristics separately, typically comprised of the clustered channel impulse responses (CIRs) and angular spread statistics. Latest works on millimetric wave channel models also follow such approach [17], [22], [23] and apply different cluster analysis techniques to the experimental data. Such approaches work very well for bands below 6 GHz, where a great number of reflected, refracted and diffracted rays are observed. However, this is no longer valid for millimetric wave with their quasi-optical behaviour. Additionally, for long distances (e.g. about 20-50 m), the PL specifics of millimetric wave signals lead to a strong attenuation of distant reflections and dominance of rays close to LoS path. Also, new approaches to characterize channel mobility, Doppler and blockage effects are needed, as well as new experimental measurements focused on the characterization of those parameters. Moreover, the dynamic nature of the busy outdoor environment leads to partial or full path blockage, which should be properly simulated. The blockage models were developed for the indoor cases [24], but rich dynamic outdoor environment with lots of cars and buses, pedestrians and cyclists may require new approaches for channel measurements and measurement data processing.
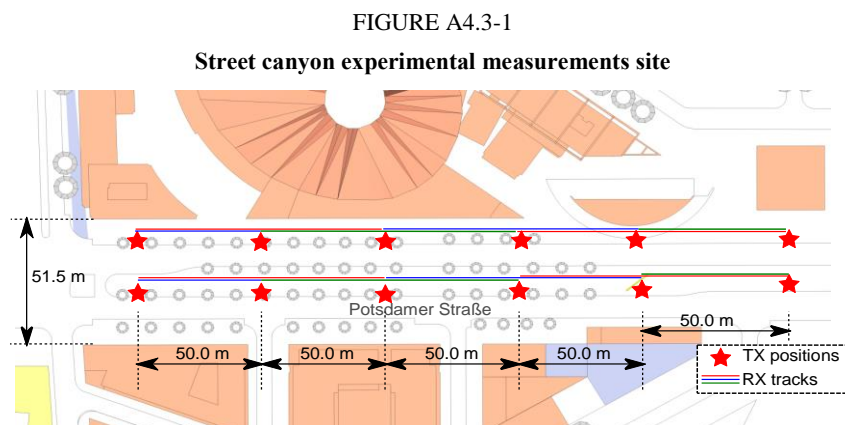
A.4.3.2 A novel methodology for experimental measurements in the 60 GHz band

This section describes a novel methodology for experimental measurements in the 60 GHz band. The novelty consists in exploiting two antenna types, omnidirectional and directional at both the TX and RX to gather experimental results. Omnidirectional antennas are used primarily for long-term millimetric wave channel measurements in a number of static environments with stationary TX and RX positions at a fixed distance, and multiple dynamic environments with a moving RX and a stationary TX. The experimental setup and traditional interpretation of the measurement results in more detail can be found in [25], [26], [27].

In previous work, [14], [15], [28], [29] the results of similar measurements were traditionally used to evaluate the propagation path loss exponents and channel power delay profiles. In the present work, we use the measurement results to justify and validate the proposed Q-D approach to channel modelling. For that purpose, directional antennas are also used in broadband millimetric wavechannel measurements for the detailed investigation of fast short-term channel fading effects.

a) Experimental measurements with omnidirectional antennas

A complex urban outdoor street canyon access scenario, see schematic top view in Fig. A4.3-1, was selected for the measurements with omnidirectional antennas. The measurement campaign was carried out in the Potsdamer Straße in Berlin, Germany. As can be seen, this scenario is a typical street canyon with modern buildings on both sides, multiple car lanes separated by a pedestrian walkway, medium-sized trees and street furniture such as lampposts, bus stops, bicycle stands and seats placed on the sidewalks.

FIGURE A4.3-1

Street canyon experimental measurements site

The TX antenna was mounted at a height of 3.5 m to represent a typical small cell base station being added to existing lampposts. The RX was mounted on a mobile cart with an antenna height of 1.5 m, modelling the user equipment (UE). Multiple static measurements were performed for stationary TX and RX positions separated by 25 m. Mobile measurements were conducted as well, where the RX was moved at a constant speed along the sidewalk up to a distance of 50 m to each side of the stationary TX.

The channel sounder used in the measurement campaign is based on a self-developed FPGA platform and has the key parameters listed in the Table. The primary output of the sounder is a channel impulse response (CIR) for each measurement snapshot taken every 800 µs.

TABLE A4.3-1

Measurement system parameters

Parameter	Omnidirectional measurements	Directional measurements
Frequency	60 GHz	60 GHz
Bandwidth	250 MHz	800 MHz
Output power	15 dBm	2.4 dBm
Antenna gain	TX: 2 dBi, RX:2 dBi	TX: 19.8, 34.5 dBi RX: 12.3 dBi
Antenna pattern	TX:omnidirectional RX:omnidirectional	TX:HPBW = 18°/14°, 3° RX: HPBW = 30°

During the static measurements, 62,500 of those snapshots were obtained for each given position of the TX and RX pair, resulting in a single trial observation time of 50 s. Overall, 20 different static positions have been measured and the corresponding data set comprises 1.25 million CIRs.

The measured channel impulse responses were processed by a simple threshold peak detection algorithm:

A point in the PDP $P(t_k)$ is identified as peak if:

$$P(t_{k-1}) < P(t_k) > P(t_{k+1}) \text{ and}$$

$$P(t_k) > \text{estimated noise level} + 10 \text{ dB}$$

The peaks corresponding to the strongest rays or multipath components (MPCs) resolved by the sounder are shown in Fig. A4.3-2.

The ray delay vs. observation time bitmap is shown in Fig. A4.3-3, where the appearances/disappearances of the identified strongest rays are indicated for the whole observation time of 50 s.

FIGURE A4.3-2

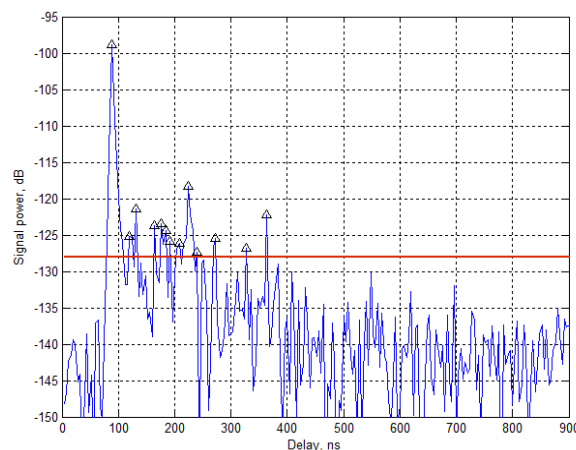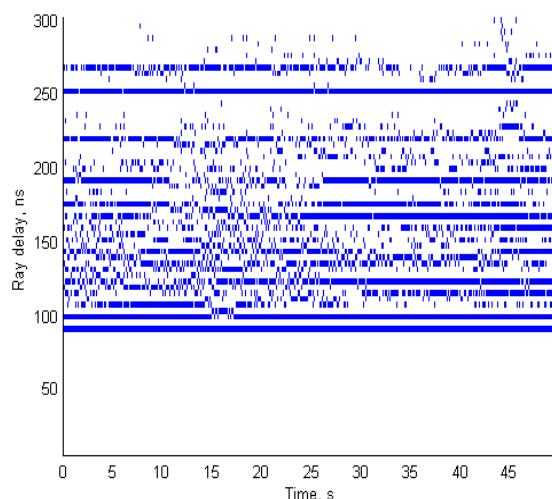**Single channel snapshot with identified peaks**

FIGURE A4.3-3

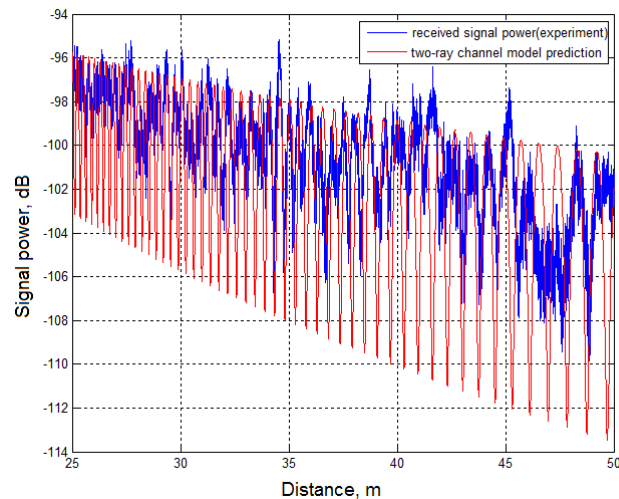**Ray delays vs. observation time bitmap**

It is worth noting that in every measurement the LoS ray arrives at 83 ns representing the delay caused by the 25 m separation between TX and RX. It can also be seen from Fig. A4.3-4 that there are other very stable rays. Those rays can be associated with the reflections from large static objects such as building walls and bus stop pavilions. At the same time, some rays are randomly appearing and disappearing due to small power and/or blockage. Those rays can be associated with the reflections from faraway objects and closely located elements of the dynamic street environment.

For the mobile measurements with the moving RX, a number of 40 measurement series with 62,500 snapshots each were done. Hence, the corresponding data set comprises 2.5 million CIRs. Since the RX was moved over 25 m during each run, a fine spatial sampling (0.4 mm spacing) over the whole section of the street canyon has been achieved.

Based on the gathered experimental data we have selected a simple two-ray channel model, taking into account only the direct ray and first (ground) reflected ray, for the initial approximation of the propagation channel. For example, Fig. A4.3-4 depicts the experimental measurement results versus a two-ray channel model approximation. From this data it can be seen that even this simple model is in good coincidence with experimental data. It should be noted that at distances of more than 25 m the ground-reflected ray is almost as strong as the direct ray due to sliding incidence with respect to the street surface. The interference between the two rays produces the large fading gaps observed in Fig. A4.3-4. Moreover, the fading depth can be used for a rough estimation of the reflection loss.

FIGURE A4.3-4

**Street canyon experimental measurement results versus two-ray model results
for the same parameters**

b) Broadband experimental measurements with directional antennas

The outdoor open-space area of the University of Nizhny Novgorod (UNN) was used to study the effect of fast fading in the broadband millimetric wave channel. A general view of the experimental scenario is shown in Fig. A4.3-5 and its schematic illustration is given in Fig. A4.3-6. The TX antenna was mounted on the vestibule roof of the university main campus building at the fixed height H1 = 6.2 m. The RX was mounted on a moving platform with adjustable antenna height H2.

For the experimental data acquisition and processing, a specially designed measurement platform was used with the key technical parameters listed in Table A4.3-I. Depending on the distance L0 the TX was equipped with antennas of different gain, e.g. the rectangular horn antenna 14×18 mm^2 with 19.8 dBi gain for distances less than 35 m or the highly directive lens antenna with large aperture (100 mm) and 34.5 dBi gain for greater distances. The RX was equipped with a round horn antenna with the diameter d = 14 mm and 12.3 dBi gain.
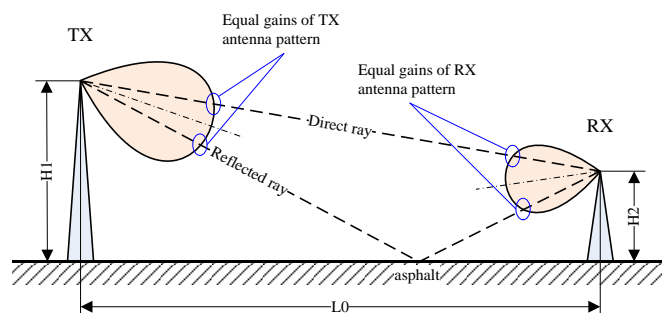
FIGURE A4.3-5

**General view of the experimental scenario for measurements with
directional antennas at both TX and RX side**

For a detailed investigation of fast-fading effects in the broadband (800 MHz) millimetric wavechannel caused by the motion of mobile users, we have minimized the impact of antenna patterns. To achieve that, the TX and RX antenna patterns had an initial orientation in 3D space as illustrated in Fig. A4.3-6 to provide equal gains for the direct and ground-reflected rays.
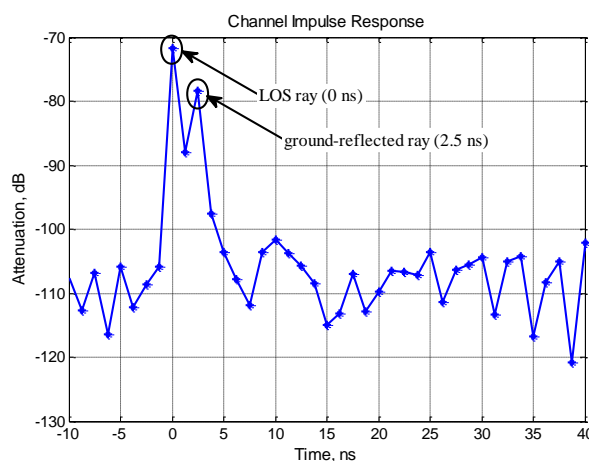
That configuration allowed keeping almost constant amplitudes of the direct and ground-reflected rays during the motion of the receiver. All other propagation paths caused by reflections from surrounding objects were more than 15-20 dB lower than these two strongest quasi-deterministic rays.

FIGURE A4.3-6

**Schematic illustration of the experimental scenario for measurements
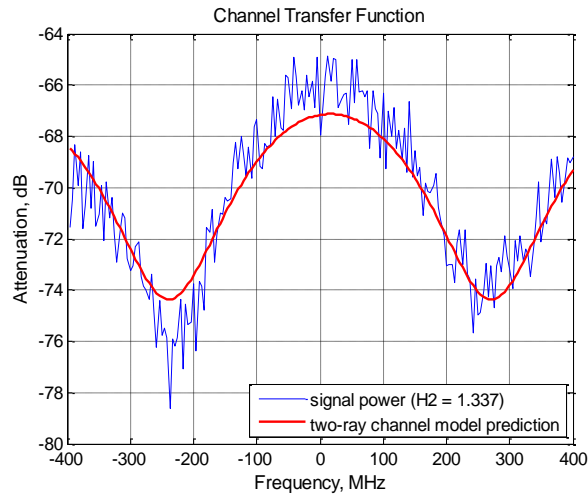with directional antennas at both TX and RX side**

An example of the measured channel impulse response is presented in Fig. A4.3-7. Two clearly distinguishable peaks in the CIR correspond to the LoS and the ground-reflected component. They are separated by 2.5 ns. The power difference between those two peaks is approximately equal to the ground reflection coefficient (–6 dB). This is in line with the given scenario geometry where $L_0 = 30.6$ m and H2 = 1.34 m. It should be stressed that the peaks were resolved for all other measured distances (20-50 m) because the sounding signal bandwidth used in those experiments was equal to 800 MHz, which provided a time resolution of up to 1.25 ns.

FIGURE A4.3-7

Channel impulse response, $L_0 = 30.6$ m
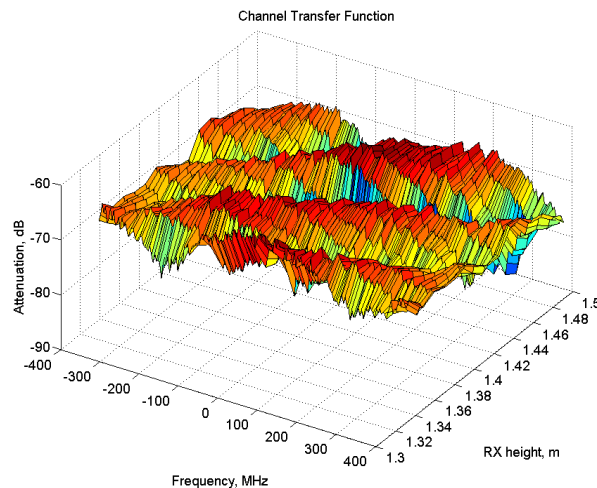

The corresponding measured channel transfer function (CTF) in frequency domain is illustrated in Fig. A4.3-8. For comparison, the result of the two-ray channel model approximation (the superposition of the direct LoS and ground-reflected ray), is also depicted. It can be seen that this simple model is in a good accordance with the experimental measurements with directional antennas.

FIGURE A4.3-8

Channel transfer function, L0 = 30.6 m

During the measurements with directional antennas, the dependence of the CTF on the RX vertical and horizontal motion was investigated for the distance $L_0 = 30.6$ m. In Fig. A4.3-9, for example, the CTF of 800 MHz bandwidth is presented when the RX height changes from 1.34 m to 1.5 m.

FIGURE A4.3-9

Dependence of the channel transfer function on the RX height H2, H-H, L_0 = 30.6 m

In these experiments the Horizontal-to-Horizontal (H-H) antenna polarization configuration was used. The measurements for other polarization configurations were also carried out to evaluate the cross-polarization ratio (XPR), which was discovered to be less than −25 dB. However, the use of the H-H configuration allowed us to exclude additional effects associated with the Brewster angle. As can be observed from Fig. A4.3-9, the channel shows a high frequency selectivity in 800 MHz bandwidth. But the most important outcome of these results is the very fast variation of the millimetric wavechannel when the RX height is changing. Moving the RX in the vertical direction by only 2-3 cm produces significant variations of the channel. Similar, but a bit smoother variations of the CTF were observed for horizontal RX movements.

Note, that due to wider bandwidth of the signal, strong fading of the total signal power like in the results for 250 MHz bandwidth is not observed.

Broadband experimental measurements with directional antennas have revealed the fine structure of the millimetric wave channel in the outdoor open-area environment. It can be concluded that a typical, i.e. moderately directional, mobile user antenna will receive two rays (the direct LoS ray and the ground-reflected ray) with rather small time delay (2.5 ns for 30 m). The interference of those two quasi-deterministic rays explains the fast fading effects observed in the experiments with omnidirectional antennas from the previous subsection and should be explicitly addressed in the channel modelling methodology.

A4.3.3 Novel quasi-deterministic channel model methodology

a) General structure of the channel model

In the IEEE 802.11ad channel modelling document (Maltsev, et al., 2010) the generalized description of channel impulse response is given by:

$$h(t, \varphi_{tx}, \theta_{tx}, \varphi_{rx}, \theta_{rx}) = \sum_i A^{(i)} C^{(i)}(t - T^{(i)}, \varphi_{tx} - \Phi_{tx}^{(i)}, \theta_{tx} - \Theta_{tx}^{(i)}, \varphi_{rx} - \Phi_{rx}^{(i)}, \theta_{rx} - \Theta_{rx}^{(i)}$$

$$C^{(i)}(t, \varphi_{tx}, \theta_{tx}, \varphi_{rx}, \theta_{rx}) = \sum_k \alpha^{(i,k)} \delta(t - \tau^{(i,k)}) \delta(\varphi_{tx} - \varphi_{tx}^{(i,k)}) \delta(\theta_{tx} - \theta_{tx}^{(i,k)}) \delta(\varphi_{rx} - \varphi_{rx}^{(i,k)}) \delta(\theta_{rx} - \theta_{rx}^{(i,k)})$$

where:

h :	generated channel impulse response.
$t, \varphi_{tx}, \theta_{tx}, \varphi_{rx}, \theta_{rx}$:	time, azimuth and elevation angles at the transmitter and receiver, respectively.
$A^{(i)}$ and $C^{(i)}$:	gain and the channel impulse response for the i-th cluster, respectively.
$\delta(\cdot)$:	Dirac delta function.
$T^{(i)}, \Phi_{tx}^{(i)}, \Theta_{tx}^{(i)}, \Phi_{rx}^{(i)}, \Theta_{rx}^{(i)}$:	time-angular coordinates of the i-th cluster.
$\alpha^{(i,k)}$:	amplitude of the k-th ray of the i-th cluster
$\tau^{(i,k)}, \varphi_{tx}^{(i,k)}, \theta_{tx}^{(i,k)}, \varphi_{rx}^{(i,k)}, \theta_{rx}^{(i,k)}$:	relative time-angular coordinates of k-th ray of the i-th cluster.

Hence the channel can be explicitly described by a set of rays and its parameters: ray powers and delays, angles of arrival and departure. This channel model may be also expanded to take into account polarization properties, see [11], [21]. Defining those parameters is required for channel model implementation.

b) Quasi-Deterministic (Q-D) channel modelling

To provide an adequate representation of the channel, the methodology of Quasi-Deterministic (Q-D) modelling is proposed. Under this approach, for each propagation scenario, the strongest propagation paths (rays which produce the substantial part of the received useful signal power) are determined first, and their contribution to the overall channel is calculated based on the geometry of the deployment and the locations of the base stations (BS) and the user equipment (UE) in a deterministic manner. Signal power delivered over each of the rays is calculated in accordance to theoretical formulas taking into account free space losses, reflections, polarization properties and UE mobility effects, i.e. Doppler frequency shift and user displacement.
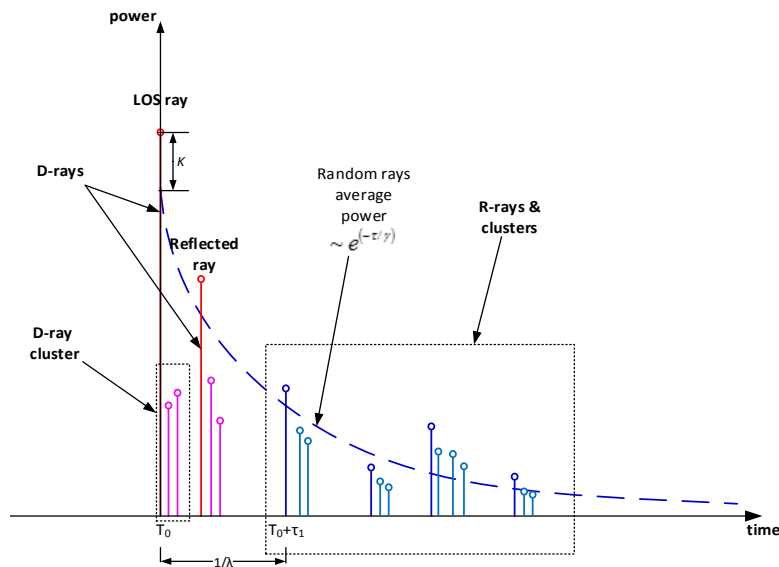
Some of the parameters in these calculations may be considered as random values (e.g. reflection coefficients) or even as random processes (e.g. UE motion). It should be noted, that the number of such quasi-deterministic rays (D-rays), which should be taken into account, depends on the considered scenario. In this respect, for outdoor open space scenarios it has been shown, that signal propagation properties are mostly determined by two D-rays – the LoS ray and the ground-reflected ray. From the measurements and the ray tracing modelling we can see that for the outdoor street canyon scenario, the propagation is determined mostly by 4 D-rays: the LoS, the ground-reflected

ray, the one reflected from the nearest wall and the one reflected from the ground and the nearest wall. For the hotel lobby (indoor access large public area) scenario more D-rays need to be modelled. For this scenario it is proposed to consider all rays with up to second order reflections as D-rays (in similar way as was adopted in the IEEE 802.11ad evaluation methodology for all considered indoor scenarios.

In real environments, numerous reflected waves arrive at the receiver from different directions in addition to the strong D-rays. For example, there are cars, trees, lampposts, benches, far big reflectors as houses, etc. All these rays are considered in the Q-D channel models as secondary random rays (R-rays) and are described as random clusters with specified statistical parameters extracted from available experimental data or more detailed ray tracing modelling.

The general time-domain structure of the Q-D model channel impulse response is shown in Fig. A4.3-10.

FIGURE A4.3-10

Channel impulse response structure

c) Effects of polarization

1) *Polarization for D-rays*

Following the proposed channel modelling methodology, all properties of the quasi-deterministic D-rays are explicitly calculated. The polarization matrix H contains all polarization information of the ray and is calculated on the basis of the reflections defined from the scenario geometry.

For the intra-cluster rays with the main D-ray, the polarization matrix is the same as for the main ray.

2) *Polarization for R-rays*

Random rays (R-rays) are defined by the power-delay profile and angular characteristics and are generated with regard to reproducing pre-defined probability distributions of these parameters. R-rays model far-away reflections and reflections from various random objects in the area. Most of the random rays may be considered as second (or higher) order reflections with corresponding polarization statistics. The channel polarization matrix distribution for second-order rays was investigated in [4] and corresponding distribution approximations were proposed. For simplicity, the distributions of the polarization matrix H components for weak R-rays are approximated as uniform in the interval [–1; 1] for diagonal elements, while the statistical distributions of the cross-coupling

components H12 and H21 are approximated by random variables, uniformly distributed in the interval (–0.1, 0.1) [21].

For the intra-cluster rays with the main random ray, the polarization matrix is the same as for the main R-ray.
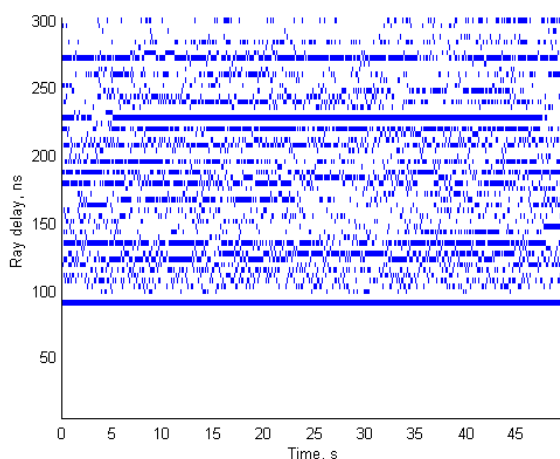
A4.3.4 Blockage modelling

In all environment scenarios considered in the MiWEBA project, the signal propagation paths are subject to blockage – by humans or vehicles interrupting the rays with static positions of the AP and UE, or by the UE movement in the areas where some rays are shadowed. The necessity of incorporating blockage in the 3D channel model is proven by experimental measurements. Another effect that should be considered is the appearance of new rays for a short time − for example reflections from passing vehicles, persons, and smaller objects the mobile RX is passing.

These effects were observed in the measurement results with omnidirectional antennas: Fig. A4.3-13 shows the ray bitmap for a measurement position close to the building walls. The nearest wall reflected rays can be identified close to LoS component (see Fig. A4.3-10). Figure A4.3-11 shows the ray bitmap for a measurement position in the middle of boulevard, far from walls, with lanes on the both sides.

FIGURE A4.3-11

Ray bitmap for middle-street measurement position

It can be seen that some steady rays in this case are interrupted due to blockage events. The blockage events can be observed also in the signal power graph (Fig. A4.3-12).

The percentage of the "ray activity" may be estimated from the ray bitmaps. Assuming ergodic properties of the blockage random process, the percentage of activity in time may be used as estimation of the blockage probability in the statistical ensemble. Figure A4.3-12 shows the bar chart of ray activity for the street canyon measurement scenario (near-wall position).

Figure A4.3-12 allows the classification of the rays with regard to the Q-D channel modelling ray categories:

−   The rays with activity percentage above 80% are the D-rays: strong and always present, until blocked.

−   The rays with activity percentage 30-80% are the R-rays: the reflections from far-away static objects, weaker and more susceptible to blockage due to longer travel distance.

– The rays with activity percentage below 30% are the R-rays of another type: the reflection from random moving objects (usually cars and buses), so called "flashing" rays, or F-rays. Such rays are not "blocked", they actually "appear".

FIGUREA 4.3-11

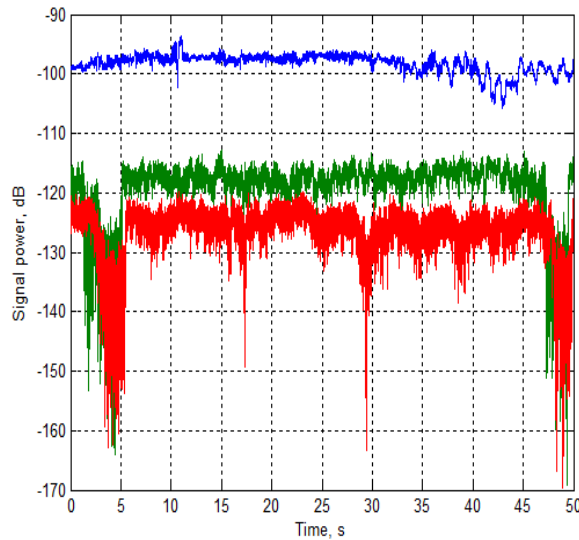**Ray blockage events in the experimental measurements**

FIGURE A4.3-12

Ray appearance probability for street canyon measurements (near-wall position)
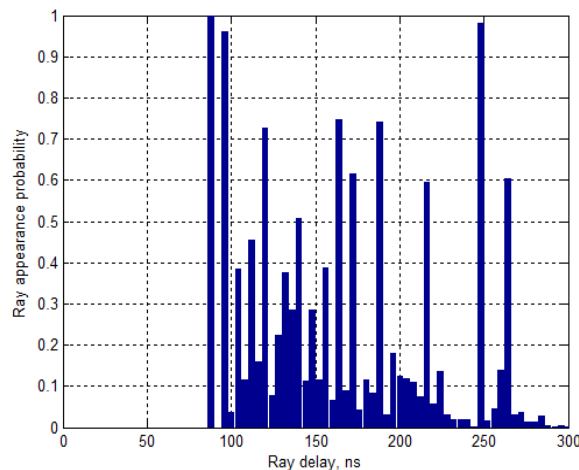

Figure A4.3-14 illustrates the mechanism of the ray blockage and ray appearance. Following the picture, the average duration of blockage and the duration of flashing reflections may be easily estimated:

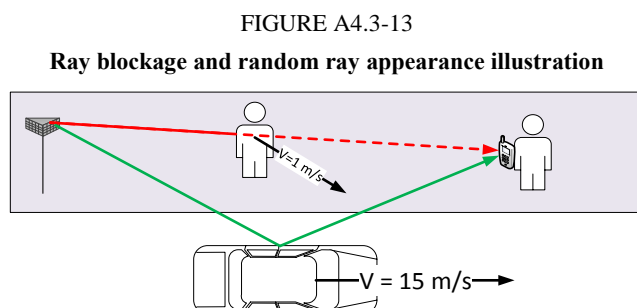Tblockage ~ 0.5 m (human diameter) / 1 m/s (average speed) ~ 0.5-1 s

Tflash ~ 4.5 m (car length) / 15 m/s (average speed) ~ 0.2-0.3 s

The analysis of the experimental data in ray diagrams Fig. A4.3-12 and Fig. A4.3-11 gives approximately the same values.

The average service period (SP, the duration of data and control frames) of the millimetric wave communication systems is equal to 1-3 ms (IEEE 802.11ad). This means that for the single blockage or flashing event period thousands service periods and tens of thousands frames will pass.

System level simulations rarely include more than thousand frames, so that blockage and appearance may be modelled as static random events, instead of dynamic stochastic process. The blockage parameters derived from the analysis are summarized in Table A4.3.4-I. During system level simulations the blockage state can be determined once per channel snapshot and retained over time.

FIGURE A4.3-13

Ray blockage and random ray appearance illustration

For VoIP and video streaming simulations, which require analysis of longer time periods, the blockage events may be introduced as Poisson process with corresponding parameters shown in Table A4.3.4-II.

TABLE A4.3.4-I

Blockage parameters for system level simulation

Parameter	Value
D-ray blockage probability, P_D	0.03
R-ray blockage probability, P_R	0.3
*F-ray appearance probability, P_F	0.2

TABLE A4.3.4-II

Blockage parameters for VoIP and video streaming simulations

Parameter	Value
D-ray blockage rate , λ_D	0.05 s^{-1}
R-ray blockage rate , λ_R	0.3 s^{-1}
D-ray and R-ray blockage duration, T	1 s
*F-ray appearance rate, λ_F	0.2 s^{-1}
*F--ray appearance duration, T_F	0.25 s

It should be noted that for the considered outdoor scenarios (open area and street canyon) we have developed channel models on the base of static reflections only (D-rays and R-rays). The parameter estimation of F-rays requires additional investigations and may be used in relation to special studies, which specifically focus on vehicle/human traffic model.

A4.3.5 Mobility effects

In the Q-D channel model mobility effects are described by introducing a velocity vector for each UE (see Fig. A4.3-14). Then, for each ray (D-ray or R-ray) the phase rotation may be simply calculated in accordance with the next expressions:

the phase rotation for the i-th ray caused by Doppler frequency shifts is defined as

$$\Delta\varphi_i(t) = 2\pi f_i^D t$$

where f_i^D is the Doppler frequency shift of the i-th ray. Its values can be calculated as

$$f_i^D = (\vec{v}, \vec{r}_i)\, F_c/c$$

where $\vec{v}$ is the vector of RX motion and $\vec{r}_i$ is the direction of the i-th ray arrival. The vector $\vec{v}$ can be decomposed as

$$\vec{v} = v_x\vec{\imath} + v_y\vec{\jmath} + v_z\vec{k}$$

It is assumed that the horizontal components of $\vec{v}$ are normally distributed random values with appropriate mean and standard deviation

$$P(v_x) = \frac{1}{\sigma_x\sqrt{2\pi}} e^{-\frac{(m_x - v_x)^2}{2\sigma_x^2}}, \; P(v_y) = \frac{1}{\sigma_y\sqrt{2\pi}} e^{-\frac{(m_y - v_y)^2}{2\sigma_y^2}}.$$

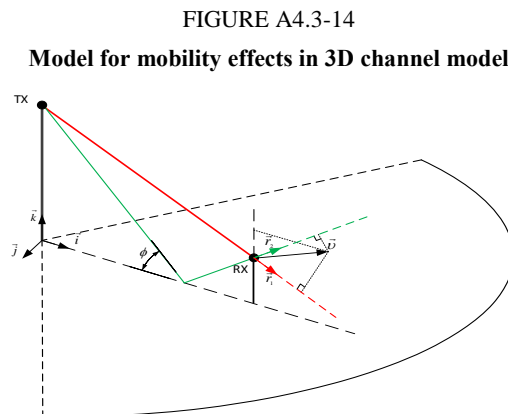The vertical component of $\vec{v}$ is defined as

$$v_z = \frac{dz}{dt},$$

Where $z(t)$ is a vertical UE displacement modelled as stationary Gaussian random process with a correlation function equal to

$$K_z(\tau) = \sigma_z^2 e^{\frac{-\tau^2}{\tau_z^2}}.$$

For this vertical motion correlation function the one-side power spectral density function of v_z can be calculated as

$$G_{v_z}(f) = 8\pi^{5/2}\sigma_z^2\tau_z f^2 e^{-(\pi\tau_z f)^2}.$$

FIGURE A4.3-14

Model for mobility effects in 3D channel model

A4.3.6 Street canyon millimetric wave 3D channel model example

The street canyon (outdoor access ultra-high-rate hot-spots) channel model represents a typical urban scenario: a city street with pedestrian sidewalks along long high-rise buildings. The access link between the APs on the lampposts and the UEs carried by persons is modelled in this scenario. The parameters of the model are summarized in TABLE A4.3.6-III.

The ray tracing analysis of the street canyon environment allows defining the most significant rays, which should be treated as D-rays. These are, in addition to the LoS ray, the ground reflected ray, and the nearest wall reflected ray and the wall-ground ray. It was shown from the experimental data and ray tracing simulation that those three NLoS rays contain more than 90% of the total NLoS ray power for all typical cases.

TABLE A4.3.6-III

Street canyon (outdoor access ultra-high-rate hot-spots) model parameters

Parameter	Value
AP height, H_{tx}	6 m
UE height, H_{rx}	1.5m
AP distance from nearest wall, D_{tx}	4.5 m
Sidewalk width	6 m
Street width	16 m
Street length	100 m
AP-AP distance, same side	100 m
AP-AP distance, different sides	50 m
Street and sidewalk material	asphalt
Street and sidewalk ε_r	$4 + 0.2j$
Street and sidewalk roughness σ_g (standard deviation)	0.2 mm
Building wall material	concrete
Building wall ε_r	$6.25 + 0.3j$
Building wall roughness σ_w (standard deviation)	0.5 mm

Table A4.3.6-III defines the scenario geometry and reflecting surface parameters, which can be used for a full description of the D-rays: the path distance, the AoA and AoD (calculated by using method of images), the ray power (obtained by using the path loss formula, Fresnel equations, and the formula that describes the losses from the rough surface):

$$P = 20\log 10\left(\lambda \middle/ 4\pi d\right) - A_0 d + R + F \ ,$$

$$R = 20\log 10\left(\frac{\sin\phi - \sqrt{B}}{\sin\phi + \sqrt{B}}\right),$$

$$B = \varepsilon_r - \cos^2\phi \ , \text{ for vertical polarization},$$

$$B = \left(\varepsilon_r - \cos^2\phi\right)\middle/ \varepsilon_r^2 \ , \text{ for horizontal polarization},$$

$$F = -\frac{80}{\log 10}\left(\frac{\pi\sin\phi\,\sigma_w}{\lambda}\right)^2 ,\text{in dB}.$$

The random ray temporal parameters are derived from the street canyon measurements with omnidirectional antennas, the distribution of angles is obtained from the ray tracing analysis. The parameters are summarized in Table A4.3.6-IV.

TABLE A4.3.6-IV

Street canyon (outdoor access ultra-high-rate hot-spots) model random ray parameters

Parameter	Value
Number of clusters, $N_{cluster}$	5
Cluster arrival rate, λ_c	0.03 ns^{-1}
Cluster power-decay constant, γ	20 ns
Ray K-factor	10 dB
AoA	Elevation: U[-20:20˚] Azimuth: U[-180:180˚]
AoD	Elevation: U[-20:20˚] Azimuth: U[-180:180˚]

The sub-rays within a ray cluster are also modelled as Poisson process with an exponentially decaying power-delay profile. The parameters are specified in Table A4.3.6-V. The intra-cluster rays are added to the D-rays and R-rays in the same way.

TABLE A4.3.6-V

Street canyon model intra-cluster parameters

Parameter	Value
Post-cursor rays K-factor, K	6 dB for LoS ray 4 dB for NLoS rays
Number of post-cursor rays, N	4
Post-cursor rays power decay time, γ	4.5 ns
Post-cursor arrival rate, λ_χ	0.31 ns^{-1}
Post-cursor rays amplitude distribution	Rayleigh
AoA and AoD distribution	$N(0,5˚)$ around main ray

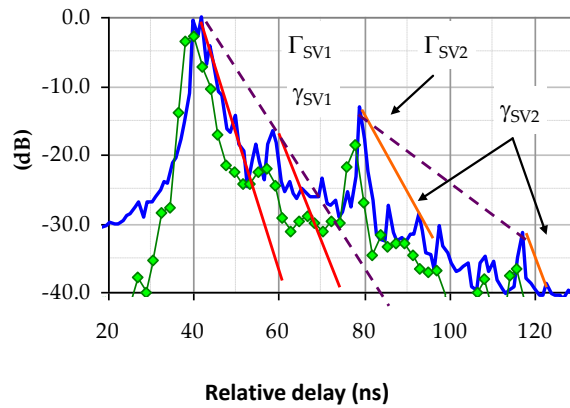## A4.3.7 Multipath modelling extension to outdoor for Hot Spots

The multipath modelling resorts from a multi-cluster approach as adopted in IEEE802.11 ad standards where intra-cluster modelling is carried out separately from inter-cluster modelling. Intra cluster modelling use indoor reference models as a first step and inter-cluster modelling resorts from dedicated experimental measurements performed in outdoor scenarios.

Indoor reference models utilizing a very large channel sounding bandwidth up to 1-2 GHz to benefit from high resolution path will be used to model intra-cluster behaviour of the 60 GHz propagation multi-cluster model as well as the CEPD (Canal Enregistré de Propagation) model derived from multi-rate theory and statistical analysis of measurements [38]. Several intra-cluster models are derived from different indoor scenarios defined in the IEEE802.11.ad standard and dedicated scenarios.

Inter-cluster modelling use outdoor multipath channel restricted to a channel sounding bandwidth size up to 250 MHz, ensuring multi-cluster resolution adjusted to 4 ns. Frequency sweeping techniques are used to evaluate the channel.
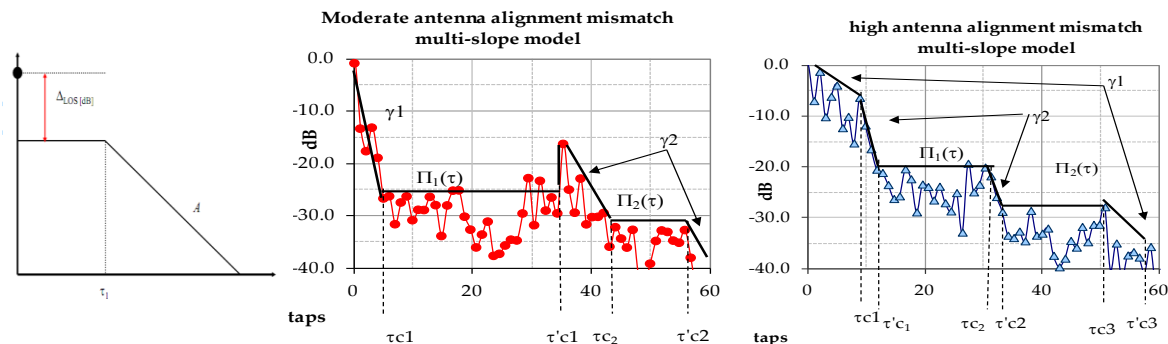
The multi-cluster model may then expressed in an analytical way, considering the combination of several Poisson distribution laws describing the time of arrival of echoes within different clusters and the time of arrival of clusters independently. This model will be built upon Kannan's model assumptions (Fig. A4.3-16), using measurements and CEPD modelling results [40].

FIGURE A4.3-16

Multi-cluster model based on multi-Poisson distribution

Another aspect to consider in the multipath propagation modelling is related to antenna alignment mismatch. When the environment is time-variant, models using the CEPD model and the Smulder's approach may be built following dedicated measurements and Smulder's model adaptation as illustrated on the Fig. A4.3-17.

FIGURE A4.3-17

Antenna alignment mismatch model concept

References

[1]   T. Rappaport, S. Sun, R. Mayzus, H. Zhao, Y. Azar, K. Wang, G. Wong, J. Schulz, M. Samimi and F. Gutierrez, "Millimeter Wave Mobile Communications for 5G Cellular: It Will Work!," *Access, IEEE,* vol. 1, pp. 335,349, 2013.

[2]   A. Maltsev, A. Sadri, A. Pudeyev, R. Nicholls, R. Arefi, A. Davydov, I. Bolotin, G. Morozov, K. Sakaguchi and T. Haustein, "MmWave Small Cells is a Key Technology for Future 5G Wireless Communication Systems," in *European Conference on Networks and Communications*, 2014.

[3]   ACTS MEDIAN project technical report, "IMST 60 GHz indoor radio channel measurement data".

[4]   Y. Azar, G. N. Wong, K. Wang, R. Mayzus, J. K. Schulz, Z. Hang, F. Gutierrez, D. Hwang and T. S. Rappaport, "28 GHz propagation measurements for outdoor cellular communications using steerable beam antennas in New York city," in *IEEE International Conference on Communications (ICC)*, 2013.

[5]   M. Peter, W. Keusgen and R. Felbecker, "Measurement and ray-tracing simulation of the 60 GHz indoor broadband channel: Model accuracy and parameterization.," in *Antennas and Propagation, 2007. EuCAP 2007. The Second European Conference on*, Edinburgh, 2007.

[6]   A. M. Hammoudeh, M. G. Sanchez and E. Grindrod, "Experimental analysis of propagation at 62 GHz in suburban mobile radio microcells," *IEEE Transactions on Vehicular Technology, vol. 48,* pp. 576-588, 1999.

[7]   A. Hammoudeh, M. Sanchez and E. Grindrod, "Modelling of Propagation in Outdoor Microcells at 62.4GHz," in *Microwave Conference, vol.1, no., pp.119,123*, 1997.

[8]   Z. Hang, R. Mayzus, S. Shu, M. Samimi, J. K. Schulz, Y. Azar, K. Wang, G. N. Wong, F. Gutierrez and T. S. Rappaport, "28 GHz millimeter wave cellular communication measurements for reflection and penetration loss in and around buildings in New York city," in *IEEE International Conference on Communications (ICC)*, 2013.

[9]   M. W. M. Peter, W. K. M. Raceala-Motoc, R. Felbecker, M. Jacob, S. Priebe and T. Kürner, "Analyzing human body shadowing at 60 GHz: Systematic wideband MIMO measurements and modeling approaches," in *IEEE 6th European Conference on Antennas and Propagation*, 2012.

[10]   A. Maltsev, R. Maslennikov, A. Sevastyanov, A. Lomayev, A. Khoryaev, A. Davydov and V. Ssorin, "Characteristics of Indoor Millimeter-Wave Channel at 60 GHz in Application to Perspective WLAN System," in *Antennas and Propagation (EuCAP)*, 2010.

[11]   A. Maltsev, V. Erceg, E. Perahia, C. Hansen, R. Maslennikov, A. Lomayev, A. Sevastyanov, A. Khoryaev, G. Morozov, M. Jacob, S. Priebe, T. Kürner, S. Kato, H. Sawada, K. Sato and H. Harada, "Channel Models for 60 GHz WLAN Systems," IEEE 802.11ad 09/0334r8, 2010.

[12]   A. Maltsev, R. Maslennikov, A. Sevastyanov, A. Lomayev and A. Khoryaev, "Statistical channel model for 60 GHz WLAN systems in conference room environment," in *Antennas and Propagation (EuCAP)*, 2010.

[13]   "WiGig MAC and PHY specification, v 1.1," 2012.

[14]   METIS2020, D1.2 "Initial channel models based on measurements", 2014.

[15]   T. S. Rappaport, S. Shu, R. Mayzus, Z. Hang, Y. Azar, K. Wang, G. N. Wong, J.K. Schulz, M. Samimi and F. Gutierrez, "Millimeter Wave Mobile Communications for 5G Cellular: It Will Work!," *IEEE Access,* vol. 1, pp. 335-349, 2013.

[16]   E. Ben-Dor, T. S. Rappaport, Q. Yijun and S. J. Lauffenburger, "Millimeter-Wave 60 GHz Outdoor and Vehicle AOA Propagation Measurements Using a Broadband Channel Sounder," in *IEEE Global Telecommunications Conference (GLOBECOM)*, 2011.

[17]   T. S. Rappaport, F. Gutierrez, E. Ben-Dor, J. N. Murdock, Q. Yijun and J. I. Tamir, "Broadband Millimeter-Wave Propagation Measurements and Models Using Adaptive-Beam Antennas for Outdoor Urban Cellular Communications," *IEEE Transactions on Antennas and Propagation,* vol. 61, pp. 1850-1859, 2013.

[18] W. Keusgen, A. Kortke, M. Peter and R. Weiler, "A highly flexible digital radio testbed and 60 GHz application examples," in *IEEE European Microwave Conference (EuMC)*, 2013.

[19] A. Maltsev, A. R. Maslennikov, Sevastyanov, A. Khoryaev and A. Lomayev, "Experimental investigation of 60 GHz wireless systems in office environment," *IEEE JSAC,* vol. 27, no. 8, pp. 1488-1499, 2009.

[20] H. Sawada, "Intra-cluster response model and parameter for channel modeling at 60 GHz (Part 3)," IEEE doc. 802.11-10/0112r1, January 2010.

[21] A. Maltsev, E. Perahia, R. Maslennikov, A. Sevastyanov, A. Lomayev and A. Khoryaev, "Impact of Polarization Characteristics on 60-GHz Indoor Radio Communication Systems," *IEEE ANTENNAS AND WIRELESS PROPAGATION LETTERS,* vol. 9, p. 413, 2010.

[22] F. Khan and Z. Pi, "Millimeter-wave Mobile Broadband (MMB): Unleashing 3-300 GHz Spectrum," in *IEEE Sarnoff Symposium*, 2011.

[23] F. Khan and Z. Pi, "An introduction to millimeter-wave mobile broadband systems," *IEEE Comm. Mag.,* vol. 49, no. 6, p. 101 – 107, 2011.

[24] M. Jacob, S. Priebe, A. Maltsev, A. Lomayev, V. Erceg and T. Kurner, "A ray tracing based stochastic human blockage model for the IEEE 802.11ad 60 GHz channel model," in *Antennas and Propagation (EUCAP), Proceedings of the 5th European Conference on*, April 2011.

[25] R. J. Weiler, M. Peter, W. Keusgen and M. Wisotzki, "Measuring the Busy Urban 60 GHz Outdoor Access Radio Channel," in *ICUWB*, 2014.

[26] R. J. Weiler, M. Peter, W. Keusgen, H. Shimodaira, K. T. Gia and K. Sakaguchi, "Outdoor Millimeter-Wave Access for Heterogeneous Networks – Path Loss and System Performance," in *PIMRC*, 2014.

[27] R. J. W. Wilhelm Keusgen, M. Peter, M. Wisotzki and B. Göktepe, "Propagation Measurements and Simulations for Millimeter-Wave Mobile Access in a Busy Urban Environment," in *IRMMW*, 2014.

[28] T. S. Rappaport and S. Shu, "Multi-beam antenna combining for 28 GHz Cellular link Improvement in urban environments," in *IEEE Global Telecommunication Conference (Globecom)*, Atlanta, 2013.

[29] K. Kitao and S. Ichitsubo, "Path loss prediction formula in Urban Area for the Fourth-Generation Mobile Communication Systems," *IEICE Trans. Comm.,* Vols. E91-B, pp. 1999-2009, 2008.

[30] A. Ghosh, T. A. Thomas, M. C. Cudak, R. Ratasuk, P. Moorut, F. W. Vook, T.S. Rappaport, G. R. MacCartney Jr., S. Sun and N. Shuai, "Millimeter wave enhanced local area systems: A high data rate approach for future wireless networks," *IEEE Journal on Selected Areas in Communications,* vol. 32, no. 6, pp. 1152-1163, June, 2014.

[31] T. S. Rappaport, S. Sun, R. Mayzus, H. Zhao, Y. Azar, K. Wang, G. N. Wong, J.K. Schultz, M. Samimi and F. Gutierrex, "Millimeter wave mobile communications for 5G cellular: It will work!," *IEEE Access,* vol. 1, pp. 335-349, 2013.

[32] W. Roh, J.-Y. Seol, J. Park, B. Lee, J. Lee, Y. Kim, J. Cho, K. Cheun and F. Aryanfar, "Millimeter-wave beamforming as an enabling technology for 5G cellular communications: Theoretical Feasibility and Prototype Results," *IEEE Communications Magazine*, pp. 106-113, February 2014.

[33] METIS, "Intermediate description of the spectrum needs and usage principles," *METIS Deliverable D5.1,* 30 August 2013.

[34] T. A. Thomas, H. C. Nguyen, G. R. MacCartney Jr. and T. S. Rappaport, "3D mmWave Channel Model Proposal," in *IEEE VTC-Fall/2014*, Vancouver, Canada, September 14-17, 2014.

[35] M. R. Akdeniz, Y. Liu, M. K. Samimi, S. Sun, S. Rangan, T. S. Rappaport and E. Erkip, "Millimeter Wave Channel Modeling and Cellular Capacity Evaluation," *IEEE Journal on Selected Areas in Communications, Special Issue on 5G,* July, 2014.

[36] "MiWEBA Project homepage http://www.miweba.eu/project.html (FP7-ICT-2013-EU-Japan, project number: 608637)," 2013.

[37] "MiWEBA project deliverable D5.1," 06 2014. [Online]. Available: http://www.miweba.eu/data/MiWEBA_D5.1_v1.01.pdf.

[38] I. Siaud, A.M. Ulmer-Moll,, N. Malhouroux-Gaffet and V. Guillet "Short-Range Wireless Communications", "An Introduction to 60 GHz Communication Systems: Regulation and Services, Channel Propagation and Advanced Baseband Algorithms", Chapter 18, SBN-13: 978-0-470-69995-9 – John Wiley & Sons Ed. Chapter 18, February 2009.

[39] S.K.Yong, "TG3c Channel Modelling sub-committee Final Report", IEEE 802.15 Working Group for WPAN, IEEE 802.15-07-0584-01_003c, March 2007.

[40] B. Kannan, C.W. Kim, S. Xu, and al., "Characterization of UWB Channels: Small-Scale Parameters for Indoor and Outdoor Office Environment", IEEE802.15.4a, n°IEEE 802.15-04-0385-00-04a, July 2004.

A4.4 Measurement and modelling of pathloss at 72 GHz

The measurement campaign was conducted at Chengdu, China. The indoor deployment scenario was in a large dining hall. The outdoor deployment scenario was in the campus. Both LoS and NLoS propagation conditions were measured.

The TX and RX locations for indoor measurement are shown in Fig. A4.4-1. For LoS scenario measurement, two TX sites are chosen close to the top sides in order to get a maximum variable distance between TX and RX. For each TX position, the RX sites were chosen in line with the TX site with the randomly chosen distance.

In NLoS scenario measurement the TX site was chosen in one aisle of the room and the RX sites were chosen randomly at the NLoS area. The TX and RX locations for outdoor measurement are shown in Fig. A4.4-2.

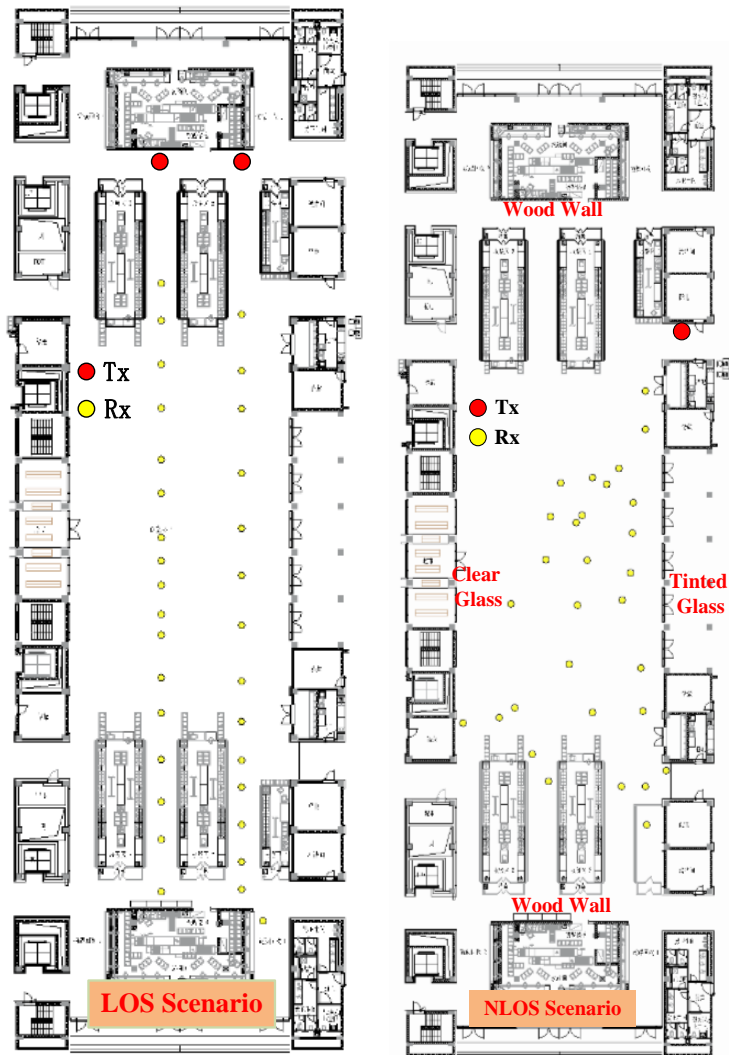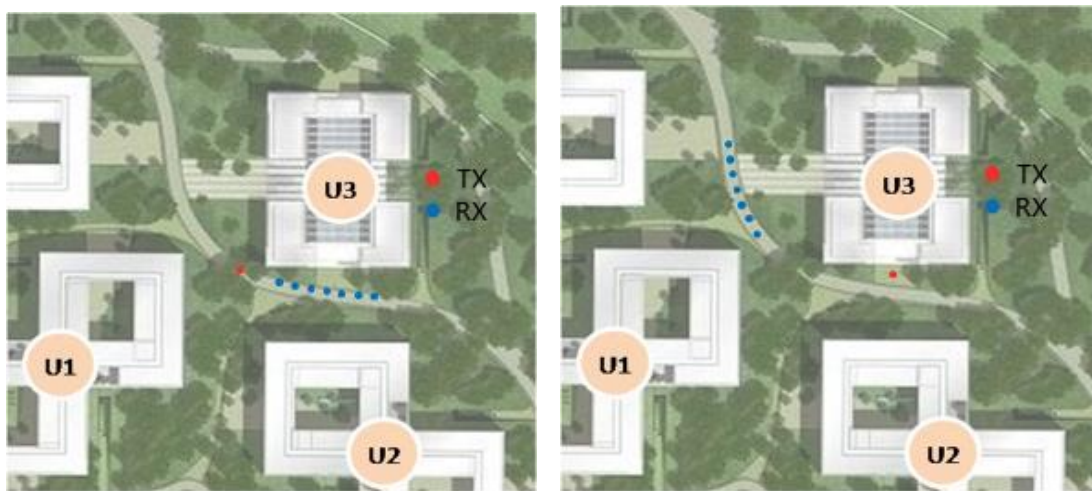FIGURE.A4.4-1

Layout of indoor measurement environment

FIGURE.A4.4-2

Layout of outdoor measurement environment

(a) Outdoor LoS measurement environment **(b) Outdoor NLoS measurement environment**

For indoor, the measurement campaign was conducted with 33 LoS TX-RX position combinations and 29 NLoS TX-RX position combinations. For outdoor, measurement campaign was conducted with 17 LoS TX-RX position combinations and 19 NLoS TX-RX position combinations. Based on the measurement data acquired, the propagation path loss model was fitted based on the framework as follows.

$$PL = \alpha + 10 \cdot \beta \cdot \log 10(\frac{d}{d_0}) + x_\sigma$$

in which $\alpha = PL_{d0} = 20 \cdot \log 10(\frac{4\pi d_0}{\lambda})$. D_0 is the reference distance. In this document d_0 was chosen as 1 m.

In Fig. A4.4-3, the model-fitting result for 72 GHz propagation path loss is provided. The strongest sample refers to the sample with strongest received power for each TX-RX position combination after beamsteering. It can represent the condition that TX and RX beams are perfectly matched in millimetric wave beamforming system A summary of the model parameters considering beamsteering for different propagation condition can be found in Table A4.4-1.

FIGURE A4.4-3
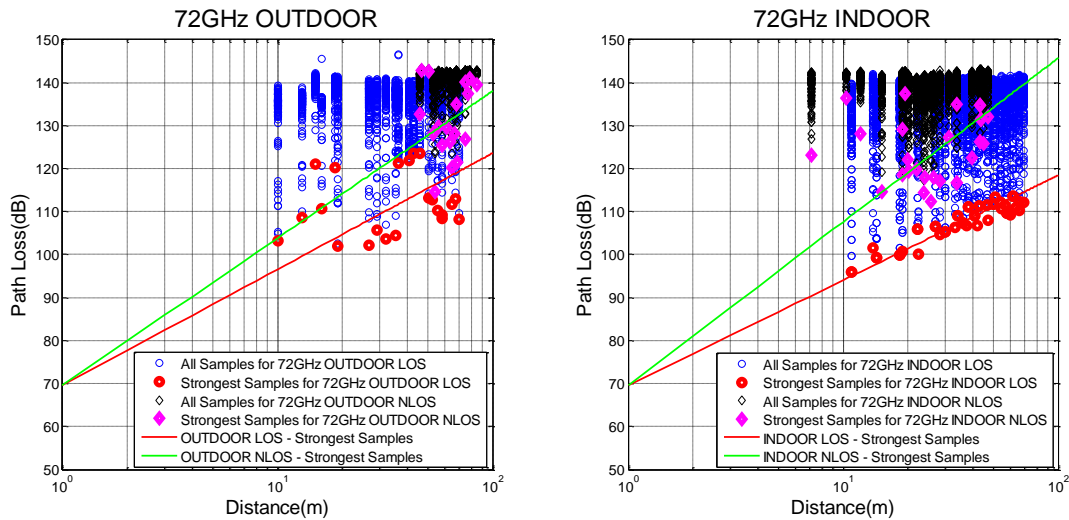
Model fitting for LoS prapagation channel

TABLE A4.4-1
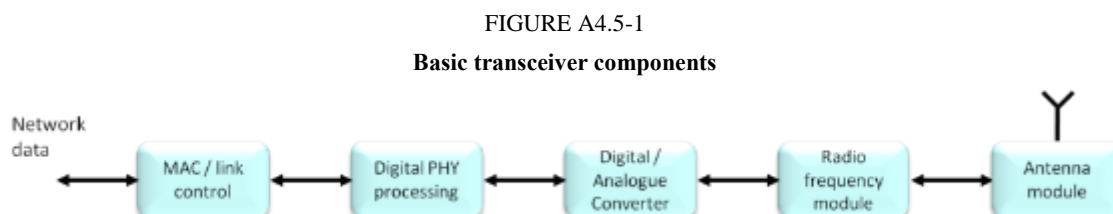
Experimentally-derived path loss model parameters

Scenarios	Parameters	LoS	NLoS
Indoor	PLE in dB(β)	2.58	4.08
	Intercept in dB(α)	69.59	69.59
	Standard deviation in dB(σ)	2.38	10.63
Outdoor	PLE in dB(β)	2.86	3.67
	Intercept in dB(α)	69.59	69.59
	Standard deviation in dB(σ)	9.75	8.33

A4.5 Introduction of MiWaveS[13] project scope and findings

A4.5.1 Prototyping millimetric use cases

A4.5.1.1 Basic features of transceiver elements

In this subsection the basic features of the demonstrator setups available in MiWaveS project are described to get an overview about general capabilities of the demonstrator.

FIGURE A4.5-1

Basic transceiver components

In Fig. A4.5-1, the basic components of one transceiver unit required to process the data before and after wireless transmission over the air channel are shown. It should be noted that one transceiver always includes one transmit and one receiver branch. The basic functionality of each component is listed in Table A4.5-1 below:

TABLE A4.5-1

Basic functionality of transceiver components

MAC / link control	- Resource and link control - Multi-user access - Beamforming control
Digital PHY processing	- Link transmission in digital baseband - Time and frequency synchronization - Channel estimation and equalization - Modulation and coding - Pulse shaping and digital re-sampling
Digital / analogue converter	- Signal sampling - Signal quantization
Radio frequency module	- Analogue up and down conversion from / to baseband - Filtering of unwanted spurious signal emissions - Signal amplification
Antenna module	- Signal radiation - Beam steering using antenna arrays

---

[13] The European project MiWaveS analyses and studies the key technologies for the implementation of millimetric wave wireless access and backhaul in future 5th generation heterogeneous cellular mobile networks. One main objective of the MiWaveS project is the demonstration of innovative millimetric wave transmission concepts that will be developed during the project time frame. The frequency bands of interest here are the band 57-66 GHz and the bands 71-76 and 81-86 GHz.
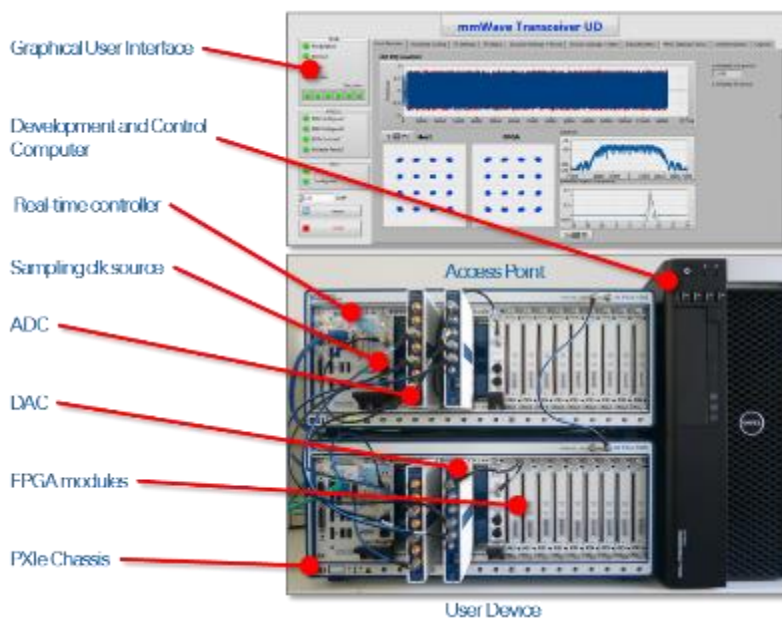
The MiWaveS demonstrator has setups for the bands 71-76 GHz and 81-86 GHz as well as the band 57-66 GHz transmissions. In Table A4.5-2, the main features of the demonstrator components are listed. It should be noted that this represents rather a high level feature description to draw conclusions about the maximum functionality and the expected outcomes in the project time frame.

TABLE A4.5-2

Basic feature list of MiWaveS hardware components

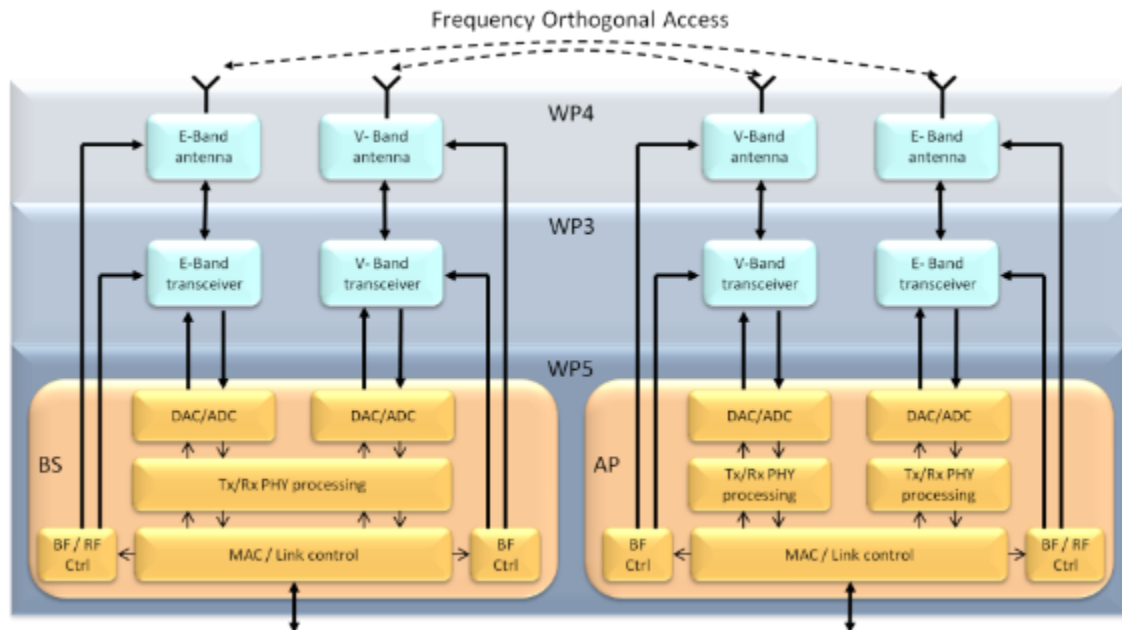|		
MAC / Link control	• Uplink and downlink closed loop operation → enable real-time channel feedback • Flexible TDD access with dynamic uplink / downlink load control • Multi-user access in time division duplex or space division duplex • Beam steering control → direction • RF control → frequency, power, receiver gains	
Digital PHY processing	• Single carrier based modulation scheme with frequency domain equalization • Real-time reconfigurable PHY • Channel estimation based on blocks of pilots. • Capable of Gbit/s high throughput PHY processing • Scalable solution to support multiple parallel high-throughput links	
Digital / Analogue converter	• DAC quantization resolution: 14 bit, sampling rate: 1.25 GHz • ADC quantization resolution: 8 bit, sampling rate: 1.5 GHz	
Radio frequency module	71-76 and 81-86 GHz	Tuneable carrier frequency range: 71 -76 GHz and 81-86 GHz Analogue transmission bandwidth: ~1 GHz Max output power: ~9 dBm
	57-66 GHz	Tuneable carrier frequency range: 57-66 GHz Analogue transmission bandwidth: ~1.2 GHz Max output power: ~9 dBm
Antenna module	71-76 and 81-86 GHz	Max antenna gain: >25dBi, 30dBi targeted Beam resolution: 5-7 beams (backhaul)
	57-66 GHz	Max antenna gain: ~30 dBi Beam resolution: ≤8 beams (backhaul), ≤16 beams (access)

FIGURE A4.5-2

Millimetric base band transceiver used in MiWaves project

A4.5.1.2 Demonstrator setups and use case mapping

In MiWaveS project backhaul and access link experiments are intended. For the backhaul link the MiWaveS demonstration and measurements are focusing on:

- **High throughput**: Use maximum available transmission bandwidth for downlink or uplink for achieving the maximum throughput. For increasing the throughput two parallel links can be used in the setup which doubles the capacity. High gain antennas should be used to maximize SNR at the receiver to allow an efficient modulation and coding scheme.

- **Hop length** (Backhaul range): Measurement of maximum distance between backhaul link hops under the constraint of achieving a certain throughput / capacity.

- **Latency**: Measure the round trip latency on PHY and MAC layer and determine the time for the system to adapt for some channel variation.

- **Ease of installation Efficiency of installation and in operation:** Demonstration of different methods, approaches and techniques which enable autonomous backhaul link adjustment in the field e.g. automated antenna beam search and locking during deployment.

Using the available hardware components for the MiWaveS backhaul link, one can setup a system as sketched in Fig. A4.5-3.

FIGURE A4.5-3
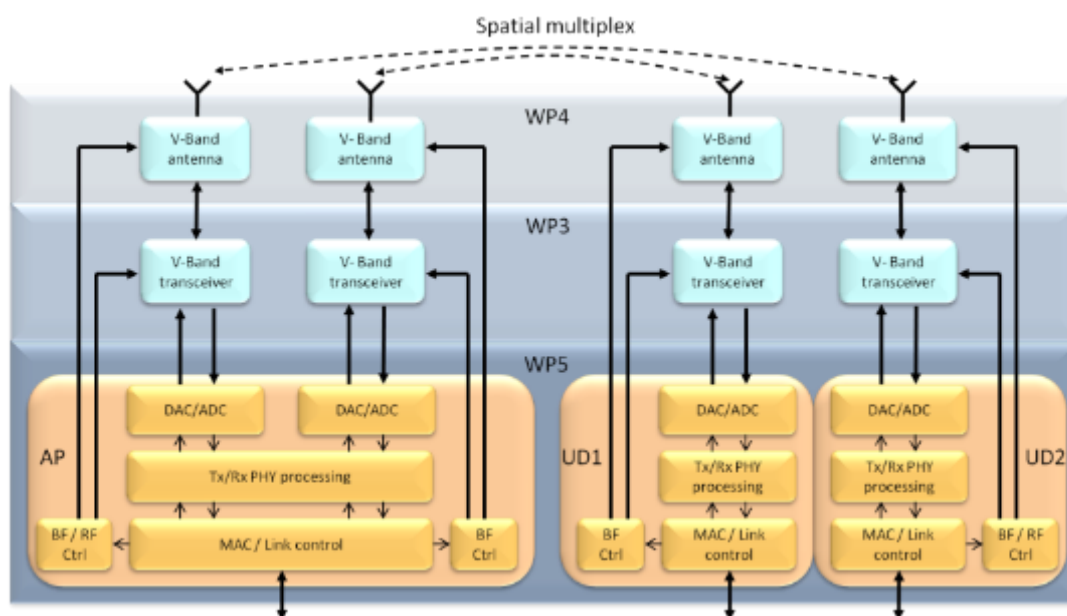
Intended backhaul link system setup

For the access link the MiWaveS demonstration and measurements are focusing on:

*   **Flexible multi-user access**: Two-user access is either possible in time or in spatial multiplex. Different users can be provided with different rates.

*   **Beam tracking**: Adaptive multi-user beamforming. Use two parallel transceiver chains with separate RF and antenna modules to allow for two independent beams. Exploit real-time feedback scheme for real-time adaptive beam tracking.

*   **Coverage**: The coverage will be provided by a sectored transceiver element with multiple antennas. Each antenna will cover one sector and thus can provide the needed gain for a sufficient SNR in an outdoor environment.

Using the available hardware components for the MiWaveS access link, one can setup a system as sketched in Fig. A4.5-4.

FIGURE A4.5-4

Intended access link system setup

A4.5.1.3 Description of experiments and KPI measurements

All the experiments will be carried out indoor (laboratories or rooms suitable for this purpose) to solve all the issues due to the nature of the realized prototype (for the base band processing) by means of PXI chassis (systems generally used indoors). At the end of this phase of the project, if a logistic solution will be available and there will be enough time the possibility to perform a measurement campaign outdoors will be considered. The main problems for which it is necessary to find a solution would be:
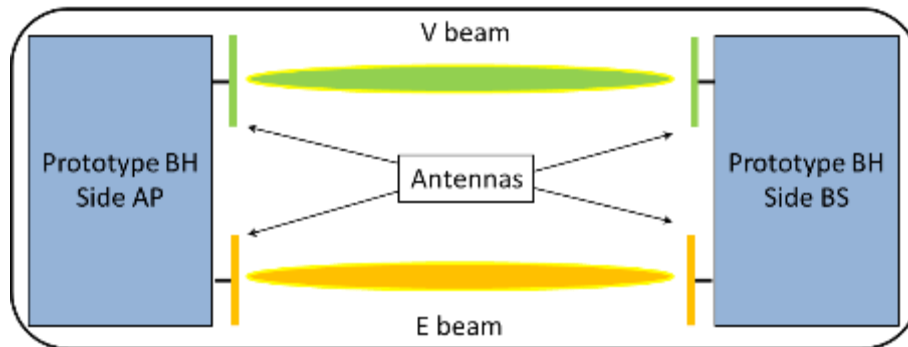
• How to install the prototype of the AP on top of a pole in safe way (both for equipment and for operators).

• If only the base band equipment is placed at the base of the pole, arranging on top radio frequency devices, how to face the losses in the RF cables (PA and LNA).

• The previous version can be changed using instead of RF cable, two coaxial cables: the first one for data transmitted and the second one for data received, both in analogue format. In any case it is necessary to check the maximum length of these coaxial cables (losses).

• Remote the RF part on top of the pole by means of an optical fibre but all the electro optical transducers are needed.

In general, except for the first case, all the other ones need the introduction in the original setup of additional hardware that must be integrated with the demonstrator.

A4.5.1.4 Backhaul link in the band 57-66 GHz and the bands 71-76 and 81-86 GHz

The Figure below shows a block diagram overview of the demonstrator.

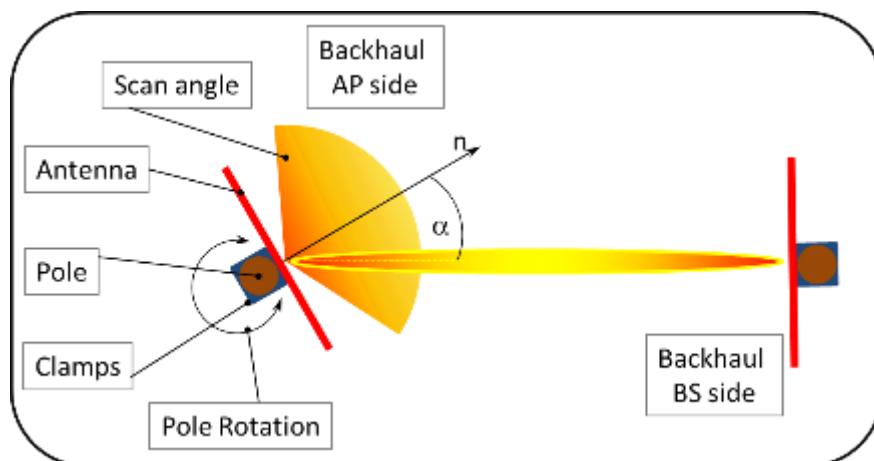**High level description of backhaul demonstrator**

Throughput, latency and SINR (by means of known pilots embedded in the stream of bits) will be evaluated. This analysis will be done with respect to the link budget checking the effect of the distance on performances and evaluating the *backhaul range* KPI. The latency obtained here is at MAC layer and some evaluations can be done to estimate the latency at the application layer. Values averaged over a time interval may better characterize this system.

As for reliability, an analysis can be done related to frequency redundancy and possible effects due to weather conditions. Simulating a failure in one of the two beams (using a physical obstacle or stopping the relative base band section) the system has to be able to operate also with a throughput reduction. Weather conditions can be emulated with an attenuation introduced in the radio link (reduction of transmitted power).

A4.5.1.5 Beamforming functionality for backhaul

In Figure A4.5-6 a possible setup is depicted for testing the beamforming on the backhaul. For sake of simplicity in this picture a horizontal configuration is considering but this description is still valid also for the case of a two-dimensional beamforming.

FIGURE A4.5-6

Beamforming demonstrator for backhaul

The pole where the antenna is mounted relative to the AP, must be rotated keeping the segment joining the two antennas inside the scan angle (see picture above). Similar considerations also apply if the antenna is equipped with a beamforming in two dimensions placing the two antennas in the setup with different heights.

The test is carried out with the following steps:

1   Switch on the antenna side AP

2   Switch on the antenna side BS

3   Measuring the time necessary to establish a connection between the two antennas

4   Monitoring throughput, latency and SINR like in the previous case

The time interval obtained in the point 3 can be used to estimate the *efficiency of installation and in operation* KPI. The point 4 is useful to check the beamforming effect comparing these results with those obtained with fixed beam antennas. The same experiment can be repeated varying the angle α represented in Figure A4.5-6, searching the true scan angle for the specific AUT and analysing the performance of the system as a function of the α angle.

With this setup the capabilities of beam searching and beam steering of the antenna relative to the AP can be shown. Another feature to check in this type of system is the beam tracking which is useful if the access point may be subjected to vibrations. Manufacturers use specific vibration tables to qualify the antennas for base stations. These tables generate sinusoidal vibrations of which amplitude and frequency can be selected.

If this apparatus will be available, tests of beam tracking can be carried out placing the scan antenna on this vibrating table and verifying the ability to maintain the radio link. Ranges for amplitudes and frequencies of these vibrations can be searched where the AP does not degrade his performance.
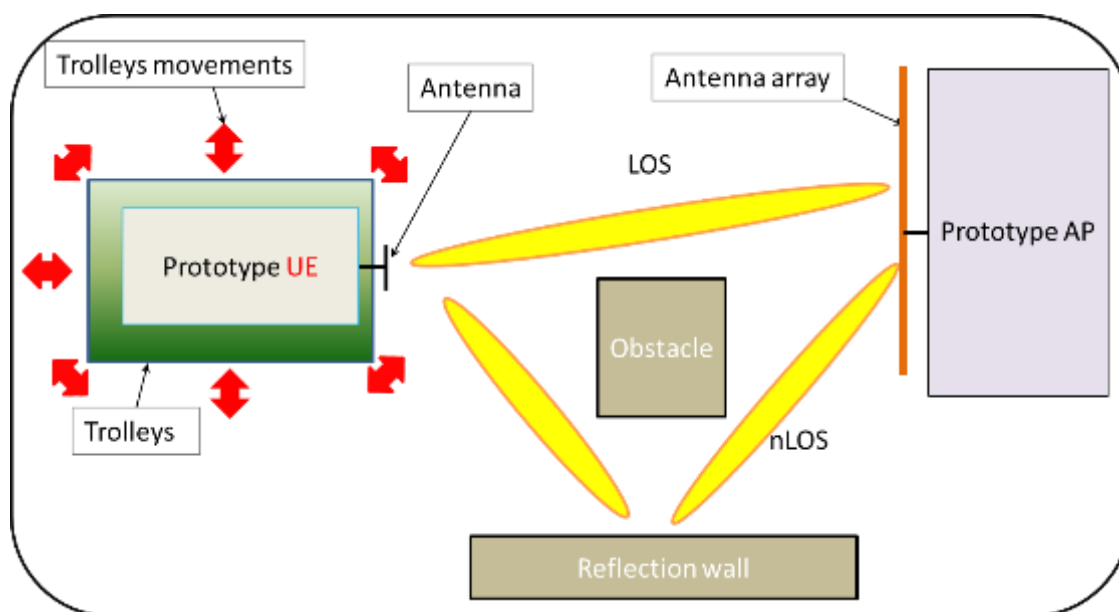
Relatively to reliability, also for the previous case, all the phenomena reported which may cause outage must be considered and estimate their occurrence probability. In this way, it is possible to obtain a general value not strictly related to the period of the measurements.

A4.5.1.6 Beamforming functionality for access

The beamforming functionality for the access link can be verified with a setup depicted in Fig. A4.5-7.

FIGURE A4.5-7

Beamforming demonstrator for access (single user).

Considering the possibility of moving the UE thanks to the trolley and its wheels and that, the propagation between the two antennas can be in LoS and/or NLoS, the available tests with this setup can be classified in:
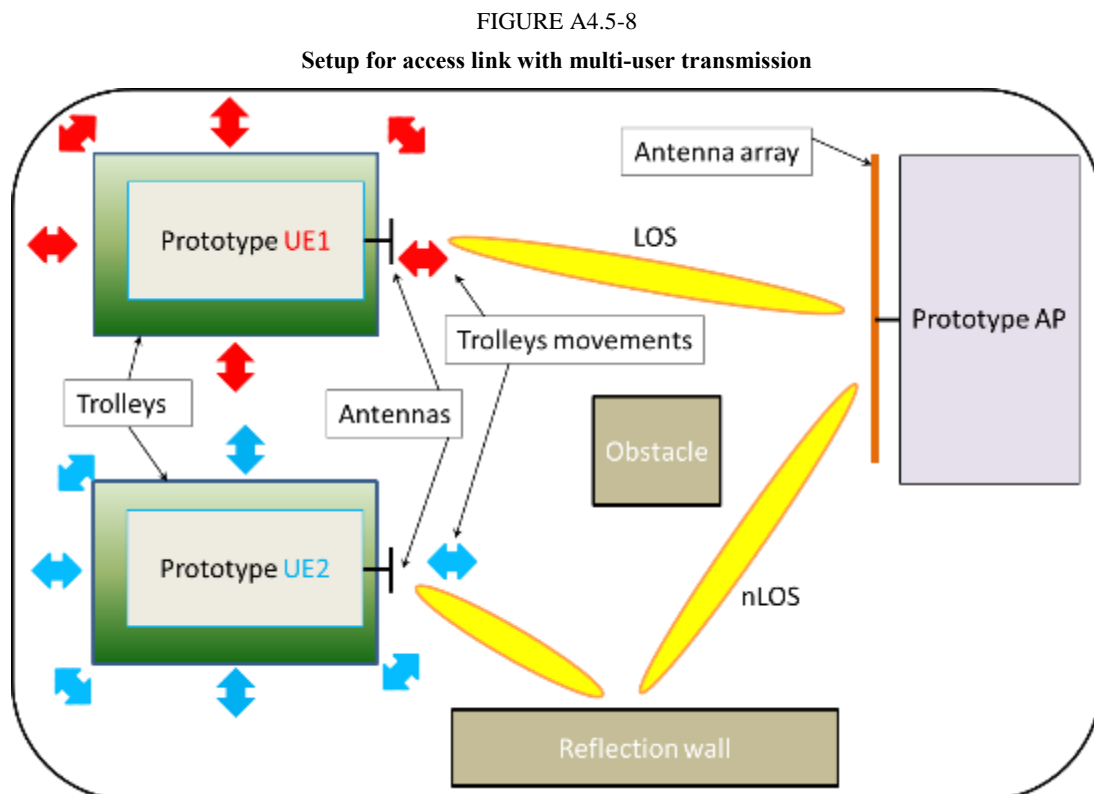
- Static LoS
- Static NLoS
- Dynamic LoS
- Dynamic NLoS

In each of these conditions, it is necessary to pay attention to the scan angle of the AP antenna, in order to allow the generation of a beam (LoS or NLoS). In all these cases it is possible to measure SINR and the *end user capacity* KPI sending and receiving files. Like for the backhaul range also here it is possible, with the link budget, to estimate the *access range* KPI tuning the transmitted power. By averaging the value of this KPI can be evaluated. Similar to the previous cases weather conditions can be emulated by means of attenuations. In the dynamic cases, if possible, record the speed and direction of the trolley could be of interest.

Specific beamforming capability can be evaluated in the static cases (beamforming search LoS and NLoS) and in the dynamic ones (beamforming tracking LoS and NLoS).

A4.5.1.7 Access link in the band 57-66 GHz with multi-user configuration

As shown in Fig. A4.5-8, this demonstrator is quite similar to the beamforming functionality for the access.

FIGURE A4.5-8

Setup for access link with multi-user transmission

All the measurements and KPI are the same but obtained in a multi-user configuration. In this case it is also possible to verify the effect of the interference that the beam related to the UE1 produce to the UE2 and vice versa. The results can be correlated with the angular separation of the two beams generated by the antenna of the AP.
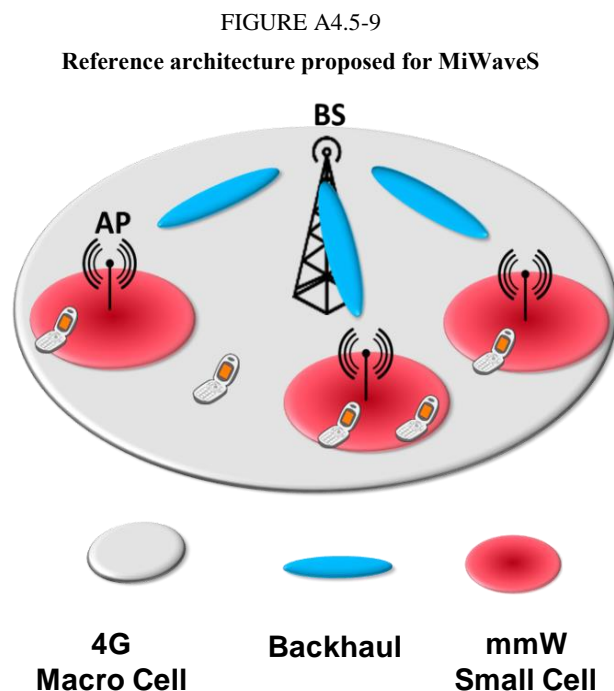
A4.5.1.8 Final demonstrator

Finally, the four previous setups will be combined in order to verify at the same time all the features of the system. Obviously, the BH will be set with, at least, one antenna with beam control.

A4.5.2 MiWaveS summary on the millimetric small cell access points and backhaul system

The MiWaveS project follows a top-down approach, starting from the definition of the global system and its requirements in terms of network organization, frequency planning, technical and environmental specifications. The relevant electromagnetic field exposure regulations are summarized by the project as well.

Then, the access and backhaul links are investigated separately. In each case, the system definition is presented taking into account the performance objectives, the main features of the physical layer, and the global specifications of the main components (power levels, antenna performances) in order to derive typical link budgets showing the feasibility of the concept. Next, the architecture and specifications of the millimetric wave modules, transceiver, antenna and sub-components are presented and analysed in view of the state-of-the-art of millimetric wave technologies planned to be used in MiWaveS.

FIGURE A4.5-9

Reference architecture proposed for MiWaveS

The reference system architecture considered in MiWaveS is illustrated in Fig. A4.5-9. It relies on macro-cellular base-stations providing a global coverage to mobile users using the legacy radio access technologies (LTE, UMTS, etc.) in sub-6 GHz bands and introduces millimetric wave small-cells enabling much higher throughput and traffic capacity to low-mobility users using a millimetric wave radio access in the band 57-66 GHz. Each small cell exhibits a radius of up to 50 m and is served by one or several collocated APs arranged in independent sectors. Each of the four IEEE channels defined in the 57-66 GHz band are divided in eight 220-MHz sub-channels in order to benefit from enhanced performances such as a longer communication range and to enable an FDMA scheme of up to eight users per AP in the same IEEE channel. Considering a small cell divided in four sectors, a maximum of 32 simultaneous users may be accommodated in FDMA; of course, a much larger number of users can be served in TDMA. The link budget analysis, taking into account an availability of 99.9% with respect to climatic conditions (rain falls), shows that maximum downlink and uplink

data rates of 7 Gbit/s and 3.8 Gbit/s, respectively, can be provided for users located at a short distance from the AP and benefiting from the maximum bandwidth allocation. Users located near the cell edge and having a single sub-channel allocation will still benefit from a minimum data rate of 300 Mbit/s in downlink and 150 Mbit/s in uplink.

Assuming a massive and dense deployment of millimetric wave small-cell APs, wireless backhaul technologies are required to provide a cost-efficient and high-capacity interconnection of the APs and the core network (Fig. A4.5-9). MiWaveS investigates the implementation of wireless backhaul using the unlicensed spectrum available in the band 57-66 GHz and the light-licensed spectrum of the bands 71-76 and 81-86 GHz. The proposed frequency plan uses the four 2.16 GHz IEEE channels of the band 57-66 GHz and the 250 MHz channelization plan proposed by ETSI standard in the bands 71-76 and 81-86 GHz. The band 57-66 GHz backhaul system is shown to be able to provide a maximum data rate of 28 Gbit/s over a distance of 100 m with an availability of 99.9%.

Based on the specifications, feasibility studies and analysis, the work-packages 2, 3, and 4 of MiWaveS project will further investigate the proposed transceiver and antenna concepts, as well as the beam-steering/beam-switching algorithms to develop and implement the suitable technologies and proof-of-concept demonstrating the feasibility and performances of the millimetric wave small-cell heterogeneous network proposed by MiWaveS consortium.

List of References

[1]   "Specifications of the mmW access point and backhaul" MiWaveS project deliverable D1.2, October 2014.

[2]   "Detailed specification of demonstrator setups and functionality" MiWaveS project deliverable D6.1, October 2014.

[3]   M. Cudak, et. al., "Experimental mmWave 5G Cellular System" in Proc. Globecomm 2014, December 2014.

_____